ON THE SENSITIVITY OF AN ATMOSPHERE IN RADIATIVE-CONVECTIVE EQUILIBRIUM TO SOIL MOISTURE

by

JAMES COLES BARNARD

B.A., University of California at Davis
(1972)

SUBMITTED IN PARTIAL FULFILLMENT
OF THE REQUIREMENTS FOR THE
DEGREE OF

MASTER OF SCIENCE

at the

MASSACHUSETTS INSTITUTE OF TECHNOLOGY

July, 1977

Signature of Author. . . . . Department of Meteorology, July 1977

Certified by. . . . . Thesis Supervisor

Accepted by. . . . . Chairman, Departmental Committee on Graduate Students

ON THE SENSITIVITY OF AN ATMOSPHERE IN RADIATIVE-CONVECTIVE EQUILIBRIUM TO SOIL MOISTURE

by

James Coles Barnard

Submitted to the Department of Meteorology in July 1977 in partial fulfillment of the requirements for the degree of Master of Science.

ABSTRACT

The sensitivity of the atmosphere to soil moisture is explored using a coupled soil-atmosphere model. The model is one dimensional (in the vertical) and diurnally forced. The atmospheric component of the model includes only radiative and free convective processes; atmospheric dynamics and condensation are not considered. In the soil, a detailed treatment of moisture and heat transfer, as developed by Philip and de Vries, is used.

With the assumption that the soil is perfectly dry, the model is integrated to find the state of diurnally forced radiative-convective equilibrium. The temperature profiles produced by this integration resemble typical profiles observed in the lower atmosphere ($z < 10$ km) under conditions of strong free convection, except that diurnal temperature fluctuations in the diurnal boundary layer are too small.

Two integrations are then performed to determine the sensitivity of the atmosphere to different amounts of soil moisture. These integrations differ only in the specification of the initial soil moisture content; in one case the soil is only slightly moist, while in the other case, a thin layer of soil ajoining the surface is assumed to be saturated. As the model contains no provision for condensation, the integrations are stopped when significant supersaturation occurs in the atmosphere.

The calculations reveal that:

1) If the soil is initially slightly moist, no appreciable effect on the atmosphere can be detected. In this case, the latent heat flux is negligible.

2) When the initial soil moisture content at the surface is high, the atmosphere is influenced, mostly by alterations in the surface energy balance. In this case, the latent heat flux is large.

3) The amount of supersaturation that occurs in the atmosphere does not appear to be greatly influenced by the initial soil moisture content.

Thesis Supervisor: Peter H. Stone
Title: Professor of Meteorology

TO

ALL

TORTOISES

Acknowledgements

I would like to express my sincere thanks to my thesis advisor, Professor Peter H. Stone, who was of immense help to me while doing this thesis. I would also like to thank Jule Charney, with whom I discussed some of the physics of the problem; Eugenia Rivas, who helped me conquer some numerical difficulties; and Peter Eagleson, who discussed with me the soil hydrology portion of the thesis. Finally, Virginia Mills must be thanked for her superb typing job.

Table of Contents

I. Introduction

It is well known that significant amounts of moisture can be found in the soil beneath the surface of the earth. In all but the driest soils, this water is not locked tightly to the soil particles but is capable of movement in all directions. Exchanges of moisture occur across the earth-atmosphere interface which can affect both the atmosphere and soil.

The nature of this interaction and the strength of its effects have yet to be extensively studied. Crude parameterizations for soil hydrology have been developed for use in atmospheric models (for example, see Manabe (1969)). These parameterizations, based on a simple moisture budget scheme for a column of soil (on the order of 1 meter in depth), fail to incorporate important physical processes such as gravitational drainage, capillarity, and adsorption. Evaporation from the soil has been calculated from formulas relating the rate of evaporation to the surface wind and surface moisture gradient. The attraction of such methods appears to be their simplicity and attendant economy of calculation; however their accuracy has not been demonstrated.

Using the crude parameterizations mentioned above, Manabe and Holloway (1975) studied the seasonal variation of the hydrological cycle over the earth using a general circulation model. Their model calculated the magnitude and distribution of evaporation, precipitation, soil moisture, and runoff. A comparison between the calculated and observed values of evaporation and precipitation showed fairly good agreement, although the rates of precipitation over continental areas

were too high.

Soil moisture in the model was controlled by the amount of solar radiation (which influences evaporation), and the rate of precipitation. For example, areas such as the Amazon basin, where the rate of precipitation exceeds the high rate of evaporation, had a high soil moisture content. On the other hand, the soil in the Sahara desert was found to be very dry because of the small amount of rainfall, and the large flux of incident solar radiation.

Philip and de Vries (1957) applied a knowledge of soil physics to derive a set of partial differential equations which govern the time-dependent moisture and heat fields in the soil. These equations were employed by Philip (1957) to study the case of steady-state evaporation from bare soil. Philip argued that evaporation is limited either by meteorological conditions (i.e. evaporation can never exceed the potential evaporation) or by the ability of the soil to transfer moisture to the surface of the earth. In the latter situation the evaporation rate is only a function of water-table depth and soil characteristics. However, for very dry soils (with depths to the water table $\geq$ 3 meters) the evaporation rate becomes sensitive to the heat flux in the soil.

Sasamori (1971) incorporated the work of Philip (1957) into a numerical study of the atmospheric and soil boundary layers. In this study a coupled atmosphere-soil system was designed which allowed both heat and moisture exchange across the soil-atmosphere boundary. The calculation simulated conditions observed by Lettau and Davidson (1957) during the Great Plains Turbulence Field Program and a fairly good agreement was found between the observed and calculated values for

temperature and humidity (temperature errors were around 2°C). However, the model was unable to accurately simulate the boundary layer winds.

Other studies suggest that the atmosphere may be quite sensitive to soil moisture. Walker and Rountree (1977) investigated the effects of soil moisture on circulation and rainfall over West Africa using an eleven layer tropical model. (This model employed the crude soil hydrology parameterization given in Manabe (1969)). Two experiments were conducted to isolate the effects of soil moisture; the only difference between them being the specification of initial soil moisture content between 14°N and 32°N. In one case a desert was simulated; in the other case, the soil was initially prescribed to be moist. The integration period varied from 10 days for the dry case to 20 days for the moist case. They found that:

(1) The initial soil moisture content had a large influence on future precipitation. In the dry case aridity was maintained north of 14° while in the moist case, rainfall occurred persistantly over what was, in the dry case, a desert.

(2) The energetics of disturbances that developed during the integrations differed. In the dry situation, the large meridional temperature gradient that was formed between the hot desert and the cooler, moist land to the south caused the production of eddy kinetic energy through baroclinic instability. In contrast, in the moist experiment condensation in the atmosphere was a significant source of energy and the eddy kinetic may have been maintained by a mechanism similar to CISK.

This thesis will make a further investigation of the interaction between soil moisture and the atmosphere. A one-dimensional (in the vertical) model will be constructed with a detailed treatment of soil hydrology. This model will simulate a diurnal cycle occuring in an arid region where free convection is the dominant form of (vertical) sensible heat and moisture transfer. To determine the sensitivity of the atmosphere to soil moisture, two integrations will be performed corresponding to initially dry and moist soil conditions. To avoid the complications of clouds and moist convection, the integrations will be stopped when significant condensation occurs.

Chapter 2 develops the basic atmospheric model used in this thesis. It includes both radiative and convective processes but does not include soil hydrology. This model is closely patterned after the radiative-convective model presented by Gierasch and Goody (1968) for a study of the Martian atmosphere.

In chapter 3 a detailed model of soil hydrology will be coupled to the atmosphere. Integrations for dry and wet soil conditions will be done and the results presented.

Chapter 4 concludes the thesis and gives some suggestions for future work.

II. The Radiative-Convective Model without Moisture

2.1 Introduction

Calculations (Manabe and Moller, 1961) have been done to determine the temperature structure of the atmosphere in pure radiative equilibrium. These calculations reveal that the lower troposphere (below 6-7 km) is hydrostatically unstable due to the existence of superadiabatic lapse rates. Therefore, as radiative processes pull the atmosphere towards radiative equilibrium and unstable lapse rates, convection will result attempting to restore the atmosphere to a condition of stability. An equilibrium situation is attained between radiative and convective processes; this state is called radiative-convective equilibrium.

This chapter will develop a model which simulates a state of diurnally forced radiative-convective equilibrium for the earth's atmosphere. To simplify matters, we shall introduce two important assumptions. These assumptions cause the neglect of important physical processes and consequently, the model should not be considered as a highly realistic representation of the earth's atmosphere. However, by including the action of both radiative and convective processes, results can be produced which resemble vertical temperature profiles found in the atmosphere.

Firstly, in keeping with the one-dimensional nature of the model, we shall ignore atmospheric dynamics. The winds are assumed to be very small for all time. An important consequence of this assumption is the neglect of mechanisms (such as advection and forced convection) for the transport of atmospheric quantities (i.e. heat, moisture).

Secondly, radiative heating rates will be calculated by using the grey approximation. This avoids the much more complicated non-grey situation found in the real atmosphere. In addition, when computing radiative heating rates, the atmosphere will be assumed transparent to solar radiation, and water vapor will be considered the only absorber of long-wave radiation.

It should be noted that in certain areas of the globe, advection is weak compared to free convective processes (i.e. advective time constants are much larger than convective time constants) and that free convection is stronger than forced convection. For example, an area that roughly meets these criteria is the Sahel in West Africa. In such situations, given accurate initial conditions, the model should be expected to give good results for integrations over a short time period. For longer times, errors caused by the neglect of dynamics and non-grey radiation will become serious, and unreliable results will be produced.

2.2 The Basic Equations

We have assumed that the velocity of the wind is very small and that advection is weak. With this realization, the basic equations for the atmosphere are:

(1) thermodynamic (heat) equation

$$\rho c_p \frac{\partial T}{\partial t} = Q_{rad} + Q_{conv} \qquad 2.2.1$$

(2) hydrostatic equation

$$\frac{\partial p}{\partial z} = -\rho g \qquad 2.2.2$$

(3) equation of state

$$p = \rho R T \qquad 2.2.3$$

with the following notation:

a. dependent variables

p, ρ, T = pressure, density, and temperature

b. independent variables

z, t = height, time

c. constants

c_p = specific heat at constant pressure (9.96×10^6 ergs/g °K)

R = gas constant for dry air (2.87×10^6 ergs/g °K)

g = acceleration of gravity (980 cm/sec^2)

d. heating terms

Q_{rad} = heating per unit volume due to radiation

Q_{conv} = heating per unit volume due to free convection

In the soil, heat transport takes place primarily by molecular conduction, as expressed by the heat conduction equation,

$$C \frac{\partial T_s}{\partial z} = - \frac{\partial}{\partial z} H_s \qquad 2.2.4$$

where T_s is the temperature of the soil, and C the volumetric heat capacity. H_s is the soil heat flux given by

$$H_s = - K_g \frac{\partial T_s}{\partial z} \qquad 2.2.5$$

where K_g is the thermal conductivity of the soil. In this chapter, the soil is assumed to be perfectly dry, and both C and K_g are taken to be constants.

Given expressions for Q_{rad} and Q_{conv}, and appropriate boundary and initial conditions, the mathematical problem is that of finding the pressure, density, and temperature profiles as functions of time. Further simplification can be made by noting that for the equilibrium solution to the equations, diurnal fluctuations in temperature are small, except in a diurnal boundary layer close to the ground. (The reasons for this will be discussed later). Hence to a good degree of approximation, the pressure and density can be considered as functions of height only, and the equations needed to calculate p and ρ (2.2.2 and 2.2.3) can be decoupled from the heat equation. (Of course, when calculating these variables, we need to use a temperature distribution which closely approximates the true, time-dependent profile. In practice, this profile is determined by trial and error).

2.3 Radiation

The assumption of a grey extinction coefficient for long wave radiation considerably simplifies the computation of radiative heating rates. The equation of radiative transfer is easily integrated, and once the mass extinction coefficient is specified and the distribution of absorbing gas known, the long wave flux can be determined. Since the atmosphere is considered to be transparent to solar radiation, the heating rate is just the negative divergence of the long wave flux.

Our first task is to find the long wave radiative flux. For a plane stratified grey atmosphere, the equation of radiative transfer is:

$$\mu \frac{\partial I}{\partial \tau} = I - B \qquad 2.3.1$$

where μ = cosine of the zenith angle

$$I = \int_{\nu=0}^{\nu=\infty} I_\nu \, d\nu$$ = integrated intensity

$$B = \int_{\nu=0}^{\nu=\infty} B_\nu \, d\nu = \frac{\sigma T^4}{\pi}$$ = integrated source function for a grey atmosphere in local thermodynamic equilibrium (σ , the Stefan-Boltzman constant, has a value of 5.67×10^{-5} ergs/(cm^{2}sec °K^4))

The optical depth, τ , is defined as

$$\tau(z) = \int_z^\infty K_m \rho_v(z)\, dz \qquad 2.3.2$$

where K_m = mass extinction coefficient (cm^2/g) and

$\rho_v(z)$ = density of absorbing gas.

Equation 2.3.1 can be easily integrated by using the integration factor $e^{-\tau/\mu}$. The limits of integration depend upon the sign of μ. For $\mu > 0$, we integrate between the reference level (i.e. τ) and the ground ($\tau = \tau_g$). The appropriate boundary condition applied at the surface of the earth is:

$$I(\tau_g) = \frac{\sigma T_g^4}{\pi} \quad \text{at } \tau = \tau_g,\ \mu > 0 \qquad 2.3.4$$

where T_g is the surface temperature. This boundary condition simply states that the earth radiates as a black body. Integration then yields,

$$I(\tau,\mu) = \frac{\sigma T_g^4}{\pi} e^{-(\tau_g - \tau)/\mu} + \frac{1}{\mu}\int_\tau^{\tau_g} \frac{\sigma T^4(\tau')}{\pi} e^{-(\tau'-\tau)/\mu}\, d\tau', \qquad \mu > 0 \qquad 2.3.5$$

(In the above expression, we have explicitly noted the dependence of T on τ by writing $T(\tau')$).

For $\mu < 0$, the integration is carried out between the top of the atmosphere $(\tau = 0)$ and the reference level. Since no long wave radiation is incident at the top of the atmosphere, the upper boundary condition is

$$I(\tau, \mu) = 0 \quad at \quad \tau = 0, \mu < 0 \qquad 2.3.6$$

After integration we have

$$I(\tau, \mu) = -\frac{1}{\mu} \int_0^{\tau} \frac{\sigma T^4(\tau')}{\pi} e^{-(\tau' - \tau)/\mu} d\tau' \qquad 2.3.7$$

for $\mu < 0$

We now find the net upward flux, F , defined as:

$$F(\tau) = \int_0^{2\pi} \left(\int_{-1}^{+1} I(\tau, \mu) \mu \, d\mu \right) d\phi \qquad 2.3.8$$

where ϕ is the azimuth angle. Now that $I(\tau, \mu)$ is known, integrations over τ, μ, and ϕ are needed to find F . Integration over the azimuth angle gives 2π , and we obtain, after simplification,

$$F(\tau) = \sigma T_g^4 \, 2\int_0^1 e^{-(\tau_g - \tau)/\mu} \mu \, d\mu$$

$$+ 2\int_0^1 \left(\int_\tau^{\tau_g} \sigma T^4(\tau') e^{-(\tau' - \tau)/\mu} d\tau' \right) d\mu$$

$$- 2\int_{-1}^0 \left(\int_0^\tau \sigma T^4(\tau') e^{-(\tau' - \tau)/\mu} d\tau' \right) d\mu \qquad 2.3.9$$

We use the above representation of the flux to find the heating rate, which is the negative divergence of F. Remembering that τ is a function of z, we write

$$Q_{rad} = -\frac{d}{dz} F(\tau(z)) \qquad 2.3.10$$

The integrations over τ and μ needed to find the flux, and the differentiation needed to find the heating rate, are best done numerically. These procedures will be taken up at a later time.

2.4 The Convective Region

Radiative processes in the model cause the formation of unstable lapse rates below about 5 km. Free convection occurs, taking heat from the earth and distributing it throughout the range of convection. This region extends from the surface of the earth, to a height z_t (which varies in time); above this height the temperature is radiatively determined. In this section, we will devise a model for finding

the convective heating, Q_{conv} , in the convective region.

When discussing turbulent convection, it is convenient to assume that the same type of equation that governs molecular transfer also applies to turbulent transfer. We write, for the atmospheric heat flux, H ,

$$H = -\rho c_p K_H \left(\frac{\partial T}{\partial z} + \Gamma \right) \qquad 2.4.1$$

where K_H is the vertical eddy diffusivity, and Γ , the dry adiabatic lapse rate (-9.8×10^{-5} °C/cm).

In our model convection is driven by unbalanced bouyancy forces which only occur under unstable conditions. Under stable conditions no free convection exists, hence

$$H = 0, \; K_H = 0 \quad for \quad \frac{\partial T}{\partial z} + \Gamma > 0 \qquad 2.4.2$$

(This also tells us that free convection can only transfer heat upwards).

For unstable conditions, the formulation of Priestly is used for K_H . We have,

$$K_H = h z^2 \left| \frac{g}{T} \left(\frac{\partial T}{\partial z} + \Gamma \right) \right|^{1/2}, \quad \frac{\partial T}{\partial z} + \Gamma < 0 \qquad 2.4.3$$

where h , a constant, is approximately 0.9.

Sundararajan and Macklin (1976) indicate that this free convection

formula does yield a reliable estimate of the heat flux in a stability range with Richardson numbers between -0.1 and -2.0. They compared three methods of computing the heat flux with observations of the flux from the 1968 Kansas surface layer data (Izumi, 1971). They found that the most accurate representation of the data was given by the free convection formula of Priestly.

Outside the convective region the heat flux is zero and there is no convective heating. In the convective region, Q_{conv} is obtained by taking the negative divergence of the heat flux:

$$Q_{conv} = -\frac{\partial}{\partial z}\left(-\rho c_p K_H \left(\frac{\partial T}{\partial z} + \Gamma\right)\right), \quad \frac{\partial T}{\partial z} + \Gamma < 0 \qquad 2.4.4$$

This expression for Q_{conv} leads to a second order differential equation for T and two boundary conditions are required.

The lower boundary of the convective region is very close to the surface of the earth, but not precisely at the surface. Even under the most turbulent conditions there is always a thin layer of air, which due to viscous and cohesive forces, adheres to the earth with great tenacity. In this laminar layer, the transport of heat (and moisture) takes place by molecular conduction and the gradients of temperature and humidity can be quite large.

For the lower boundary condition, we require that the heat fluxes match at the height of transition from molecular to turbulent transfer. Hence,

$$-\rho c_p K_H \left(\frac{\partial T}{\partial z} + \Gamma\right) = H_1 \quad \text{at} \quad z = z_{LL} \qquad 2.4.5$$

where z_{LL} is the thickness of the laminar layer (of order 1 cm, as we shall see) and H_1 is the heat flux through the layer.

An expression for H_1 and an estimate of z_{LL} are needed. Since the flux across the laminar layer is due only to molecular conduction, we expect it to depend on the temperature difference across the layer. Kraichnan (1962) made a theoretical study of heat transfer in fluids contained between two horizontal flat plates. This theory was applied by Gierasch and Goody (1968) to get an expression for the diffusive flux. (Although Gierasch and Goody were concerned with the Martian atmosphere, their expression is also valid for any atmosphere with appropriate values of parameters). The flux is proportional to the four-thirds power of the temperature difference, and is given by the formula:

$$H_1 \cong .089 \rho c_p K \left(\frac{g}{\bar{T} K \nu}\right)^{1/3} 2^{4/3} (T_g - \bar{T})^{4/3} \qquad 2.4.6$$

where ρ is the density of the air at the earth's surface, K is thermal diffusivity of air, ν the kinematic viscosity, and $\bar{T}$ the temperature at the top of the laminar layer. (For a heuristic derivation of the above equation, see appendix I).

Equation 2.4.6 has not been subject to direct experimental verification in the atmosphere, and it should only be relied upon to give approximate results.

By rearrangement of equation 2.4.6, the temperature junp across the laminar layer can be estimated. We have,

$$T_g - T \simeq \left(\frac{H_1}{.089 \rho c_p K \left(\frac{g}{\bar{T} K \nu} \right)^{1/3} \alpha^{4/3}} \right)^{3/4} \qquad 2.4.7$$

A rough guess is made for H_1 by taking it to be about 40% of the net average solar flux. (i.e. net solar flux $\sim \sigma T_e^4$, where T_e is the effetive temperature of the earth $\sim$ 251 °K). This estimate of H_1 applies specifically to a dry surface. Taking

$$H_1 \sim 10^5 \text{ ergs/(cm}^2\text{sec)} \qquad K \sim .22 \text{ cm}^2\text{/sec}$$

$$\rho \sim 10^{-3} \text{ g/cm}^3 \qquad \nu \sim .16 \text{ cm}^2\text{/sec}$$

$$c_p \sim 10^7 \text{ ergs/(g °K)} \qquad \bar{T} \sim 300° K$$

we have

$$T_g - \bar{T} \sim 17°$$

The thickness of the laminar layer can be estimated by considering the Rayleigh number, Ra , defined as

$$Ra \equiv \frac{g d^3 \Delta T}{K \nu \bar{T}}$$

where ΔT is the temperature difference across the distance d. At a

critical value of the Rayleigh number, Ra_c , which divides regimes of molecular and turbulent transfer, d corresponds roughly to the thickness of the laminar layer, and ΔT , to the temperature jump across the layer. Hence, solving for z_{LL} , we obtain:

$$z_{LL} \sim (Ra)^{1/3} \left(\frac{K\nu\bar{T}}{g\Delta T}\right)^{1/3} \text{ at } Ra = Ra_c \qquad 2.4.9$$

With $Ra_c \sim 10^3$, and using the estimate for ΔT given above, we obtain

$$z_{LL} \sim 1 \text{ cm}$$

The laminar layer is indeed thin, and the gradients of temperature and moisture can be quite large across it.

At the top of the convective region, the heat flux vanishes and therefore we take

$$\frac{\partial T}{\partial z} + \Gamma = 0 \qquad \text{at } z = z_t \qquad 2.4.10$$

as the upper boundary condition. This assumes that convection simply stops where $\frac{\partial T}{\partial z} + \Gamma = 0$. In reality, it is possible for some of the convective eddies to "overshoot" this level, and the temperature profiles above z_t will be influenced. In this thesis, we assume that the effect of convective overshoot is small, and we make no attempt to include it in the model.

The upper boundary condition does not prevent a temperature discontinuity between the radiative and convective regions. Yet observational evidence indicates that such discontinuities do not exist for reasons that we shall presently elucidate.

Let T_c and T_R be the temperatures infinitesimally below and above the level of transition between the radiative and convective zones. (For lack of a better word, we shall refer to this level as the "tropopause"). Above the tropopause, the convective heat flux disappears, and the temperatures are solely determined by the radiative flux. When equilibrium has been attained, these temperatures assume their radiative equilibrium values.

A positive discontinuity $(T_R - T_c > 0)$ is shown in figure 2.4.1a. As convection only carries heat upwards, the region just below the tropopause must be convectively heated, and for a stable discontinuity to exist, radiative cooling must take place in this region. However, this is not possible in a equilibrium situation. As T_c is less than its radiative equilibrium temperature (which we may safely take to be T_R, since T_c is just an infinitesimal distance below T_R), in actuality, radiative heating must occur. Hence a layer of stability will be formed, convection will cease, and the tropopause will drop until the discontinuity vanishes.

For a negative discontinuity $(T_R - T_c < 0)$ as depicted in figure 2.4.1b, molecular heat conduction will cause the formation of a shallow layer of great instability. Hence convection will result, and the tropopause will move up until the discontinuity is ironed out.

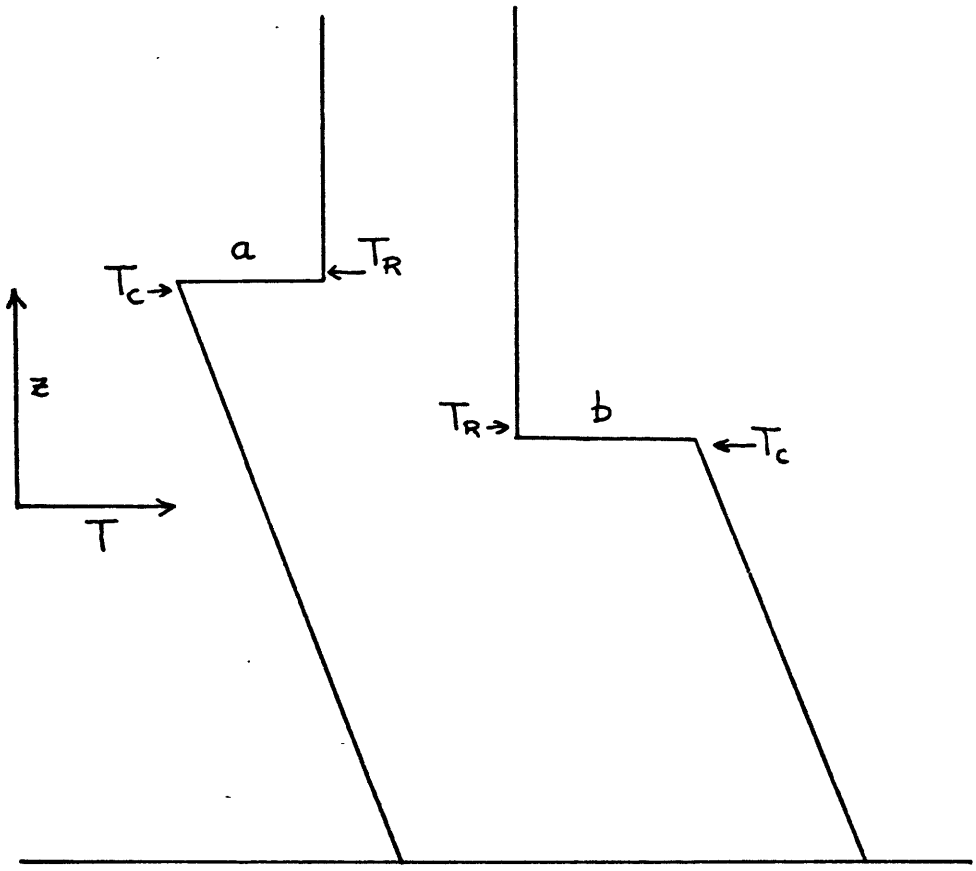

Figure 2.4.1. The profile labelled "a" shows a positive temperature discontinuity; "b" shows a negative temperature discontinuity.

Therefore, for the reasons stated above, we also require continuity of temperature at the upper boundary of the convective region,

2.5 Boundary Conditions

The boundary conditions for the convective region and the boundary conditions applied to the equation of radiative transfer have already been given. At the surface of the earth, the atmosphere and soil are coupled together via the surface energy balance equation,

$$H_s + F^- + S(t) - H_1 - \sigma T_g^4 - LW_1 = 0 \qquad 2.5.1$$

where $S(t)$ is the solar forcing function (written as $S(t)$ to explicitly show its time dependence), L the latent heat of condensation $(2.45 \times 10^{10} \frac{ergs}{g})$, and W_1, the net upward moisture flux from the surface. (Since we are assuming dry conditions for the calculations carried out in this chapter, W_1 is equal to zero.) F^- is the downward long-wave flux incident at the earth's surface, given by

$$F^- = 2\int_{-1}^{0} \left(\int_{0}^{\tau_g} \sigma T^4(\tau') \, e^{-(\tau'-\tau)/\mu} \, d\tau' \right) d\mu \qquad 2.5.2$$

In addition, continuity of temperature must also exist at the earth's surface, or

$$T_s\big|_{z=0} = T_g \qquad 2.5.3$$

In the soil, a no-flux boundary condition is specified below the depth of diurnal fluctuations, which we take to be 1 meter. Therefore

$$\frac{\partial T_s}{\partial z} = 0 \quad \text{at} \quad z \sim -1 \text{ meter} \qquad 2.5.4$$

It is easy to show that the diurnal temperature wave dies out well before reaching a depth of 1 meter. The skin thickness (d) of the temperature wave, associated with the time scale τ, is given by

$$d \sim (\tilde{\kappa}\tau)^{1/2}$$

where $\tilde{\kappa}$ is the thermal diffusivity of the soil ($\sim 2 \times 10^{-3} \frac{cm^2}{sec}$, see section 2.7). For diurnal fluctuations $\tau \sim$ 24 hours, and we have

$$d \sim 13 \text{ cm.}$$

For all practical purposes, the diurnal wave is completely attenuated at a depth of 4 skin thicknesses, and it is clear that our lower boundary condition is well below this level.

2.6 The Numerical Model

For the system of equations stated in the previous sections, it is very difficult, if not impossible, to find analytic solutions. Unfortunately, we must resort to numerical techniques. In this section, we develop the structure of the model, and then show how the equations can be solved numerically.

a. Structure of the Model

The vertical coordinate in our model is z, with the origin at the ground surface. There are 59 grid points for z; this divides the atmosphere into 58 layers. Some variables are calculated at the grid points, while others $(T, q, \rho, \ldots)$ are calculated between two z levels. With the subscript n as the index, figure 2.6.1 shows the indexing used for the model, and the variables to be calculated. (W, the vapor flux, and q, the specific humidity, are needed for the work presented in chapter 3). The layer n is between z_n and z_{n-1} and we regard T_n, $\rho_n, q_n, n \geq 2$, as the values of these variables at the point $\frac{z_n + z_{n-1}}{2}$. Vertical derivations of T (and q) are given by

$$\left.\frac{\partial A}{\partial z}\right|_n \approx \frac{A_n - A_{n-1}}{\delta_{n-1}} \qquad 2.6.1$$

where A is either T or q, and δ_n is the distance between the midpoints of layer n and layer $n-1$. For $n=1$, all variables are calculated at the surface.

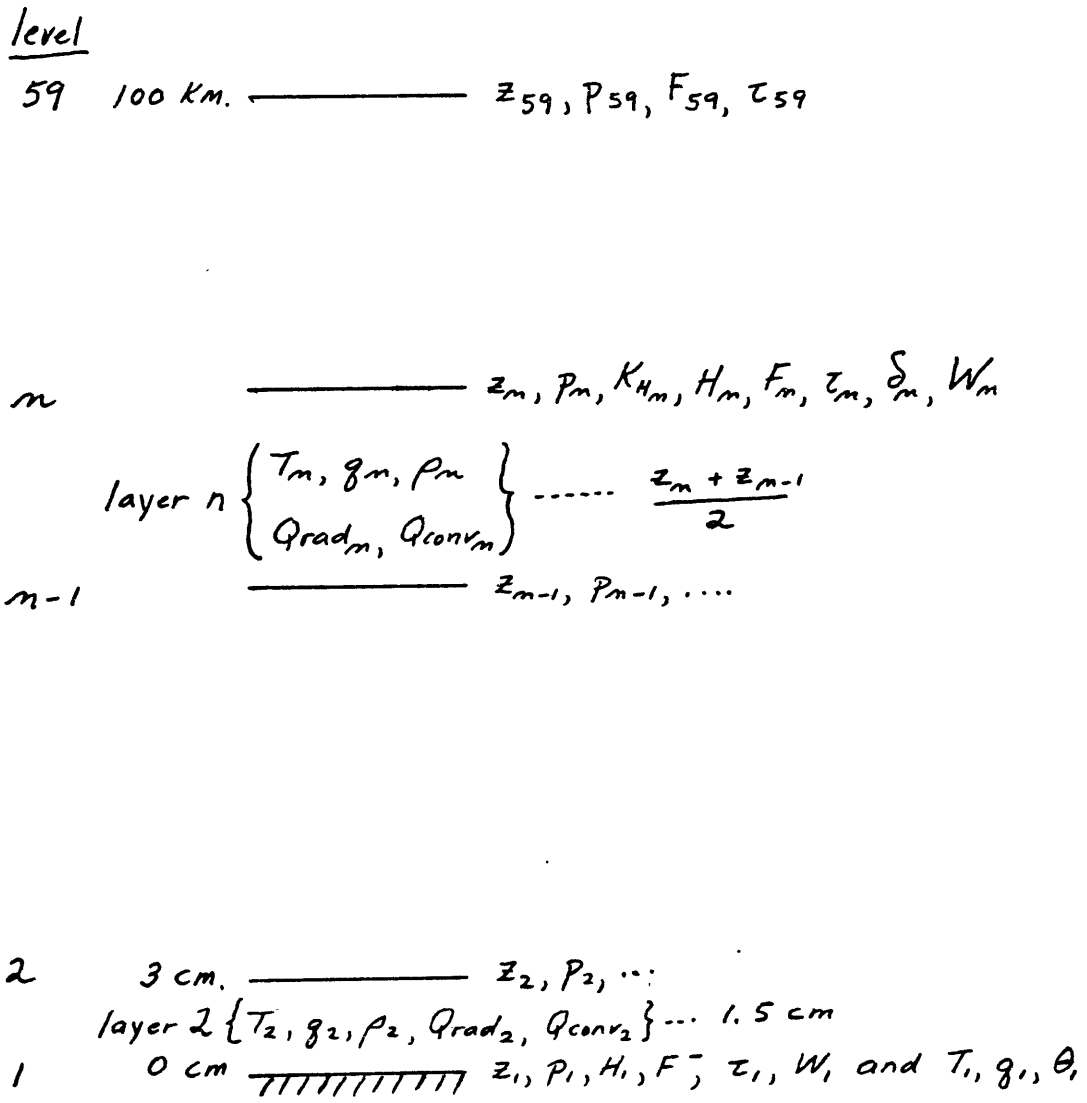

Figure 2.6.1. The coordinate system for the atmosphere. The layer "n", $n \geq 2$, is between the levels n and n-1.

The spacing of the grid points is designed to give accuracy where it is needed, while also attempting to minimize the amount of computation time. This is achieved by dividing the atmosphere into layers of variable thickness.

Near the earth's surface, the resolution is high, to pick up details of the diurnal boundary layer. Above this, moderate resolution is necessary to represent the convective region, and to accurately locate its upper boundary. A coarse resolution is satisfactory in the upper atmosphere $(z > 10\ km)$, as the temperature does not vary much with height or time.

The spacing of z levels is adopted with the above requirements in mind. z is prescribed as follows:

$$
\begin{aligned}
z_1 &= 0\ cm \\
z_2 &= 3\ cm \\
z_n &= 10^{.2(n+1)}\ cm, \quad 3 \le n \le 19 \\
z_n &= .25 \times 10^5 \cdot (n-19)\ cm, \quad 20 \le n \le 55 \\
z_{56} &= 9.5 \times 10^5\ cm \\
z_{57} &= 10.0 \times 10^5\ cm \\
z_{58} &= 16.0 \times 10^5\ cm \\
z_{59} &= 100.0 \times 10^5\ cm
\end{aligned}
$$

The values of z for all n are shown in Table 1.

As stated in section 2.2, the pressure and density are considered as functions of height only. Once they are calculated, they are known for all time. When finding these values, we need to choose a temperature profile which is close to the one to be calculated using the

Table 1

Values of z_n and the pressure, p_n, at each level "n". The density, ρ_n, is defined for the layer between the levels n and n-1.

n	z_n (cm)	p_n (mb)	$\rho_n \times 10^3$ (g/cm^3)
1	0.0	1000	-----
2	3.0	1000	1.16
3	6.3	1000	1.16
4	10.0	1000	1.16
5	16.	1000	1.16
6	25.	1000	1.16
7	40.	1000	1.16
8	63.	1000	1.16
9	100.	1000	1.16
10	158.	1000	1.16
11	251.	1000	1.16
12	398.	1000	1.16
13	631.	1000	1.16
14	1000.	999	1.16
15	1585.	998	1.16
16	2511.	997	1.16
17	3981.	996	1.16
18	6309.	993	1.16
19	10000.	989	1.15
20	$.25 \times 10^5$	972	1.14
21	$.5 \times 10^5$	944	1.13
22	$.75 \times 10^5$	917	1.10
23	1.0×10^5	891	1.08
24	1.25×10^5	865	1.06
25	1.5×10^5	840	1.04
26	1.75×10^5	815	1.01
27	2.00×10^5	791	.991
28	2.25×10^5	767	.970
29	2.50×10^5	743	.949
30	2.75×10^5	721	.928
31	3.0×10^5	698	.908
32	3.25×10^5	677	.888
33	3.5×10^5	655	.867
34	3.75×10^5	635	.848
35	4.0×10^5	614	.829

Table 1 (continued)

n	z_n	p_n	ρ_n
36	4.25×10^5	594	.810
37	4.5×10^5	575	.791
38	4.75×10^5	556	.773
39	5.0×10^5	538	.754
40	5.25×10^5	520	.736
41	5.5×10^5	502	.718
42	5.75×10^5	485	.701
43	6.0×10^5	468	.684
44	6.25×10^5	452	.667
45	6.50×10^5	436	.650
46	6.75×10^5	420	.633
47	7.0×10^5	405	.617
48	7.25×10^5	390	.601
49	7.50×10^5	376	.585
50	7.75×10^5	362	.570
51	8.0×10^5	349	.555
52	8.25×10^5	335	.566
53	8.50×10^5	321	.543
54	8.75×10^5	309	.522
55	9.0×10^5	296	.501
56	9.5×10^5	273	.471
57	10.00×10^5	252	.435
58	16.00×10^5	95	.267
59	100.00×10^5	10^{-4}	.011

heat equation. Our profile is:

$$T(z) = \begin{cases} 300^\circ - \Gamma z, & 0 \le z \le 8\ km \\ 210^\circ, & z > 8\ km \end{cases} \qquad 2.6.2$$

or, in other words, a constant lapse rate atmosphere ($\Gamma = 9.8^\circ C/km$) to 8 km; and above 8 km, and isothermal atmosphere with a temperature of 210°.

Using the hydrostatic equation and the equation of state, it is a very simple exercise to derive a pressure distribution for the profile specified above. (For example, see Hess (1959), chapter 6). We obtain:

$$p(z) = p_s \left(1 - \frac{\Gamma z}{300}\right)^{\frac{g}{R\Gamma}}, \quad 0 \le z \le 8\ km \qquad 2.6.3$$

$$p(z) = p_{8km} \exp\left[-\frac{g}{R}\left(\frac{z - 8\ km}{210}\right)\right], \quad z > 8\ km \qquad 2.6.4$$

where p_s is the surface pressure taken to be 1000 mb, and $p_{8\,km}$ the pressure at 8 km calculated by using equation 2.6.3.

Once p is known at all levels, the hydrostatic equation, cast in finite difference form, is used to find the density for each layer. We have

$$\rho_n = -\frac{1}{g}\left(\frac{P_n - P_{n-1}}{z_n - z_{n-1}}\right), \quad n \geq 2 \qquad 2.6.5$$

Table 1 shows the values of P and ρ used in the model. (Remember that ρ_n corresponds to the density of the layer just below z_n).

These density values depend upon the pressure, calculated from the assumed temperature profile (eq 2.6.2). However, the results of the model integration, presented in figure 2.8.3 indicate that the actual profile is more like

$$T(z) = \begin{cases} 290 - \Gamma z, & 0 \leq z \leq 7\,km \\ 215, & z > 7\,km \end{cases} \qquad 2.6.6$$

Fortunately, the difference between the "actual" profile and the assumed profile does not cause large errors in the density values. The density values can be re-calculated using the above profile and compared to the densities given in table 1. This procedure reveals that the errors are quite small. For example, for the layer between .75 and 1 km (layer #23), table 1 shows that the density equals $1.08\text{x}10^{-3}\ \frac{g}{cm^3}$. The "re-calculated" density is $1.12\text{x}10^{-3}\frac{g}{cm^3}$ giving an error of about 4%. Other errors are of this size or smaller.

In the ground, 22 grid points are used with the spacing very small near the earth's surface and increasing with depth. This is

acheived by using the coordinate transformation, $\zeta = \ln(1+z)$, with equal intervals in $\Delta\zeta$, of $\Delta\zeta = .227$. This value of $\Delta\zeta$ was chosen so that the first layer would have a thickness equal to $(2\tilde{\kappa}\Delta t)^{1/2}$, where $\tilde{\kappa}$ is the thermal diffusivity of the soil, and Δt, the time step. This is the minimum thickness necessary for the computational stability of an explicit difference scheme.

b. Numerical Methods

Starting with an initial temperature profile, a time marching scheme is used to find the equilibrium solutions to the atmospheric and soil heat equations. For the atmosphere, at each time step (denoted by the superscript j), the radiative temperature change, ΔT_{rad_m}, and the convective temperature change, ΔT_{c_m} are calculated for the layer $m, (m \geq 2)$. The new temperature is found by adding these changes to the old temperature:

$$T_m^{j+1} = T_m^j + \Delta T_{rad_m} + \Delta T_{c_m}, \quad m \geq 2 \qquad 2.6.7$$

(The temperature of the ground T_1^{j+1} is found by using the surface energy balance equation).

ΔT_{rad_m} is given by

$$\Delta T_{rad_m} = \frac{Q^j_{rad_m}}{\rho_m c_p} \Delta t \qquad 2.6.8$$

where $Q^{j}_{rad_m}$ is calculated from the finite-difference analogue of equation 2.3.10. In the numerical calculations, $Q^{j}_{rad_m}$ is a row matrix of 59 elements, and is determined by the matrix multiplication

$$Q^{j}_{rad_m} = \sum_{i=1}^{59} A_{mi} \cdot T_i^{j\,4}, \quad m = 1, 2, \ldots, 59 \qquad 2.6.9$$

("$Q^{j}_{rad_1}$" conveniently turns out to be the downward long wave flux at the surface, F^-). $[A_{mi}]$ is a square (59x59) matrix whose elements depend only on the distribution of the absorbing gas. $[T_i^{j\,4}]$ is a column matrix of length 59 whose elements are the fourth power of the temperatures at the time step j . The calculation of $[A_{mi}]$ is a lengthly algebraic exercise which is done in appendix II.

Equations 2.6.8 and 2.6.9, along with an equation to find the surface temperature,

$$\sigma T_1^{\,4} = F^- + SW$$

(where SW is the net incoming solar flux $\sim \sigma T_e^{\,4}$) can be incorporated in a time marching scheme to calculate a steady state radiative equilibrium profile for the atmosphere. If we assume that the distribution of τ is given by

$$\tau(z) = 4\, e^{-\frac{z}{2\,km}}$$

(i.e. see Goody (1964), pg. 333), we find the radiative equilibrium

profile shown in figure 2.6.2.

Also shown is a profile computed by using the Eddington approximation. We see that there is good agreement between both methods, particularly in the middle atmosphere, and the similarity of the two profiles allows us to conclude that our method has an accuracy comparable to the Eddington approximation. However, we must keep in mind that the response of the grey atmosphere to diurnal forcing may be significantly different from the real, non-grey case, particularly near the earth's surface; and, without resorting to lengthy calculations, we have no means of accurately determining this difference.

Finding the convective temperature change at each time step presents special computational problems. With K_H sometimes assuming values as high as 10^8 cm^2/sec, and with a maximum grid spacing of $.25 \times 10^5$ cm in the convective region, an explicit difference scheme exhibits computational instability unless the time step is made very small ($\Delta t \lesssim$ 3 sec). Such a small time step requires too much computer time, and it is necessary to employ an implicit scheme where the time step can be made much larger. Unfortunately, an implicit scheme results in a highly non-linear set of algebraic equations which reflect the non-linear character of equation 2.4.1. This set is difficult to solve.

One way out of this dilemma is to use a linearized implicit technique and we adopt a linearized centered-implicit (Crank-Nicolson) scheme to calculate the convective temperature change. This method requires a small time step ($\Delta t \sim$ 1 minute) for the linearization to be accurate, but the time step is not so small as to make the computation time excessively large. Appendix III gives the

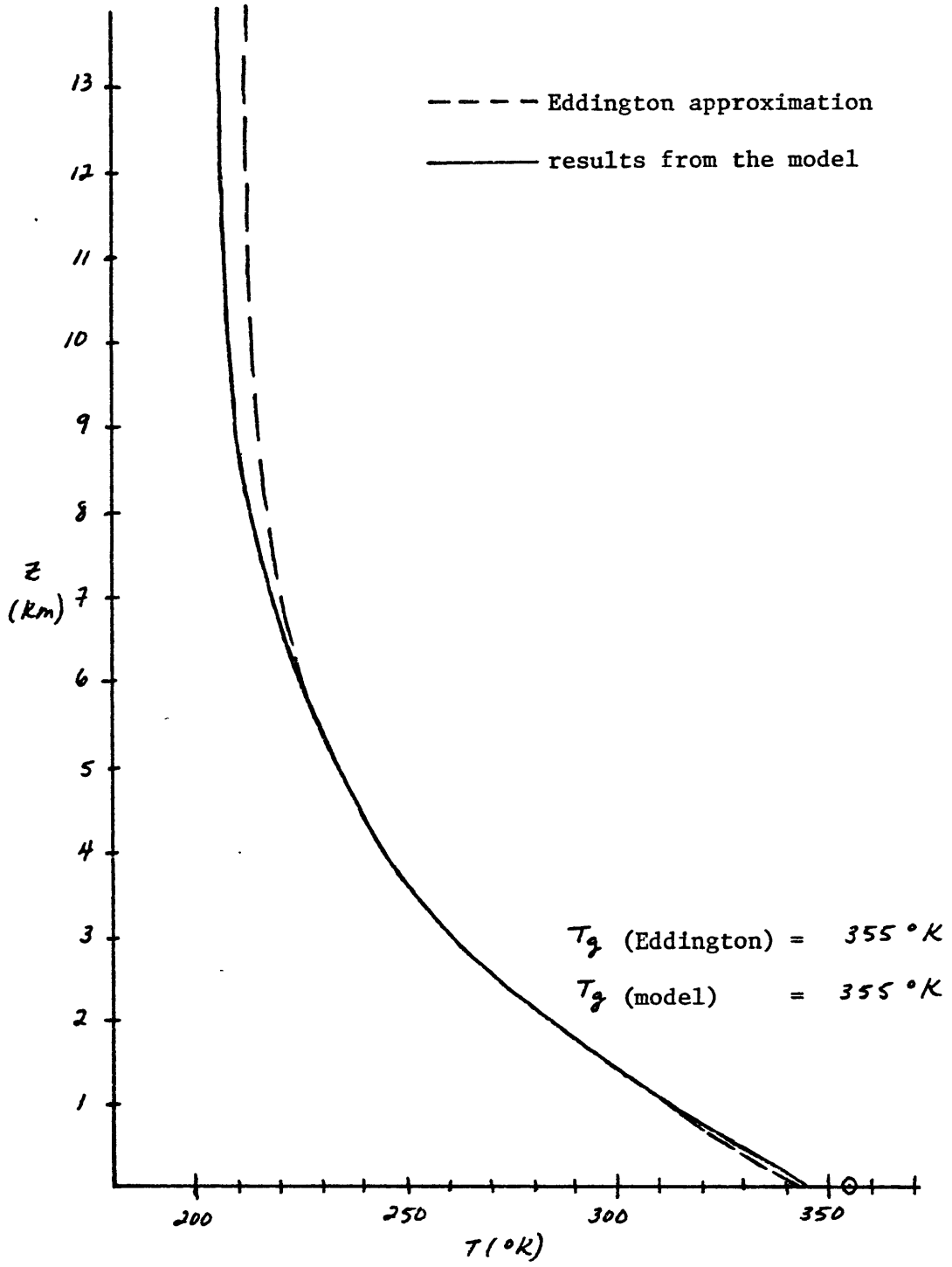

Figure 2.6.2. Radiative equilibrium profiles. The solid line is the profile calculated using the method presented in section 2.3; the dashed line is the profile calculated using the Eddington approximation. Between 1 km and 6 km the two profiles are indistinguishable.

details of this method as applied to the model.

To check the validity of the numerical technique persented above, a different scheme was devised for finding the convective temperature change. This scheme employed a "convective adjustment". For each time step, the radiative temperature change was calculated and added to the existing temperature profile , to give the new "radiative" temperatures, $T_{rad_m}^{j+1}$, $(m \geq 2)$. The new profile was checked to determine the extent of the convective region, and then the lapse rates and temperatures were adjusted to account for heat transport by free convection.

This adjustment method used an iterative scheme at each time step to find the new temperatures T_m^{j+1} in the convective region, the top of which has an indcx of $"\ell"$. These temperatures are found so that:

1) energy is conserved in each layer, or

$$\rho_m c_p (z_m - z_{m-1}) \left(T_m^{j+1} - T_{rad_m}^{j+1} \right) = \left(H_{m-1}^{j+1} - H_m^{j+1} \right) \cdot \Delta t \qquad 2.6.10$$

2) the surface energy balance is obeyed. (The ground temperature is calculated from this requirement).

3) the lapse rate at each level $"m"$ in the convective region, $\left(\frac{\partial T}{\partial z}\right)_m^{j+1}$, corresponds to the heat flux through the level m by the relationship:

$$H_m^{j+1} = \rho_m c_p h z_m^2 \left(\frac{g}{T_m^{j+1}} \right)^{1/2} \left| \left(\frac{\partial T}{\partial z} \right|_m^{j+1} + \Gamma \right|^{3/2} \qquad 2.6.11$$

which upon rearrangement yields,

$$\left(\frac{\partial T}{\partial z}\right)_m^{j+1} = -\Gamma - \left(\frac{H_m^{j+1}}{\rho_m c_p h z_m^2 \left(\frac{g}{T_m^{j+1}}\right)^{1/2}}\right)^{2/3} \qquad 2.6.12$$

If, after the iteration is complete, the increase in temperature of layer ℓ has made the lapse rate $\left(\frac{\partial T}{\partial z}\right)_\ell^{j+1}$ superadiabatic, we replace ℓ by $\ell+1$ and repeat the iteration.

The convective adjustment used a time step of 30 minutes, as opposed to the 15 second time step used in the Crank-Nicholson procedure. Both of these methods were used to find the diurnally forced equilibrium solution to the heat equation. The results were virtually identical, with maximum errors in temperature less than 1°K. This finding increases our confidence in the accuracy of the numerical techniques we have adopted.

The heat equation in the soil is solved using an explicit scheme. In explicit difference form the soil heat equation (eq 2.2.4) becomes:

$$C\left(\frac{T_{s_m}^{j+1} - T_{s_m}^{j}}{\Delta t}\right) = \frac{-H_{s_{m-1}}^{j} + H_{s_m}^{j}}{\Delta z_{s_m}} \qquad 2.6.13$$

with the soil heat flux given by

$$H_{s_m}^{j} = -K_g\left(\frac{-T_m^{j} + T_{m-1}^{j}}{\Delta z_{s_m}}\right) \qquad 2.6.14$$

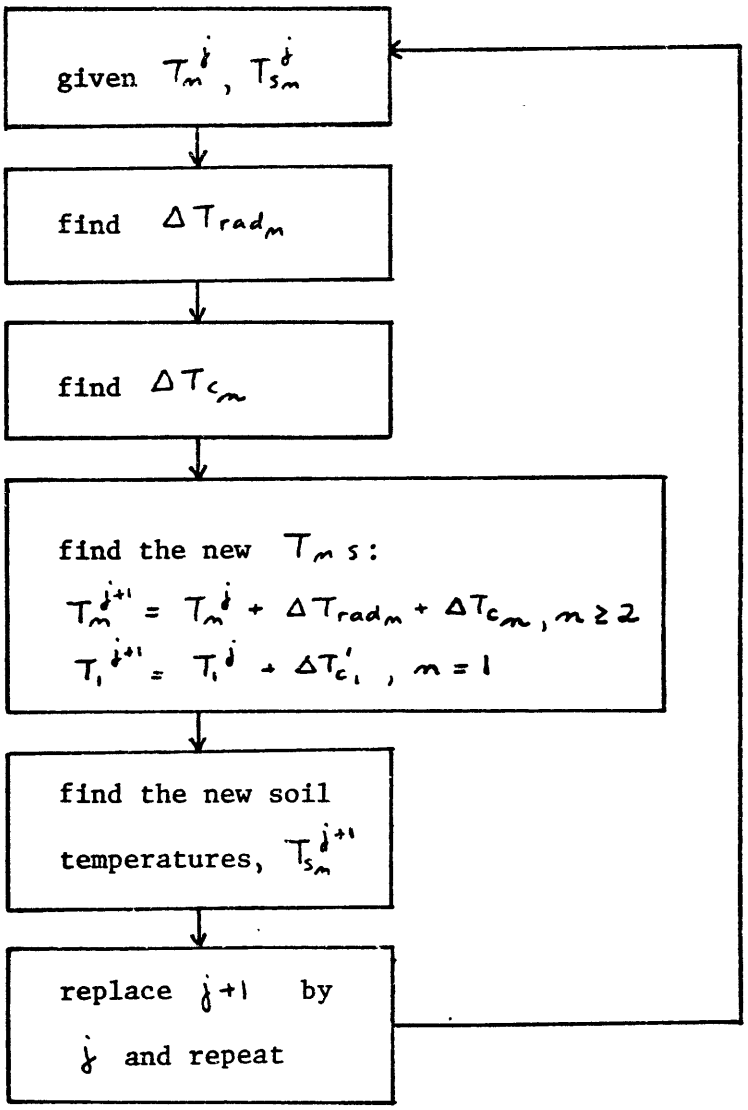

Figure 2.6.3. The computational procedure.

(Δz_{s_m} is the distance between the grid points m and $m-1$ in the soil).

The order of the calculations as performed by the computer at each time step is shown in figure 2.6.3. This procedure is repeated again and again until convergence is attained.

2.7 Description of the Calculation

Before doing any calculation, various parameters of the model must be specified. We choose an area of the earth where the model is most applicable; that is, where free convection is strong and advection weak on a diurnal scale. One area which roughly meets these requirements is the Sahel in West Africa - an arid strip of land paralleling the southern border of the Sahara desert, and lying between the latitudes of 15°N to 20°N. It is for this region that the parameters are defined.

The solar forcing function, $S(t)$, is expressed as:

$$S(t) = \begin{cases} S_o(1-\alpha)\varepsilon, & \varepsilon > 0 \\ 0, & \varepsilon < 0 \end{cases} \qquad 2.7.1$$

where S_o = solar constant (2 cal/cm^2 = 1.4×10^6 ergs/cm^{2}sec)

α = albedo

ε = cosine of the zenith angle

In terms of the latitude θ, the solar declination ϕ, and the earth's rotation rate Ω,

$$\varepsilon = \cos\theta\cos\phi\cos\Omega t + \sin\theta\sin\phi \qquad 2.7.2$$

where t is measured from local noon. For the Sahel, the soil is dry and light-colored, and the albedo is taken to have a relatively high value of $\sim$ 0.33. We specify θ as 18°N, and ϕ is 0° (i.e. the equinox).

The soil is assumed to be perfectly dry, and for its thermodynamic properties, we take:

$$C = 9.63 \times 10^{6} \text{ ergs/cm}^3 \text{ °K}$$

$$K_g = 2.09 \times 10^{4} \text{ ergs/cm sec °K}$$

$$\tilde{\kappa} = 2.17 \times 10^{-3} \text{ cm}^2\text{/sec}$$

These values are for a soil known as Yolo light clay, a soil found in California. It would be preferable to use soil parameters which are representative of the Sahelian region, but unfortunately we lack information as to the soil types of the region and their thermodynamic properties. (However, it is entirely possible that there is enough natural variation in soil properties over the region that the above specification would be as "representative" as any other).

A distribution of absorbing gas (water vapor) and a mass extinction coefficient are needed to compute the radiative heating rates. Newell (1972) presents maps showing the horizontal distribution of specific humidity over the Sahelian region at different pressure levels

and for different months. The vertical vapor content can be estimated by picking a point on the maps (we choose 18°N latitude, 0° longitude), and for each pressure level, averaging the value of q at this point over a year. This "averaged" value of q is then used to find the water vapor density, ρ_v, by using the relation $\rho_v = q\rho$. Table 2 shows the "annual averages" of these quantities at each pressure level. (Also shown is the height corresponding to each pressure level).

It is convenient to have an analytical expression for ρ_v as a function of z. After plotting ρ_v vrs. z, we see that a good expression for ρ_v is:

$$\rho_v = 9.0 \times 10^{-6} e^{-\frac{z}{1.55 \times 10^5 cm}} \qquad 2.7.3$$

The values of ρ_v calculated from Newell's data and the curve that we use to represent ρ_v are shown in figure 2.7.1. The curve fits the data fairly well.

To calculate radiative heating rates, a value is needed for the mass extinction coefficient, K_m. From a rearrangement of the definition of the optical depth (eq. 2.3.2), we obtain for K_m:

$$K_m = \frac{\tau^*}{\int_0^\infty \rho_v \, dz} = \frac{\tau^*}{M_v} \qquad 2.7.4$$

where τ^* is the total optical depth of the atmosphere and M_v is the total columnar mass associated with the value of τ^*. Given

Table 2

"Annual Average" of q and ρ_v over the point (18°N, 0°).

z(km)	p(mb)	q(g/kg)	ρ_v (g/cm^3)
0	1000	7.6	8.9×10^{-6}
1.4	850	3.5	3.7×10^{-6}
3.0	700	1.6	1.5×10^{-6}
5.5	500	.6	4.3×10^{-7}
7.1	400	.3	1.8×10^{-7}

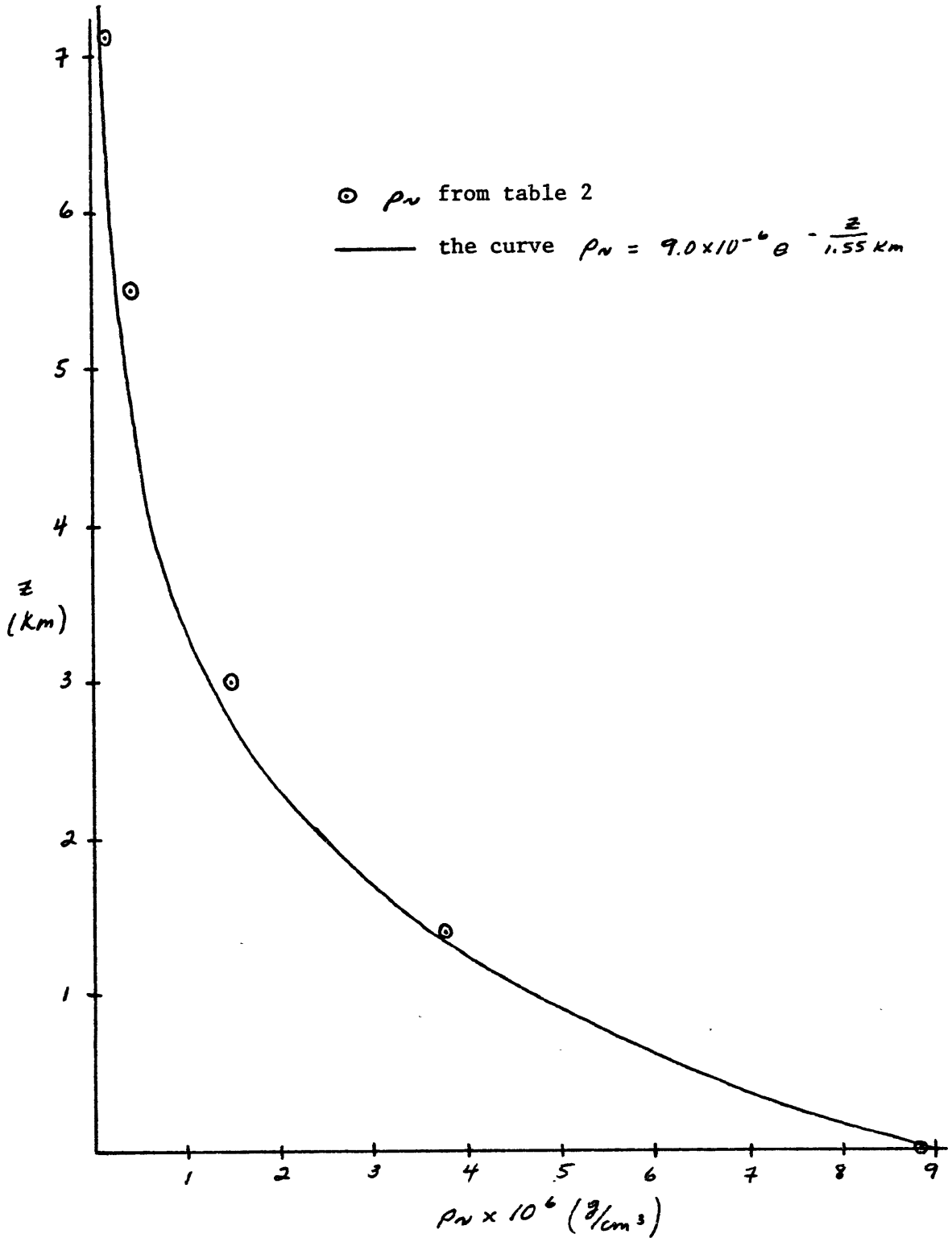

Figure 2.7.1. The density of water vapor ρ_v, as a function of height. The encircled dots are the values of the density from table 2; the solid line is the curve that is fit to these points.

approximate values for τ^* and M_v, this relationship can be used to estimate K_m.

Non-grey radiative equilibrium calculations done for mid-latitude conditions (Moller and Manabe, 1961) correspond closely below 10 km to a grey radiative equilibrium profile with $\tau^* = 4$. A value for M_v for mid-latitudes, say 35°N, can be estimated from the specific humidity data presented by Oort and Rasmusson (1971). (Table A6, page 47, gives year and seasonal values of the vertically averaged mean specific humidity $[\bar{q}]$ at different latitudes). The vertically averaged annual value of $[\bar{q}]$ at 35°N, which we denote by $\tilde{q}$, is 2.4 g/kg. $\tilde{q}$ is related to M_v by the expression

$$M_v = \frac{\Delta p}{g}\,\tilde{q} \qquad 2.7.5$$

With $\Delta p = 10^6 \frac{dynes}{cm^2}$, we obtain $M_v = 2.55$ g/cm^2. Using this value for M_v and with $\tau^* = 4$, we have for K_m:

$$K_m = \frac{4}{2.55 \frac{g}{cm^2}} = 1.57 \frac{cm^2}{g} \qquad 2.7.6$$

We must keep in mind that this value of K_m is chosen so that the grey radiative equilibrium profile simulates closely the non-grey profile below 10 km. However when using the grey approximation, radiative heating rates, for temperature perturbations away from radiative equilibrium, cannot be accurately determined for perturbations of all spatial scales.

To examine this point in greater detail, it is instructive to consider radiative relaxation times for sinusoidal perturbations imposed on the radiative equilibrium profile of a non-grey atmosphere. (This is discussed in Goody (1964), section 9.1). Given a sinusoidal disturbance with wavelength λ, there is only one value of the grey coefficient, which when used with the grey approximation to calculate heating rates, yields the "correct" relaxation time, i.e., the relaxation time associated with the scale of the disturbance in a non-grey atmosphere.

To illustrate this point, table 3 presents in column 6 appropriate values of the grey mass extinction coefficient K_m, for a wide range of perturbation wavelengths in a non-grey atmosphere with a distribution of water vapor as shown in figure 2.7.1. These values of K_m give the "correct" relaxation times for the scale lengths ($\frac{\lambda}{2\pi}$) shown in column 1. They were determined by first finding the effective volume absorbtion coefficient, $\tilde{K}_\nu$, shown in column 4. The effective coefficient is taken from figure 9.3 (pg 365) of Goody (1964), and therefore it takes into account the non-grey behavior of water vapor. (When calculating $\tilde{K}_\nu$, we used values for ρ_ν given in column 3. These are the average values of ρ_ν between the surface and a height $z = \frac{\lambda}{2\pi}$). Next, the grey volume coefficient $\bar{K}_\nu$, presented in column 5, is found. It is related to $\tilde{K}_\nu$ through the expression

$$\tilde{K}_\nu = \bar{K}_\nu \left(1 - \frac{\bar{K}_\nu}{m} \tan^{-1} \frac{m}{\bar{K}_\nu}\right) \qquad 2.7.7$$

Table 3

$\frac{\lambda}{2\pi}$	ν (cm^{-1})	ρ_ν (g/cm^3)	$\tilde{k}_\nu$ (cm^{-1})	$\bar{k}_\nu$ (cm^{-1})	k_m (cm^2/g)
1 cm	1	9×10^{-6}	1.92×10^{-3}	1.93×10^{-3}	214
10 cm	10^{-1}	9×10^{-6}	9.00×10^{-4}	9.13×10^{-4}	101
1 m	10^{-2}	9×10^{-6}	2.85×10^{-4}	2.99×10^{-4}	33.2
10 m	10^{-3}	9×10^{-6}	2.85×10^{-5}	2.99×10^{-5}	3.3
100 m	10^{-4}	8.7×10^{-6}	3.67×10^{-6}	3.90×10^{-6}	.45
1 km	10^{-5}	6.7×10^{-6}	5.32×10^{-7}	5.83×10^{-7}	.09
10 km	10^{-6}	1.4×10^{-6}	8.44×10^{-8}	9.88×10^{-8}	.07

where n is the wavenumber $\left(\frac{2\pi}{\lambda}\right)$. Finally the mass extinction coefficient is determined by dividing $\bar{K}_\nu$ by ρ_ν.

From the table we see that in order to accurately calculate relaxation times (or equivalently, heating rates) for a perturbation of 10 meters (approximately the scale of the diurnal boundary layer), a mass extinction coefficient of about 3.3 cm^2/g is appropriate. In contrast, a wavelength with a scale of 1 km, roughly the scale of the convective region, requires a mass extinction coefficient of .09 cm^2/g. If one of these values is chosen for our use, we sacrifice the accurate determination of the heating rates associated with the other important scale of our problem, and furthermore, we will be working from a radiative equilibrium profile which is far from realistic. The value of K_m that we have adopted (1.57 cm^2/g) appears to be a reasonable compromise. It gives accurate radiative relaxation times for an intermediate scale between the diurnal and convective scales and it also represents quite well the true non-grey radiative equilibrium temperature profile.

By substituting the expressions for ρ_ν and K_m into equation 2.3.2, it is possible to find the relationship between τ and z. We have

$$\tau(z) = \int_z^\infty 1.57 \frac{cm^2}{g} \left(9\times10^{-6}\frac{g}{cm^3}\right) e^{-\frac{z}{1.55\times10^5 cm}} dz \qquad 2.7.8$$

which when integrated yields

$$\tau(z) = 2.2\, e^{-\frac{z}{1.55\times10^5 cm}} \qquad 2.7.9$$

At $z = 0$, we have $\tau^* = 2.2$. The total optical depth for the arid Sahel, with its relatively small amount of atmospheric moisture, is much less than the optical depth of more humid areas of the earth.

For the calculations done in this chapter, we assume that the turbulent atmospheric motions do not alter the moisture distribution, and therefore the profile of τ is fixed for all time. In chapter 3, this condition will be relaxed.

2.8 Results

The calculation was carried out by starting with an initial condition very close to the actual solution. (The initial condition was determined by trial and error during the development of the model). The time step was 15 seconds. The temperatures were assumed to have reached their equilibrium values when the temperature differences between successive days were less than .03°K, or about 1° per month. As the initial profile was within 1°K of the final profile, and convergence took about 3 days, the e-folding time for convergence is about 1 day.

The ground temperature T_1 , the temperature at 1.5 cm T_2 , and the height of the convective region are shown in figure 2.8.1. The solar forcing S , and the heat flux through the laminar layer (H_1), are shown in figure 2.8.2. From these figures we see that the difference between the extremes in the ground temperature is about 50°K, and the maximum jump across the laminar layer (i.e., $T_1 - T_2$) is about 37°K and occurs at 1300 hours. This corresponds to a heat flux of about $3 \times 10^5 \frac{ergs}{cm^2 sec}$, or about $3/8$ the solar flux at that time.

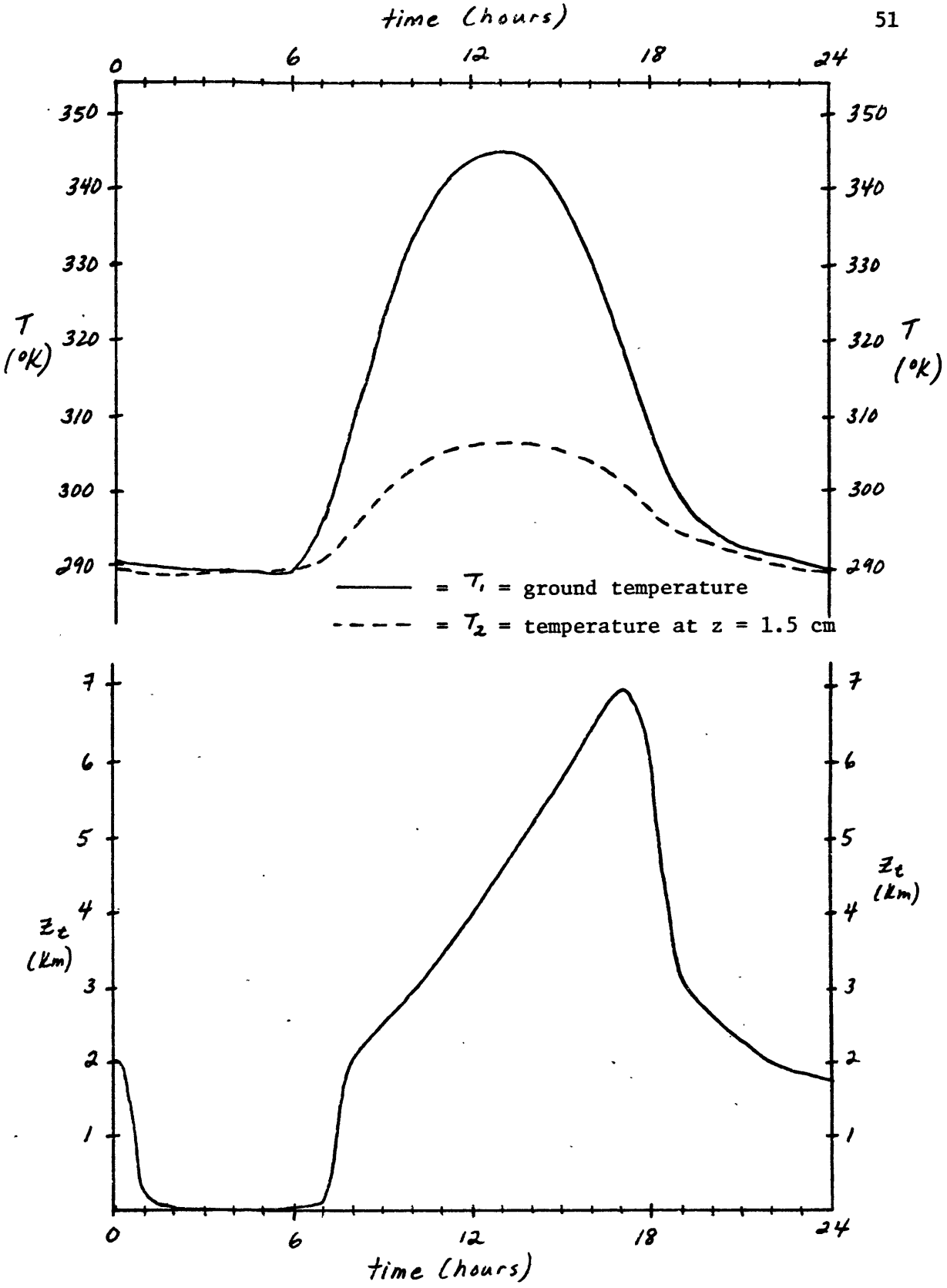

Figure 2.8.1. The lower graph is the height of the convective region z_t, as a function of time. The upper graph depicts the the ground temperature T_1, and the temperature at a height of 1.5 cm, T_2.

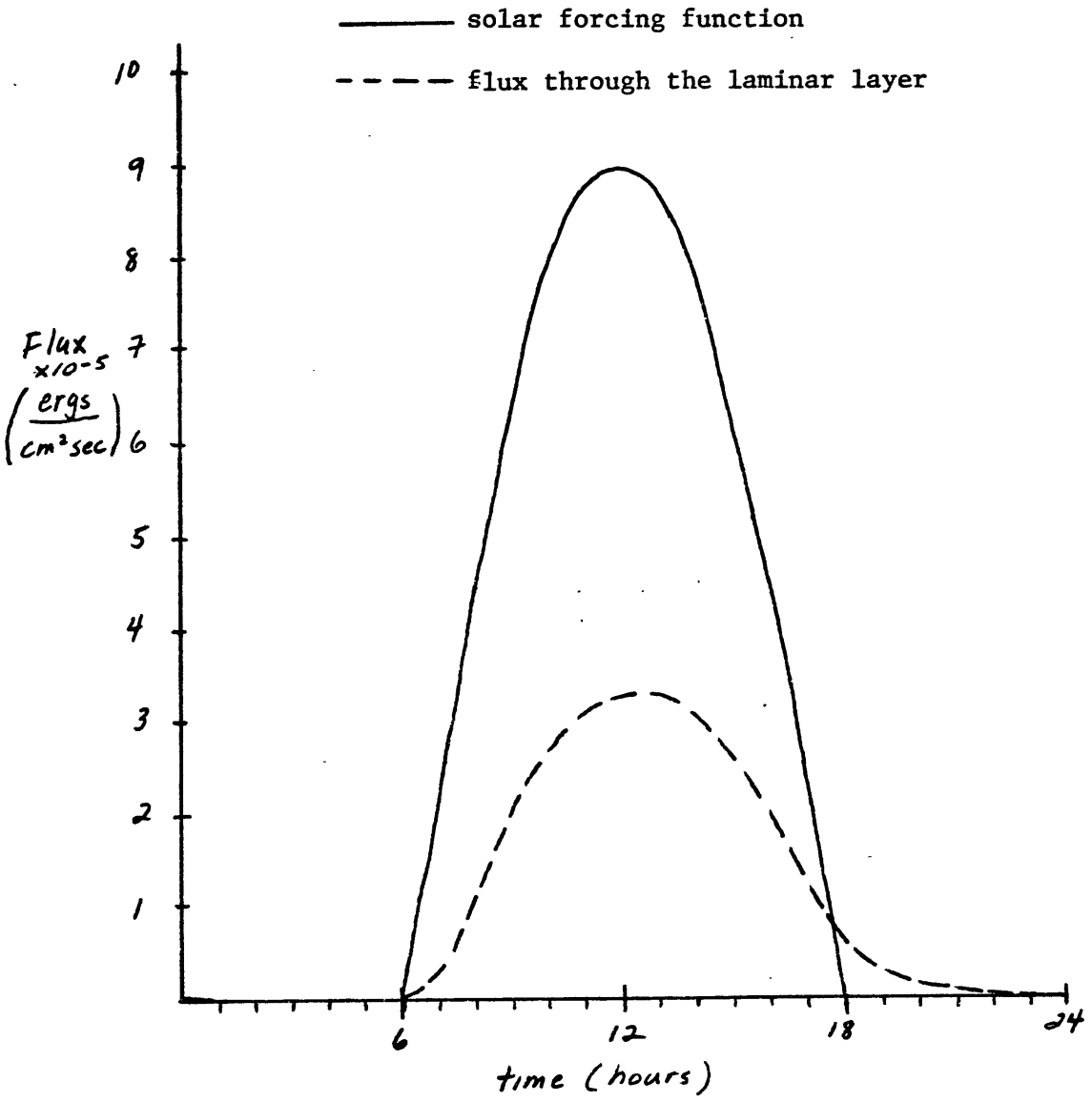

Figure 2.8.2. The solar forcing S is represented by the solid line; the flux through the laminar layer H_1 is represented by the dashed line.

It is interesting to note that the heat flux is not symmetric about 1200 hr. This is because during the morning and early afternoon hours, the soil near the earth's surface accepts energy, which is given back to the atmosphere, some in the form of sensible heat, during the late afternoon and throughout most of the night. In addition, the thermal inertial of the atmosphere contributes to the lag of the heat flux behind the solar forcing.

Figure 2.8.3 shows two temperature profiles - one at 0600 hr and the other at 1800 hr. These two profiles bracket the profiles observed at other times. During the day, convection extends to a maximum height of 7 km. Above this height, the temperature is essentially constant, while below 7 km the diurnal temperature changes range from less than 1°K at 5 km to about 3°K at 1 km.

Very close to the surface ($z < 10$ meters), there is a diurnal boundary layer where large diurnal temperature fluctuations take place. Figure 2.8.4 shows profiles below 7 meters for four different times during the day. The largest variations in temperature occur below 1 meter.

Within the framework of assumptions that have been made, the results seem physically reasonable. For the earth's atmosphere, the radiative time constant τ_{RAD}, is about 10^7 seconds, which is much greater than the diurnal time scale, 10^5 seconds. Hence, from a consideration of radiative processes alone, we expect that diurnal fluctuations in the atmosphere will be quite small, except very close to the ground ($z < 10$ meters in our model).

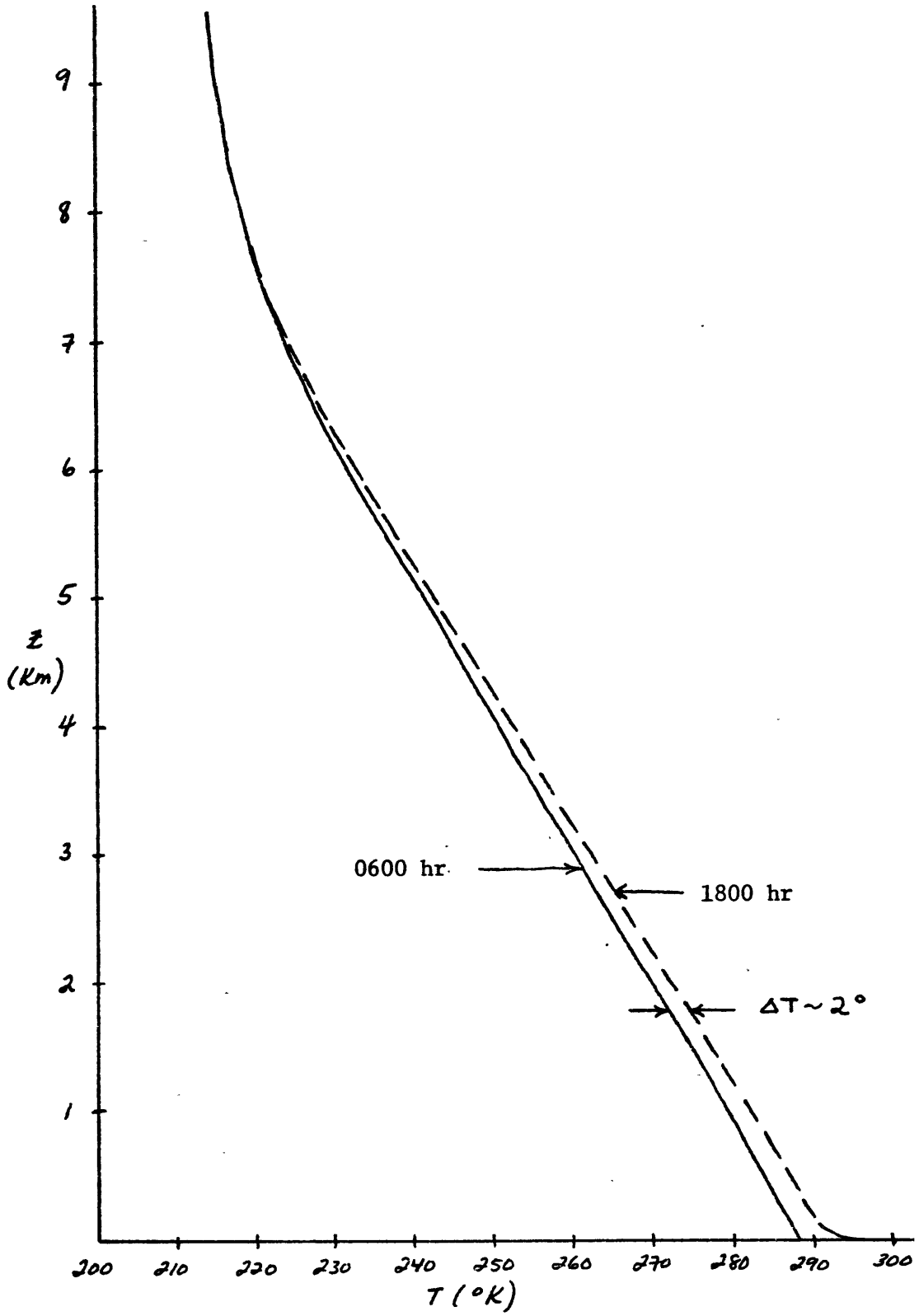

Figure 2.8.3. Atmospheric temperature profiles at 0600 hr and 1800 hr. These two profiles bracket the profiles observed at other times. The 0600 hr profile is the solid line; the dashed line is the 1800 hr profile.

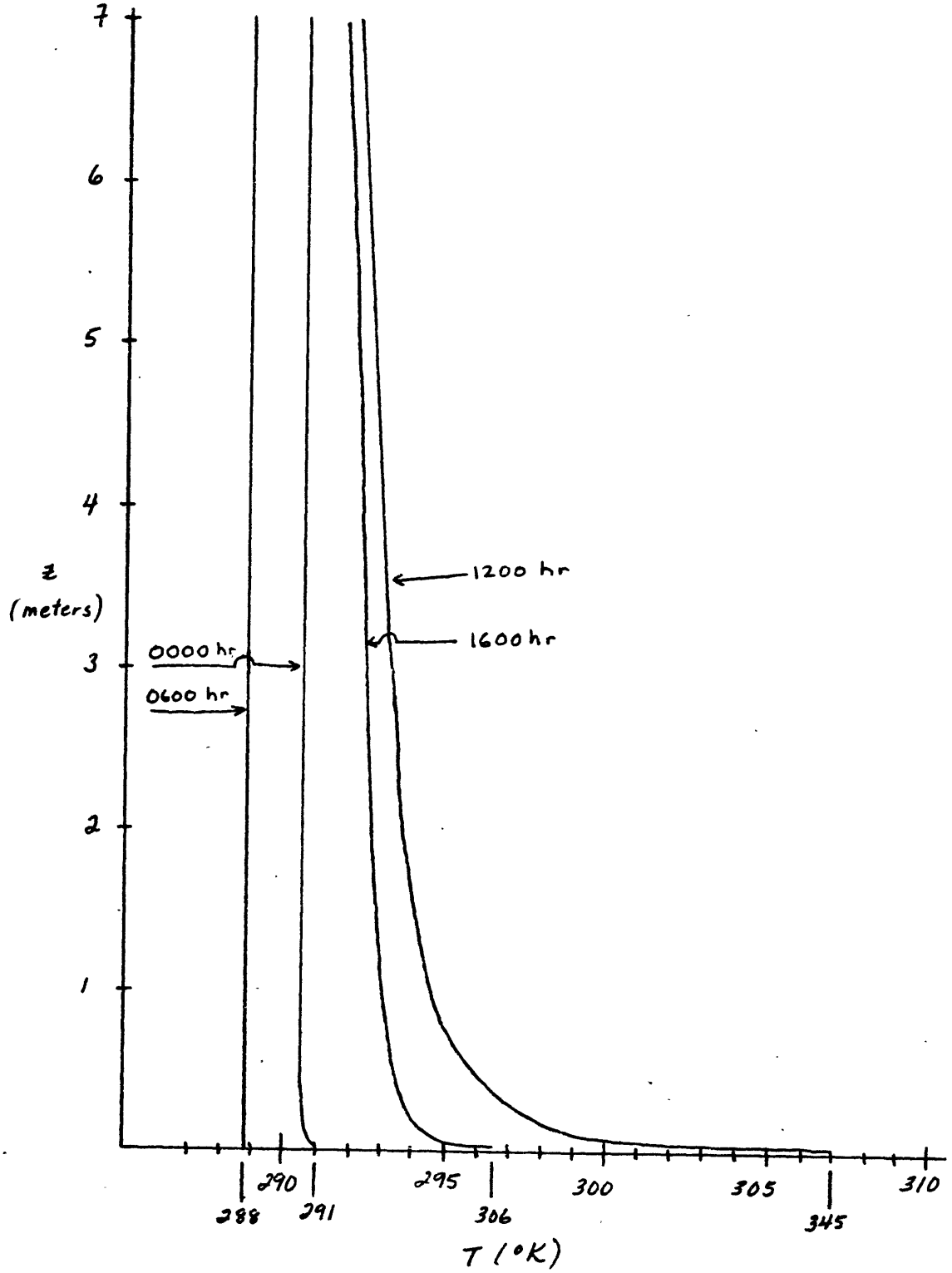

Figure 2.8.4. The temperature profiles below seven meters at four different times during the day. The tags below each curve are the ground temperatures.

As seen from figure 2.8.3, the daily temperature change in the convective region, above the diurnal boundary layer, is about 20°K. If we assume that all solar energy arriving at the earth during a 24 hour period goes into a uniform heating of the convective region, we can estimate an upper bound for the daily change in temperature above the diurnal layer. Denoting ΔT_{max} as this upper bound, we have

$$\Delta T_{max} \sim \frac{E_o}{\rho c_p z_t} \qquad 2.8.1$$

where

E_o = total solar heating = $\int_{24\ hours} S(t)\,dt$

$= \sim 2.5 \times 10^{10}\ \frac{ergs}{cm^2}$

$\rho \sim 10^{-3}\ g/cm^3$

$c_p \sim 10^7\ \frac{ergs}{g\ ^\circ K}$

$z_t \sim 5 \times 10^5\ cm$

With the above values we get

$$\Delta T_{max} \sim 5^\circ K$$

The actual temperature variation is less than ΔT_{max} but of the same order of magnitude. This result adds to the physical reasonableness of our results.

The convective time constant τ_c, is defined as

$$\tau_c \sim \left[\frac{g}{\theta}\frac{\partial\theta}{\partial z}\right]^{-1/2} \qquad 2.8.2$$

Using typical values from the model

$$\theta \sim 300\,^{\circ}K$$

$$\frac{\partial\theta}{\partial z} \sim .1 \times 10^{-5}\,^{\circ}K/cm$$

we have

$$\tau_c \sim 10^3 \text{ seconds}$$

This is much shorter than τ_{RAD} - therefore convective processes act much more quickly than radiative processes, and in our model, the temperature profile is convectively determined (below 7 km). This is shown vividly in figure 2.8.3 as the lapse rate of temperature departs very little from the dry adiabatic lapse rate during the entire day.

The model seems to faithfully represent the physics that has been built into it. However, there are some differences between what the model predicts and what actually occurs in an arid region, particularly in the diurnal boundary layer. In the model, daily temperature fluctuations in the diurnal layer seem too small; the difference between temperature extremes at 2 meters (a height where a thermometer is likely to be hung!) is only 5°K. Surface synoptic observations for a desert region show diurnal changes which are much larger than

this, and also, these changes are not uncommonly associated with temperature inversions during the night. Our model predicts no inversion, which may account for the small temperature change.

The poor results in the diurnal layer may be due to the use of the grey raidation approximation. In this layer the important scales of radiative transfer are less than 10 meters. As our mass extinction coefficient corresponds to a radiative scale between 10 and 100 meters (as discussed in 2.7), some error in the computation of heating rates will occur; these errors could contribute to the poor simulation of daily temperature fluctuations in the diurnal layer.

III. The Model with Moisture

3.1 Introduction

In the previous chapter, we considered a model that did not explicitly contain any moisture. In this chapter, additions are made to the model to allow moisture transfer in a coupled system consisting of both the soil and the atmosphere.

The mere inclusion of moisture has the potential to significantly affect the atmosphere in many ways. Soil water affects the atmosphere by its influence on the surface energy balance (as stated by the surface energy balance equation). The soil heat flux depends upon the thermodynamic properties of the soil which are functions of the soil moisture content. Soil water can evaporate and become atmospheric moisture and the resulting latent heat flux can greatly alter the surface energy balance. The thermodynamic consequences of atmospheric moisture are well known and include the role of vapor as an absorber of radiant energy, the latent heat released by the condensation of water, the albedo effect of clouds, etc.

In this chapter we ignore clouds and the processes that are involved in their genesis, such as condensation. Hence to maintain realism in the results, the integrations are stopped when significant condensation occurs. Furthermore, the action of vegetation, which can influence moisture transfer across the air-soil boundary (and other aspects of the surface energy balance), is ignored.

3.2 Equations of Moisture and Heat Transfer in the Soil

Moisture transfer in the soil occurs in both the liquid and vapor phases. Transport in the liquid phase is caused mainly by the action of capillary forces and gravity, while vapor transfer takes place primarily by molecular diffusion down gradients of specific humidity. In addition, during the course of moisture transfer, evaporation and condensation occur within the soil, thereby influencing the soil heat flux. Equations have been derived that govern these processes, and what follows is a brief outline of the derivation. For a more detailed account, the interested reader is referred to the papers of Philip (1957) and Philip and de Vries (1957).

The basic equation for flow in porous media, including soils, is Darcy's law:

$$\overline{W}_s = -\rho_\ell \bar{\bar{K}}_w \cdot \nabla \Phi \qquad 3.2.1$$

where $\overline{W}_s$ is the vector moisture flux ($\frac{g}{cm^2\ sec}$), ρ_ℓ the density of liquid water (1 g/cm^3), $\bar{\bar{K}}_w$ the hydraulic conductivity tensor (cm/sec), and Φ the total potential (cm). As we are only concerned with flow in the vertical direction in isotropic media, equation 3.2.1 becomes

$$W_s = -\rho_\ell K_w \frac{\partial \Phi}{\partial z} \qquad 3.2.2$$

Equation 3.2.2 holds for both "saturated" and "unsaturated" flow. Unsaturated flow, with which we are concerned, takes place when the

pore spaces between the soil particles are not completely filled with water. In this case K_w and Φ are strong functions of the volumetric moisture content, θ . (θ is the volume of water per unit volume of bulk soil). Figure 3.2.1 shows the relationship between K_w and θ for Yolo light clay.

The total potential Φ is comprised of a capillary potential ψ, and a gravitational component z , the height above some datum level. We have

$$\Phi(\theta) = \psi(\theta) + z \qquad 3.2.3$$

We may define ψ as the energy required to pull a unit mass of water from an unsaturated soil. Since this definition calls for the expenditure of energy to overcome capillary forces, ψ is negative. It is conveniently expressed as a length, somewhat analogous to the concept of "head" in hydraulics. Figure 3.2.1 shows the relationship between ψ and θ . We see that as θ decreases, ψ becomes more negative. This reflects the fact that as the soil becomes drier, the surface-volume ratio of intersticial water increases with a consequent increase in capillary forces (per unit mass). (For a more complete explanation of ψ , see Kirkham and Powers, (1972)).

When the expression for Φ is substituted into equation 3.2.2, we obtain

$$W_s = -\rho_\ell \left(K_w \frac{\partial \psi}{\partial z} + K_w \right) \qquad 3.2.4$$

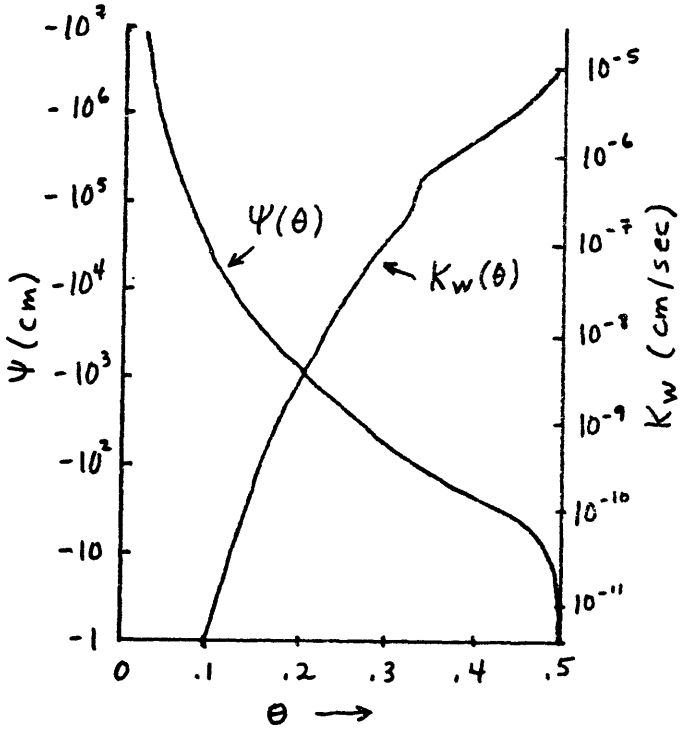

Figure 3.2.1. The capillary potential Ψ , and the hydraulic conductivity K_w , plotted against the volumetric moisture content, θ .

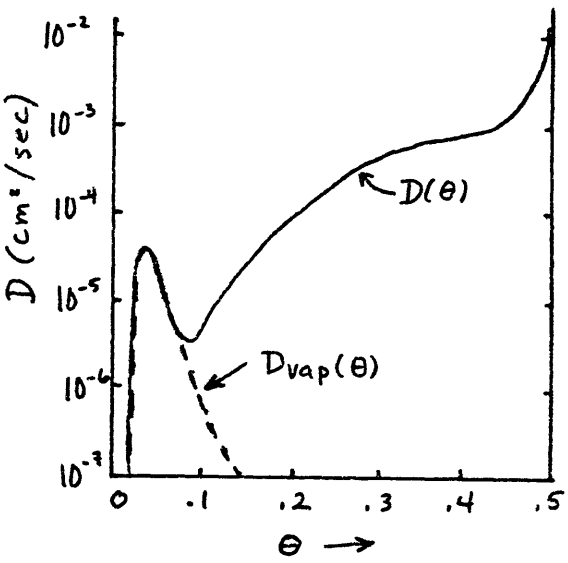

Figure 3.2.2. The moisture diffusivity $D(\theta)$, and the vapor moisture diffusivity $D_{vap}(\theta)$, plotted against the volumetric moisture content, θ .

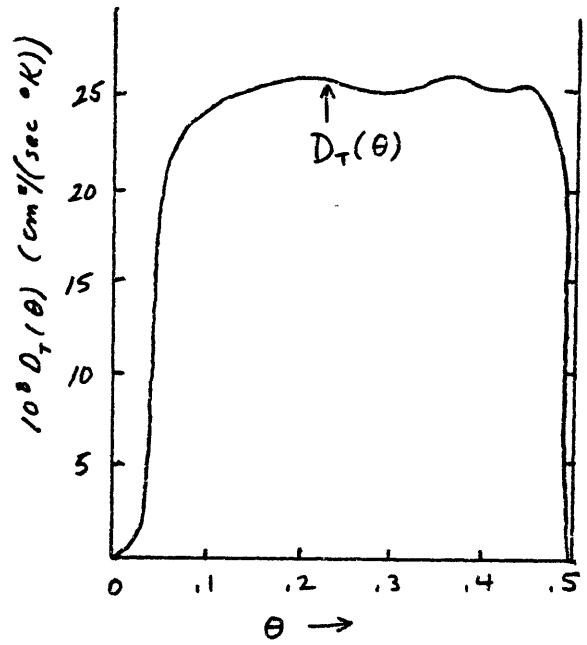

Figure 3.2.3. Thermal moisture diffusivity $D_T(\theta)$, plotted against θ .

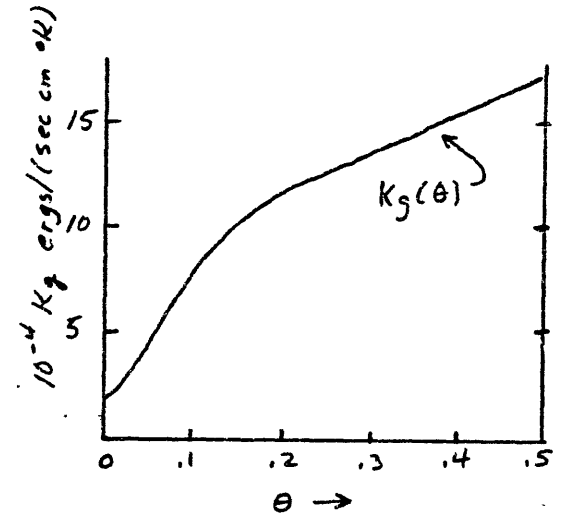

Figure 3.2.4. Thermal conductivity as a function of θ .

With the definition

$$D(\theta) \equiv K_w \frac{d\psi}{d\theta} \qquad 3.2.5$$

equation 3.2.4 becomes

$$W_s = -\rho_\ell \left(D(\theta) \frac{\partial \theta}{\partial z} + K_w \right) \qquad 3.2.6$$

The quantity $D(\theta)$ is called the "moisture diffusivity" with dimensions of $^{cm^2}/_{sec}$. Figure 3.2.2 is a graph of $D(\theta)$ for Yolo light clay. The hump on the curve centered about θ equal to .04 is due to moisture transfer in the vapor phase down gradients of moisture. This mechanism becomes important under dry conditions.

Equation 3.2.6 is valid only for isothermal systems as thermal gradients in the soil can also induce moisture movement. To include this effect, it is necessary to add a term

$$-\rho_\ell D_T(\theta) \frac{\partial T_s}{\partial z} \qquad 3.2.7$$

to the right hand side of equation 3.2.6. $D_T(\theta)$ is called the "thermal moisture diffusivity" with units of $\frac{cm^2}{sec\ ^\circ K}$. It is also a function of θ and is plotted in Figure 3.2.3.

We now have for the moisture flux

$$W_s = -\rho_\ell \left(D(\theta) \frac{\partial \theta}{\partial z} + K_w + D_T(\theta) \frac{\partial T_s}{\partial z} \right) \qquad 3.2.8$$

By combining the above equation with the requirement of continuity

$$\rho_\ell \frac{\partial \theta}{\partial t} = - \frac{\partial}{\partial z} W_s \qquad 3.2.9$$

we obtain

$$\frac{\partial \theta}{\partial t} = \frac{\partial}{\partial z} \left(D(\theta) \frac{\partial \theta}{\partial z} + K_w(\theta) + D_T(\theta) \frac{\partial T_s}{\partial z} \right) \qquad 3.2.10$$

This equation governs the transport of moisture in unsaturated soils. The boundary conditions associated with this equation will be stated later.

The existence of moisture in the soil requires the modification of the expression for the soil heat flux. Both temperature and moisture gradients can cause "distillation" effects. That is, heat energy can be transfered by the evaporation and condensation of water within the soil. With this effect in mind the heat flux is:

$$H_s = - K_g(\theta) \frac{\partial T_s}{\partial z} - \rho_\ell L D_{vap}(\theta) \frac{\partial \theta}{\partial z} \qquad 3.2.11$$

The thermal distillation effect is incorporated in the functional form of the thermal conductivity, K_g . (K_g is graphed in Figure 3.2.4). The second term on the right hand side of equation 3.2.11 represents the distillation effect induced by moisture gradients. $D_{vap}(\theta)$ is called the "isothermal vapor diffusivity" and it is shown in Figure 3.2.3. Since $D_{vap}(\theta)$ is very small, this term is usually not important unless $\frac{\partial \theta}{\partial z}$ is very large. In our calculations, it contributes only about 2% to the soil heat flux.

With the new expression for H_s , the soil heat equation becomes:

$$C(\theta)\frac{\partial T_s}{\partial t} = -\frac{\partial}{\partial z}\left(-k_g(\theta)\frac{\partial T_s}{\partial z} - \rho_l L D_{vap}(\theta)\frac{\partial \theta}{\partial z}\right) \qquad 3.2.12$$

where $C(\theta)$, the volumetric heat capacity, is given by:

$$C(\theta) = (.23 + \theta) \times 4.187 \times 10^7 \ \frac{ergs}{cm^3\ ^oK} \qquad 3.2.13$$

Equations 3.2.10 and 3.2.12 govern the simultaneous moisture and heat fields in the soil.

3.3 Moisture Transfer in the Atmosphere

As in the case with heat transfer, it is convenient to assume that the equation governing moisture transfer by turbulent eddies has the same form as a diffusion equation. For the moisture flux we have,

$$W = -\rho K_w \frac{\partial q}{\partial z} \qquad 3.3.1$$

where K_w is the eddy moisture diffusivity. As the same physical mechanism (turbulence) transfers both heat and moisture, K_w is taken to be the same as K_H .

The rate of change of the atmospheric specific humidity is found by taking the negative divergence of the moisture flux:

$$\rho \frac{\partial q}{\partial t} = -\frac{\partial}{\partial z}\left(-\rho K_H \frac{\partial q}{\partial z}\right) \qquad 3.3.2$$

Two boundary conditions are required for equation 3.3.2 which are analogous to the two needed for determining the convective heating (equation 2.4.4).

At the bottom of the convective region, moisture is transfered via molecular conduction across the laminar layer, and we have

$$-\rho K_H \frac{\partial q}{\partial z} = W_1 \quad \text{at} \quad z = z_{LL} \qquad 3.3.3$$

where W_1 is the moisture flux through the laminar layer, given by

$$W_1 = .089\, 2^{\frac{4}{3}} \rho D_m \left(\frac{g}{T_2 K \nu}\right)^{1/3} (T_1 - T_2)^{1/3} (q_1 - q_2) \qquad 3.3.4$$

q_2 is the value of the specific humidity at the top of the laminar layer. D_m , the diffusivity of vapor in air, has a value of about .25 $\frac{cm^2}{sec}$. (Equation 3.3.4 is derived heuristically in appendix I and is analogous to Kraichnan's expression for the heat flux).

At the top of the convective region, turbulence ceases, and we have

$$-\rho K_H \frac{\partial q}{\partial z} = 0 \quad \text{at} \quad z = z_t \qquad 3.3.5$$

Since K_H is equal to zero at $z = z_t$, it is not necessary for the gradient of q to be zero.

To allow interchange of moisture between the atmosphere and soil, the equation governing moisture transfer in the atmosphere and the soil must be coupled together in a physical manner.

First, fluxes at the surface must balance in accordance with the surface energy balance equation (eq. 2.5.1). For the calculations in this chapter the term LW_1, is not neglected.

Second, continuity of the moisture flux is required at the earth-atmosphere interface. We have

$$W_a = W_s \quad \text{at} \quad z = 0 \qquad 3.3.6$$

where W_a is the atmospheric moisture flux at the surface. For the calculations carried out in this chapter, W_a is identical to the flux through the laminar layer, W_1.

The final condition, applied at the soil surface, states that the liquid soil water must be in thermodynamic equilibrium with the atmospheric water vapor. At a given temperature, the vapor pressure in the soil is less than that over a plane surface of water. This is because the water molecules, besides being attracted to themselves, are also attracted to the soil by cohesive (i.e. capillary) forces. A measure of this attraction is the capillary potential ψ. By associating $g\psi$ with the specific Gibbs function for the soil water, it is possible to derive an expression for the relative humidity in terms of the volumetric moisture content. We have

$$r = e^{\frac{g\psi(\theta)}{R_w T}} \qquad 3.3.7$$

where r is the relative humidity (relative to a plane surface of water), and R_w the gas constant for water vapor $(4.615 \times 10^6 \frac{ergs}{g\ ^\circ K})$. (In the above expression we have written ψ as $\psi(\theta)$ to explicitly show its dependence upon θ). The above equation is analogous to Kelvin's law for raindrops and it is derived in a similar manner. (For example, see Businger and Fleagle (1963), pg. 81). Figure 3.4.1 shows r as a function of θ for a temperature of 300°K. (As r is not highly sensitive to changes in T , graphs for other values of T would be similar). Above a moisture content of .1, the soil presents to the atmosphere a surface, which in effect, acts as if it is saturated.

For our calculations, it is necessary to have an expression for the surface specific humidity. q_1 can be written as

$$q_1 = \epsilon \frac{e}{P_s} \qquad 3.3.8$$

where ϵ is a constant (.622) and e is the vapor pressure, given by the relation

$$e = r e_s \qquad 3.3.9$$

r , of course, is found from equation 3.3.7. e_s is the saturation

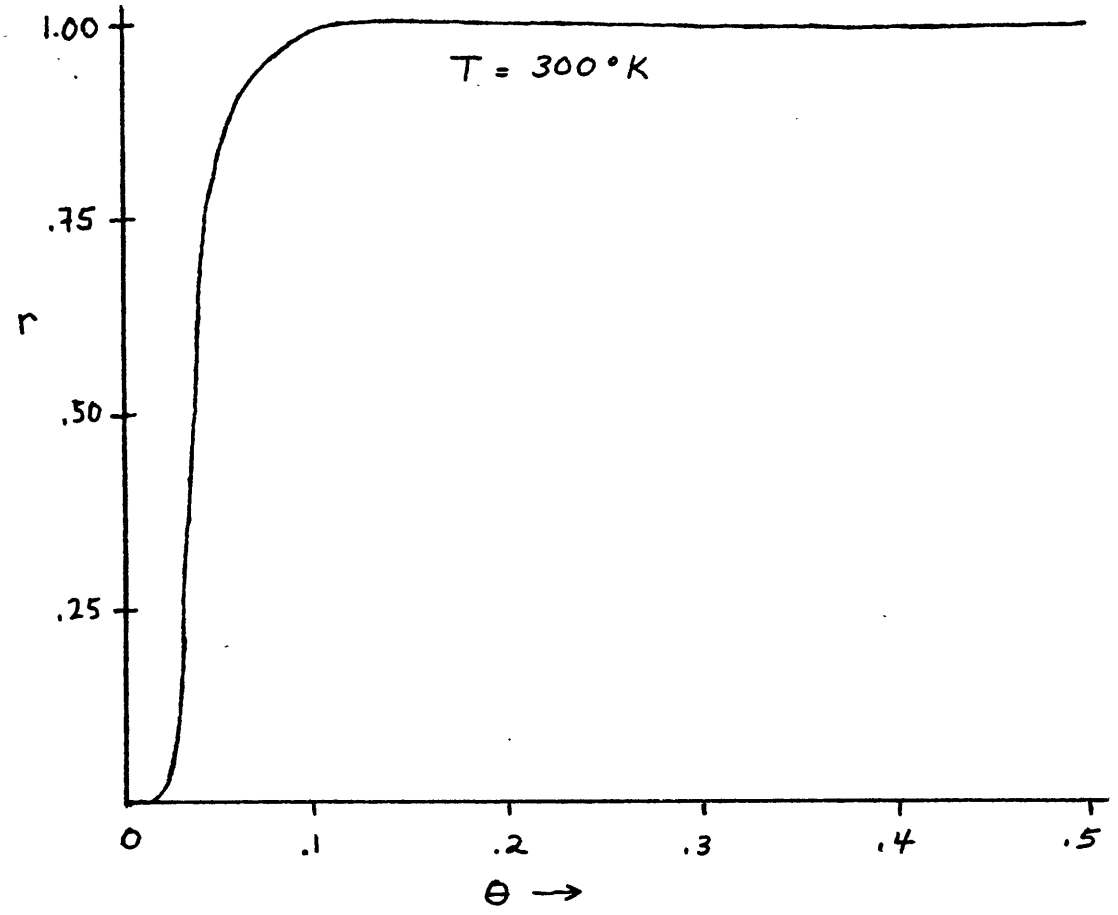

Figure 3.4.1. Relative humidity r, plotted against the volumetric moisture content θ, for a temperature of 300°K. Above $\theta = .1$, the relative humidity has a value of 100%.

vapor pressure, expressed as a function of T by the Clausius-Claperyon equation,

$$e_s = 6.11mb \cdot e^{\frac{L}{R_w}\left(\frac{1}{273} - \frac{1}{T}\right)} \qquad 3.3.10$$

By combining the above three equations and our expression for r (eq 3.3.7), we obtain for q_1

$$q_1(\theta, T) = \frac{\epsilon}{p_s} e^{\frac{g\psi(\theta)}{R_w T}} \cdot 6.11mb \cdot e^{\frac{L}{R_w}\left(\frac{1}{273} - \frac{1}{T}\right)} \qquad 3.3.11$$

q_1 is both a function of the volumetric moisture content and the surface temperature.

3.4 Numerical Procedures

In chapter 2, we found the new atmospheric temperatures T_m^{j+1}, and the new soil temperatures, $T_{s_m}^{j+1}$, at each time step. When moisture is added to the calculations, it is also necessary to find the specific humidity q_m^{j+1}, the optical depth at each level τ_m^{j+1}; and in the soil, the moisture content, θ_m^{j+1}. To calculate these five variables the following procedure is employed:

1) Given T_m^j and τ_m^j, calculate ΔT_{rad_m}. With moisture present, the values for ΔT_{rad_m} are affected not only by the atmospheric temperatures, but also by the time-dependent distribution of optical depth, which influences radiative heating rates. Hence the matrix $[A_{mi}]$ has to be calculated at each time step.

2) Find ΔT_{conv_m} . This is done in exactly the same manner as given in appendix III, except that the term $"-LW_1"$ is not omitted from the left hand side of the surface energy balance equation (eq. 2.5.1). When finding the surface temperature T_1^{j+1} , we use the moisture flux from the previous time step, W_1^j . Since the time step is so small ($\leq$ 15 seconds), this is an excellent approximation.

3) Given $K_{H_m}^j$, θ_1^j (the surface moisture content), and q_m^j , calculate θ_1^{j+1} and the q_m^{j+1}s , such that the conditions given in section 3.3 are fulfilled. Details of this step are shown in appendix IV.

4) Find the T_m^{j+1}s:

$$T_m^{j+1} = \begin{cases} T_m^j + \Delta T_{rad_m} + \Delta T_{conv_m}, & m \geq 2 \\ T_1^j + \Delta T'_{conv_1}, & m = 1 \end{cases}$$

5) Given θ_m^j and $T_{s_m}^j$, calculate θ_m^{j+1} and $T_{s_m}^{j+1}$ for $m \geq 2$ (To accomplish this, the soil moisture equation (3.2.11) and the soil heat equation (3.2.12) are written in explicit difference form).

6) Using the q_m^{j+1}s found in step 3, calculate the τ_m^{j+1}s . This is done by multiplying the q_m^{j+1}s by $\rho_m K_m$ to find the optical thickness of each layer, A simple summing procedure, starting from the top of the atmosphere where $\tau = 0$, then yields the new distribution of the optical depth.

When computing the soil temperatures in step 5, the variation of

K_g and C with respect to θ is taken into account. Table 4 shows the values of K_g and θ used for the calculations. In the expression for the soil heat flux (eq 3.2.11), the "moisture gradient" term $\left(-\rho_\ell L D_{vap}(\theta) \frac{\partial \theta}{\partial z}\right)$ is much smaller than the diffusive flux $\left(-K_g \frac{\partial T_s}{\partial z}\right)$ and it is neglected. To show the validity of this approximation we consider both wet and dry soils. For wet soils $(\theta \geq .15)$, the moisture gradient term is zero since $D_{vap}(\theta)$ is essentially zero. In a dry soil with θ roughly equal to .03, and with the typical values (as observed during the "slightly moist" integration presented in section 3.6, for example see figure 3.6.3):

$$D_{vap}(\theta) \sim 10^{-5} \frac{cm^2}{sec}$$

$$\frac{\partial \theta}{\partial z} \sim .01/cm$$

we obtain

$$-\rho_\ell L D_{vap}(\theta) \frac{\partial \theta}{\partial z} \sim 2.5 \times 10^3 \frac{ergs}{cm^2\, sec}$$

With the diffusive term having a typical value of $10^5 \frac{ergs}{cm^2\, sec}$, the neglect of the moisture gradient term is justified.

The coordinate system for the soil temperatures is found by using the coordinate transformation mentioned in chapter 2, with $\Delta \zeta$ specified as .252. The resulting grid spacing is wide enough to avoid problems of computational instability when an explicit differencing scheme is used, but not so wide as to be inaccurate. In explicit finite difference form the soil heat equation becomes:

Table 4

Values of K_θ, the thermal conductivity; C, the volumetric heat capacity; and $\tilde{K}$, the thermal diffusivity.

θ	K_θ ($\times 10^{-4}$) ergs/(sec cm °K)	C ($\times 10^{-7}$) (ergs/cm^3)	$\tilde{K}$ ($\times 10^3$) (cm^2/sec)
0	2.1	.96	2.17
.025	2.9	1.07	2.71
.05	4.3	1.17	3.68
.1	8.0	1.38	5.80
.15	10.0	1.59	6.29
.20	11.8	1.80	6.56
.25	12.9	2.01	6.42
.30	13.6	2.22	6.13
.35	14.3	2.43	5.88
.40	15.4	2.64	5.83
.45	16.4	2.85	5.75
.495	17.1	3.04	5.63

$$C(\theta)_m\left(\frac{T_{s_m}^{j+1} - T_{s_m}^{j}}{\Delta t}\right) = \frac{H_{s_m}^{j} - H_{s_{m-1}}^{j}}{\Delta z_{s_m}} \qquad 3.4.1$$

with the soil heat flux given by

$$H_{s_m}^{j} = -K_g(\theta)_m\left(\frac{T_{s_m}^{j} - T_{s_{m+1}}^{j}}{\Delta z_{s_m}}\right) \qquad 3.4.2$$

The coordinate system used for calculating the soil mositure content is identical to the soil coordinate system, except that an extra grid point is placed just below the surface at a depth of .07 cm. (This is done in the interests of accuracy).

The soil moisture equation is also solved using an explicit technique. With "m" as the vertical index, equation 3.2.9 can be written in finite difference form as:

$$\rho_l\left(\frac{\theta_m^{j+1} - \theta_m^{j}}{\Delta t}\right) = \frac{W_{s_m}^{j} - W_{s_{m-1}}^{j}}{\Delta z_{h_m}} \qquad 3.4.3$$

with the soil moisture flux given by

$$W_{s_m}^{j} = -\rho_l\left[D(\bar{\theta}_m^{j})\left(\frac{\theta_m^{j} - \theta_{m+1}^{j}}{\Delta z_{h_m}}\right) + K_w(\bar{\theta}_m^{j}) + D_T(\bar{\theta}_m^{j})\left(\frac{\partial \bar{T}_s}{\partial z}\right)_m^{j}\right] \qquad 3.4.4$$

Δz_{h_m} is the distance between the grid points m and $m+1$,
$\bar{\theta}_m^{j}$ is the average value of θ_m^{j} and θ_{m+1}^{j}, and $\left(\frac{\partial \bar{T}_s}{\partial z}\right)_m^{j}$

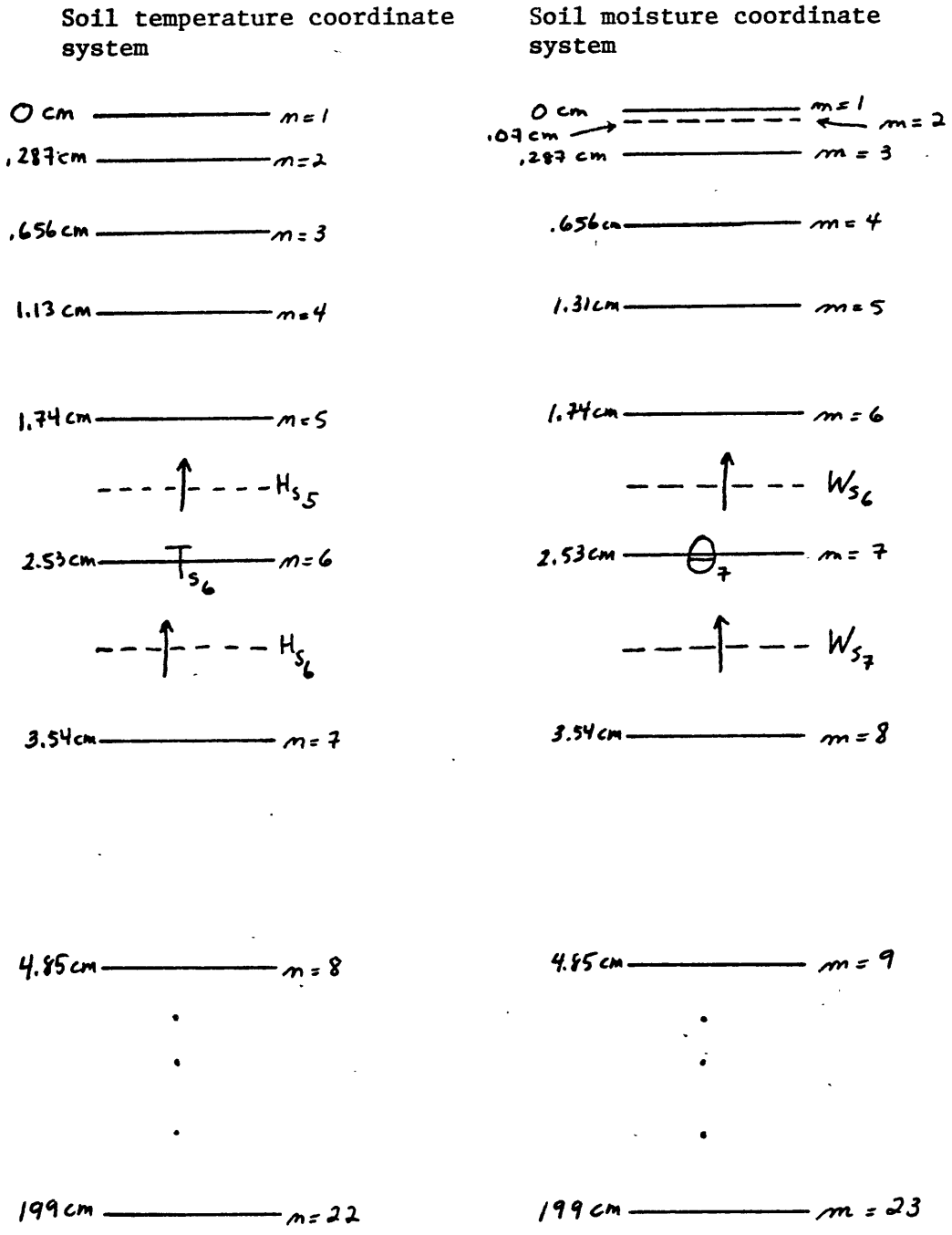

Figure 3.4.1. The soil temperature and soil moisture coordinate systems. The grid points between 4.85 cm and 199 cm are not shown because of lack of space.

is the soil temperature gradient evaluated between the grid points m and $m+1$.

Figure 3.4.1 illustrates the two systems. The soil heat flux $H_{s_K}^{i}$ and the soil moisture flux $W_{s_K}^{i}$ are evaluated at the mid-point between the level K and $K+1$.

3.5 Initial Conditions

In the calculations that follow, the integrations start at 0600 hours and run until significant condensation occurs in the atmosphere. Initial profiles are needed for the soil moisture content, the atmospheric specific humidity, and the soil and atmospheric temperatures.

Data on the soil moisture content at various depths is not readily available for the Sahelian region, if it exists at all. However, an approximate distribution for the soil moisture can be derived by considering steady-state evaporation from a water table. We assume that the steady-state case roughly represents an annually-averaged moisture profile.

In the steady-state situation, $\frac{\partial \theta}{\partial t} = 0$ and the moisture flux is constant. By neglecting the thermal term, which has little net effect when averaged over a long period of time, equation 3.2.8 can be rearranged to yield:

$$dz = \frac{D(\theta)}{W_s + K_w(\theta)} d\theta \qquad 3.5.1$$

Since $D(\theta)$ and $K_w(\theta)$ are only functions of θ, and W_s is a constant (to be determined), equation 3.5.1 can be

integrated to give z as a function of θ . We have

$$z(\theta) = \int_{\theta_0}^{\theta} \frac{D(\theta')}{W_s + K_w(\theta')}\, d\theta' \qquad 3.5.2$$

θ_0 is the soil moisture content at the surface, which can be determined from equation 3.3.7. (With $T \sim$ 300°K, and $r \sim .3$, $\theta_0 \sim .028$). The maximum value of θ occurs when the pore spaces in the soil are completely filled with water. At this depth, which corresponds to the depth of the water table, z_w, θ assumes its saturated value, θ_s . (θ_s = .495 for Yolo light clay).

In order to integrate 3.5.2 W_s must be known. W_s is only a function of the water table depth; this functional relationship is shown by a graph published by Philip (1957). According to a map of West Africa published by Michelin (1973), a typical value for z_w in the Sahel is about 10 meters. For this depth the moisture flux is about $1.6 \times 10^{-8} \frac{g}{cm^2 sec}$. By using this value for W_s in equation 3.5.2 and integrating between θ_0 and θ_s , the steady-state profile of θ can be produced as shown in figure 3.5.1. With this distribution of θ , the soil is very dry; such conditions would prevail only in an arid region.

As diurnal fluctuations in soil moisture do not occur below about 10 centimeters, it is convenient to specify a value of θ below this level to serve as a lower boundary condition for equation 3.2.10. In the numerical calculations, θ is specified as .17 at the last soil moisture grid point, 199 cm below the surface. The profile between 0 and 199 cm is the initial condition for θ.

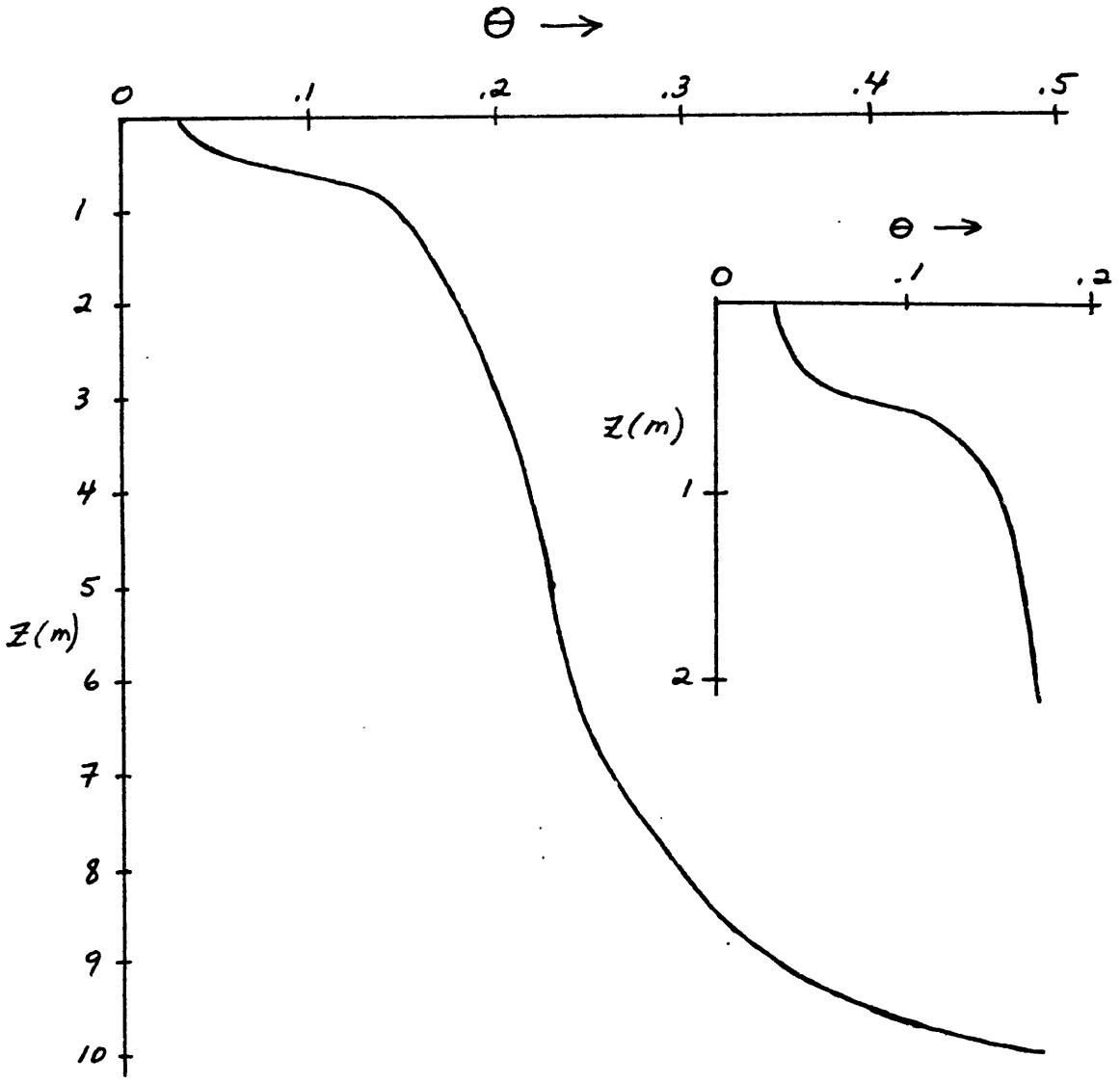

Figure 3.5.1. Steady-state soil moisture profile for a depth to water table of ten meters. The insert to the right is a "blow-up" of the profile between 0 and 2 meters.

With this moisture profile, the thermal conductivity and heat capacity of the soil have different values than they would have if the soil were perfectly dry. This alteration of the thermodynamic properties of the soil has some effect on the atmospheric and soil temperatures. To isolate the magnitude of this effect, the model of chapter 2 can be integrated with the single change that the thermodynamic properties of the soil correspond to the moisture profile of figure 3.5.1. A comparison of the results of this integration and the perfectly dry case reveals that this effect is small. (However, it could be much larger for a soil which contains more moisture). Figure 3.5.2 shows tha quasi-steady ground temperatures comptuted for the "slightly moist" case and the perfectly dry case. The maximem difference in temperature is about 2°K.

For the initial condition of the atmospheric temperatures, the temperature profile at 0600 hr from the "slightly moist" calculation is used. This condition is designated as PROFILE I in figure 3.5.3. The initial soil temperatures, shown in the figure, are also taken from the 0600 hr of the slightly moist calculation.

The humidity profile of figure 2.7.1 is used as the initial condition for the specific humidity.

3.6 Results

Starting from 0600 hr , the model was integrated with the initial conditions as specified in section 3.5. (The results of this integration will be referred to as the slightly moist case, abbreviated as "SM"). Saturation in the atmosphere occurred just after 0700 hr,

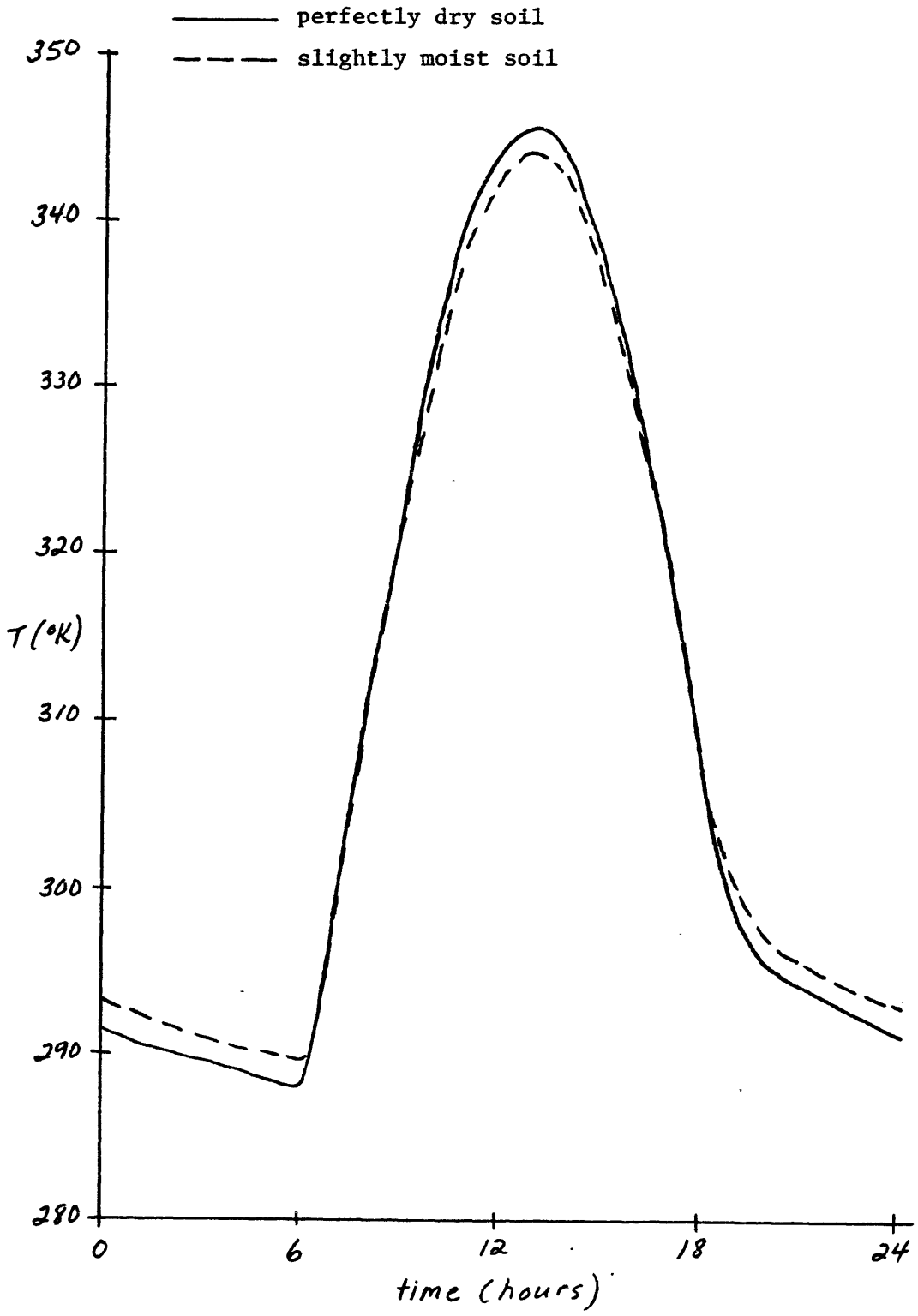

Figure 3.5.2. The temperature of the ground. The dashed line is for the slightly moist soil; the solid line is for the perfectly dry soil.

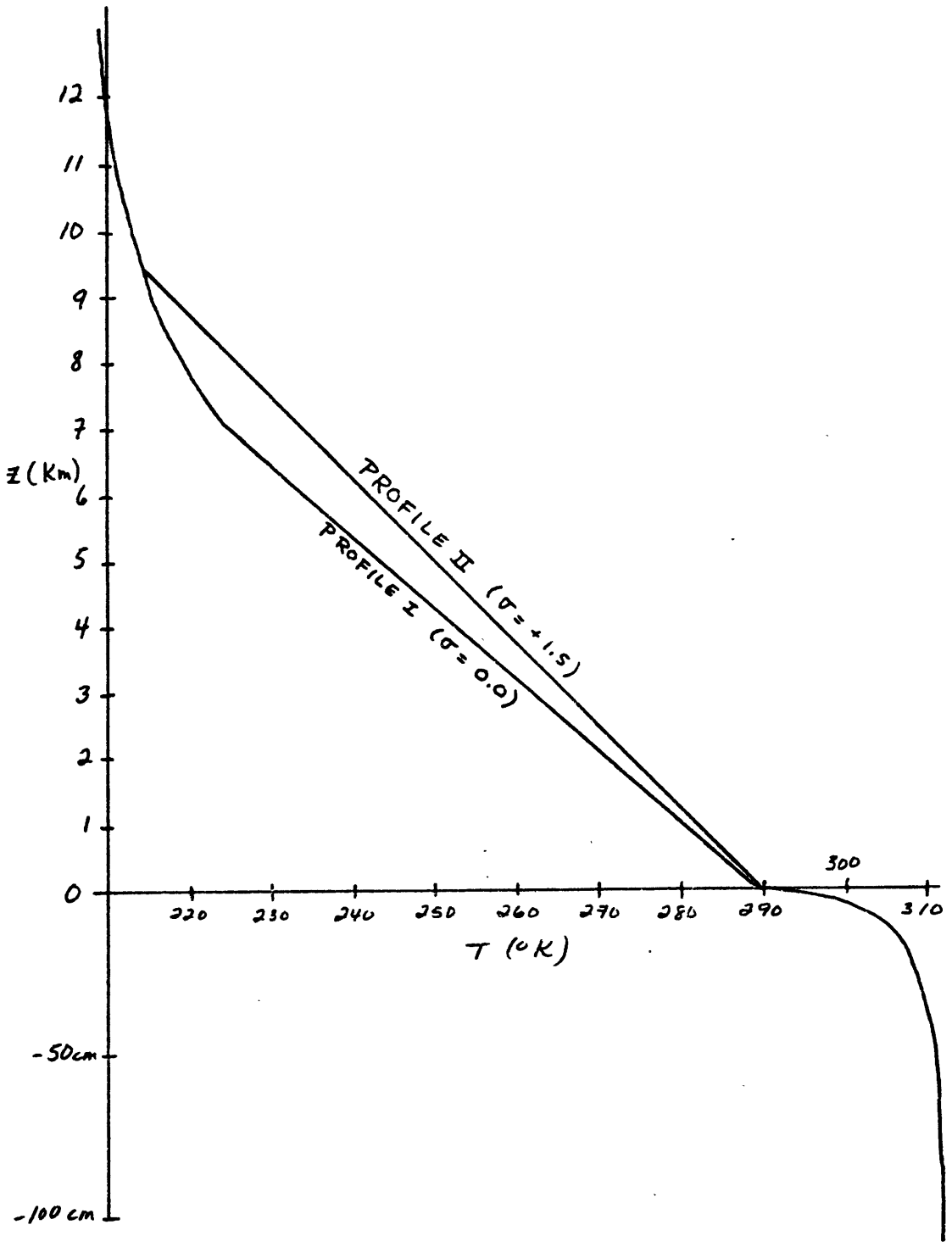

Figure 3.5.3. The initial conditions for the soil and atmospheric temperatures. (The vertical distance scale for the soil is greatly exaggerated). σ is the static stability (°K/km).

yet the calculation was not stopped until 1000 hr. Figure 3.6.1 shows the ground temperature T_1, the solar forcing S, and the surface fluxes of sensible heat (H_1) and latent heat (LW_1). (Also shown for the purpose of comparison is the ground temperature T_{1dry} and the sensible heat flux H_{1dry}, calculated in chapter 2 for the dry case). The latent flux is negligible, and the ground temperatures and sensible heat fluxes of the two cases are almost identical. Small differences do exist; these can be attributed to differences in the thermal properties of the soil (as discussed in the previous section). The atmospheric temperature profiles for the SM case are almost exactly the same as for the dry situation, and consequently they will not be shown.

Figure 3.6.2 shows the distribution of specific humidity at 0600, 0700, and 1000 hrs. With values of K_H as large as $.5 \times 10^7 \frac{cm^2}{sec}$, convection is very efficient in transfering moisture upwards from the lower part of the convective zone. The transfer of moisture across the earth-soil boundary is small ($\sim 10^{-7} \frac{cm}{sec}$), since for the dry soil, capillary forces hold the soil moisture tightly (i.e., $|\psi|$ is large). Hence, with essentially no input of moisture from the soil, the lower part of the convective region experiences a loss of moisture with time. This is shown vividly in figure 3.6.2 as the specific humidity decreases markedly below 1 km as the day progresses. (The dashed part of the 1000 hr curve indicates that the specific humidity equals or exceeds its saturated value - at this time saturation has occured between 2 and 3.25 km).

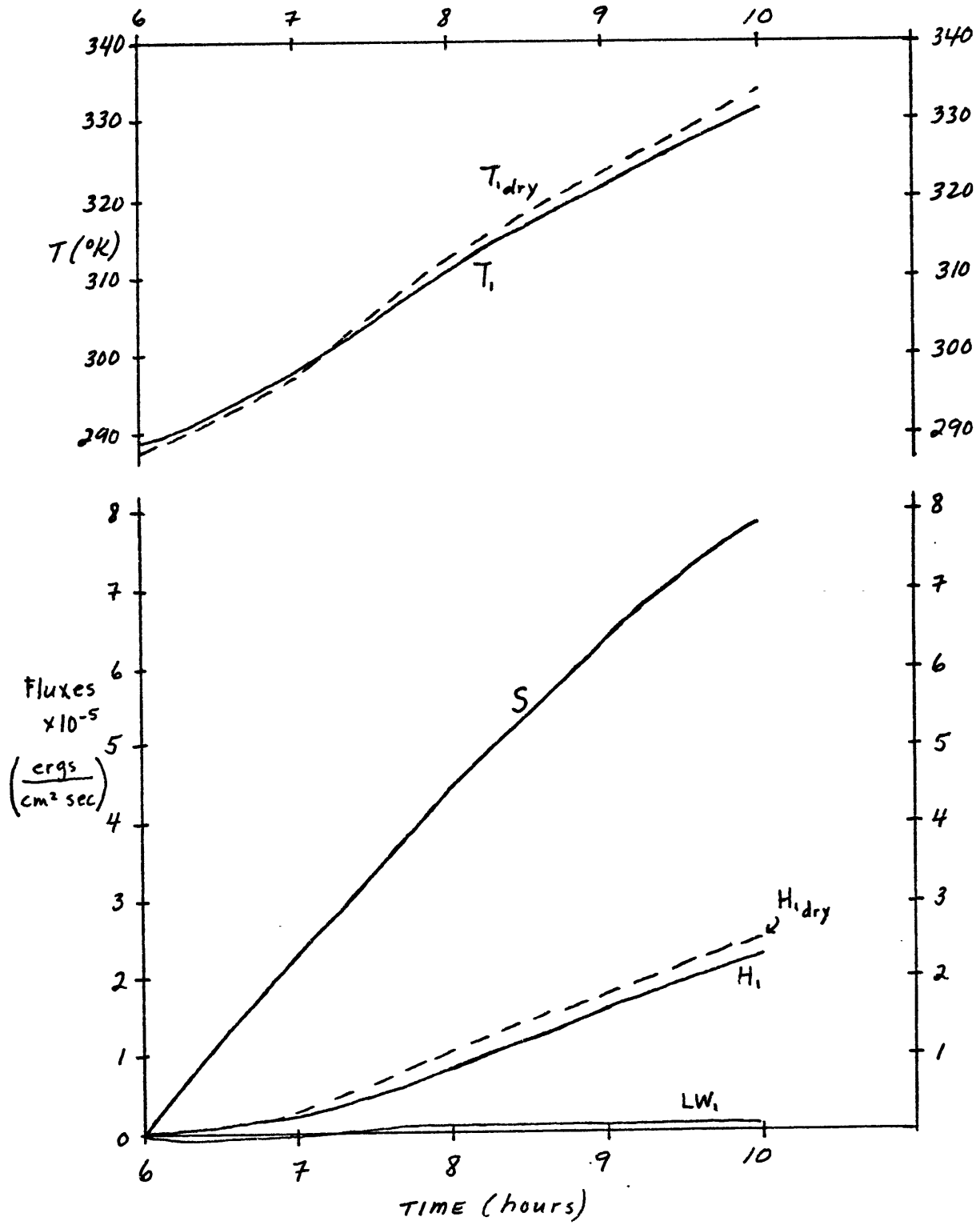

Figure 3.6.1. The temperature of the ground T_1, the solar flux S, and the surface fluxes of sensible heat H_1 and latent heat LW_1. $T_{1\,dry}$ and $H_{1\,dry}$ are the calculated values for the dry case.

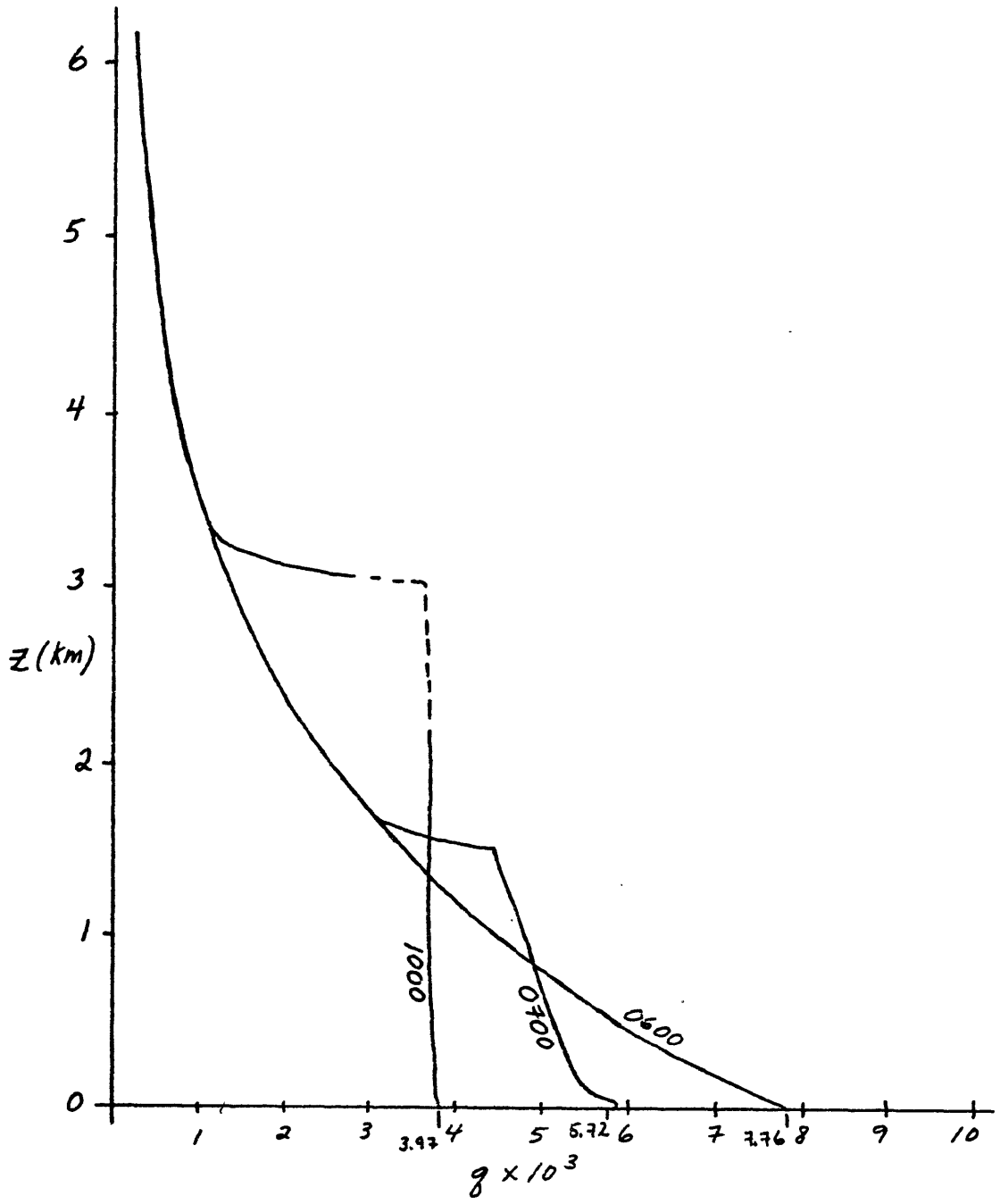

Figure 3.6.2. Specific humidity profiles for different times. The dashed portion of the 1000 hr profile indicates that q equals or exceeds its saturated value. The tag below each curve indicates the surface specific humidity. Note that the humidity jump across laminar layer is small.

The abrupt bends in the 0700 and 1000 hr profiles represent "discontinuities" in the moisture profile. As convection transfers moisture upwards, it "accumulates" below the top of the convective region because of the no flux boundary condition, and a discontinuity is formed.

Figure 3.6.3 shows soil moisture profiles between the surface and a depth of 5 cm. Most of the variations in soil moisture content occur within 3 cm of the surface; below this level the values of θ are essentially constant. At 0600 hr, with a surface soil moisture content of 0.28 and a surface temperature of $\sim$ 290°K, the surface specific humidity is about 2×10^{-3}. Immediately above the surface, the humidity is higher ($\sim 8 \times 10^{-3}$) and consequently moisture is transfered from the atmosphere into the soil. This downward transfer is still continuing at 0700 hr, as shown by the positive moisture gradient in the soil. Also at this time, a positive moisture gradient exists in the atmosphere, but only up to a height of about 1 meter.

At 1000 hr the upward transfer of moisture by convection has left the atmosphere near the earth's surface in a relatively dry condition. The potential for evaporation is high, and the atmosphere "demands" moisture from the soil. In an attempt to meet this demand, a large gradient of θ is formed just below the surface as shown in the figure. This happens because in the expression for the moisture flux (eq. 3.2.8), the moisture diffusivity is very small (since the capillary forces are large); and also, as $\frac{\partial T_s}{\partial z}$ is positive in this instance, the thermal term acts in opposition to the upward transport of moisture. (The gravitational term is negligibly small for such dry soils).

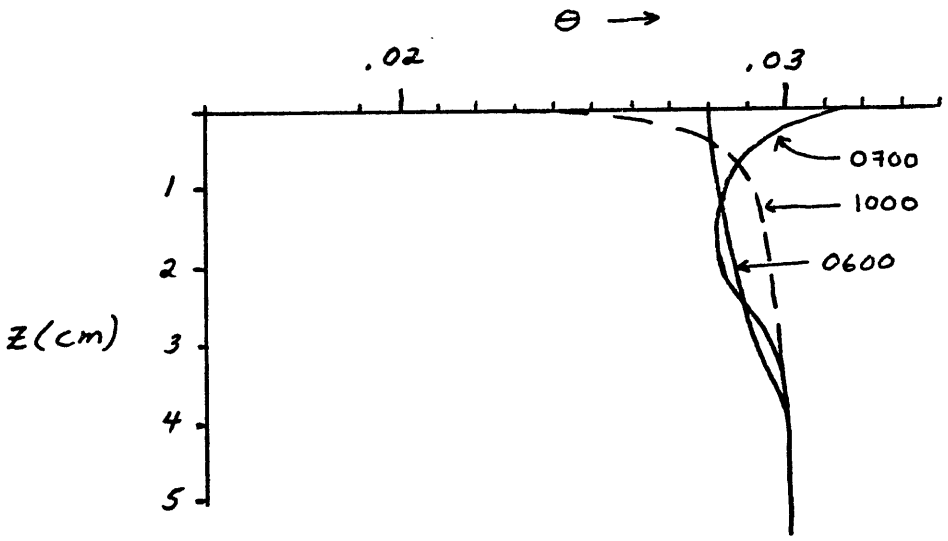

Figure 3.6.3. Profiles of the soil moisture content θ, in the first five centimeters below the soil surface.

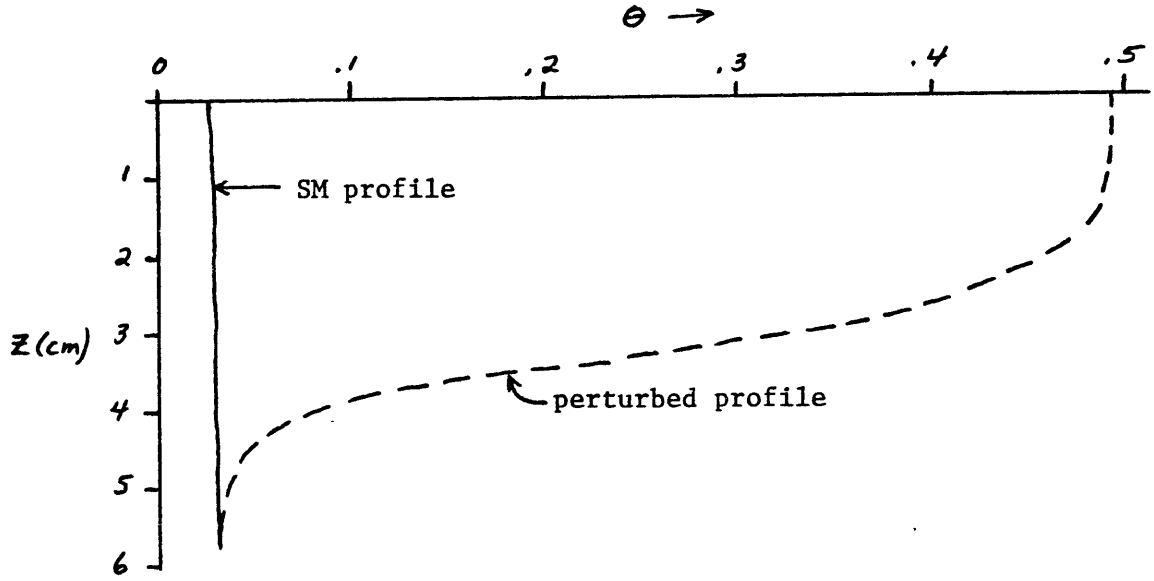

Figure 3.6.4. The initial SM profile is shown by the solid line; the perturbed profile is indicated by the dashed line. Below 6 centimeters both profiles are identical.

From an examination of the results presented above, one could conclude that the presence of a very small amount of soil moisture has no appreciable effect on the atmosphere. However, the moisture content in the upper part of the soil is not always so dry; it can increase rapidly due to precipitation, and it is possible that the atmosphere can be significantly influenced by such a change. Therefore, a study of the response of the model to a perturbation in soil moisture content, presumably caused by precipitation, seems merited.

To undertake this study, we first construct a soil moisture profile that includes a "precipitation perturbation". Then the model is integrated, starting from 0600 hr and using the same initial conditions as the SM case, except for the inclusion of the perturbation. By comparing the results of this integration to the SM case, the importance of the perturbation can be determined.

To construct a precipitation perturbation we start with the soil moisture profile used as the initial condition in the SM case. Next, we assume that rainfall occurs, the surface becomes immediately saturated (i.e. $\theta_1 = \theta_s$), and water infiltrates into the soil. After two hours, 1 1/2 cm of water has been accepted by the soil, and the moisture profile existing at this time is considered as the perturbed profile. (Mathematically speaking, the profile was generated by numerically integrating the equation governing soil moisture moisture transport (3.2.10), with the thermal term being neglected. The initial condition was the initial SM profile. The upper boundary condition of $\theta_1 = \theta_s$ was applied at the surface; at a depth of 10 cm the lower boundary condition was specified as θ = .031. The integration

was carried on for two hours).

This profile is shown in figure 3.6.4. As can be seen, the soil is almost completely saturated to a depth of about 3 centimeters. When using this profile in the calculations that follow, it is necessary to change the grid spacing of the soil moisture coordinate system, and the time step, to avoid computational instability. The new grid spacing consists of equal intervals in Δz_s, with Δz_s equal to .2 cm; with this spacing a time step of 2.5 seconds is used.

Figure 3.6.5 shows the ground temperature $T_{1,p}$, the latent heat flux LW_p and the sensible heat flux $H_{1,p}$ for the "perturbed" case. (Also shown is the solar forcing, S). With the precipitation perturbation, the surface energy balance is much different than for the SM situation, and there are large differences in the ground temperatures and the fluxes of latent and sensible heat. The total energy transmitted to the atmosphere by the latent and sensible heat fluxes is larger in the perturbed case; and in this situation the latent flux is much larger than the sensible heat flux. This is in contrast to the SM situation, where the latent flux is neglibibly small.

The atmospheric moisture profiles at different times are shown in figure 3.6.6. The gradients of moisture are very large close to the surface of the earth ($z \leq$ 10 meters) as evidenced by the long "tails" or the 0700 and 1000 hr curves. The large gradient is due to the inefficiency of convection close to the ground, where K_H is samll. Condensation occurs just after 0700 hr and by 1000 hr , the atmosphere is saturated between 1.75 and 2.75 km. (In comparison, recall that in the SM case, saturation occurs between 2 and 3.25 km

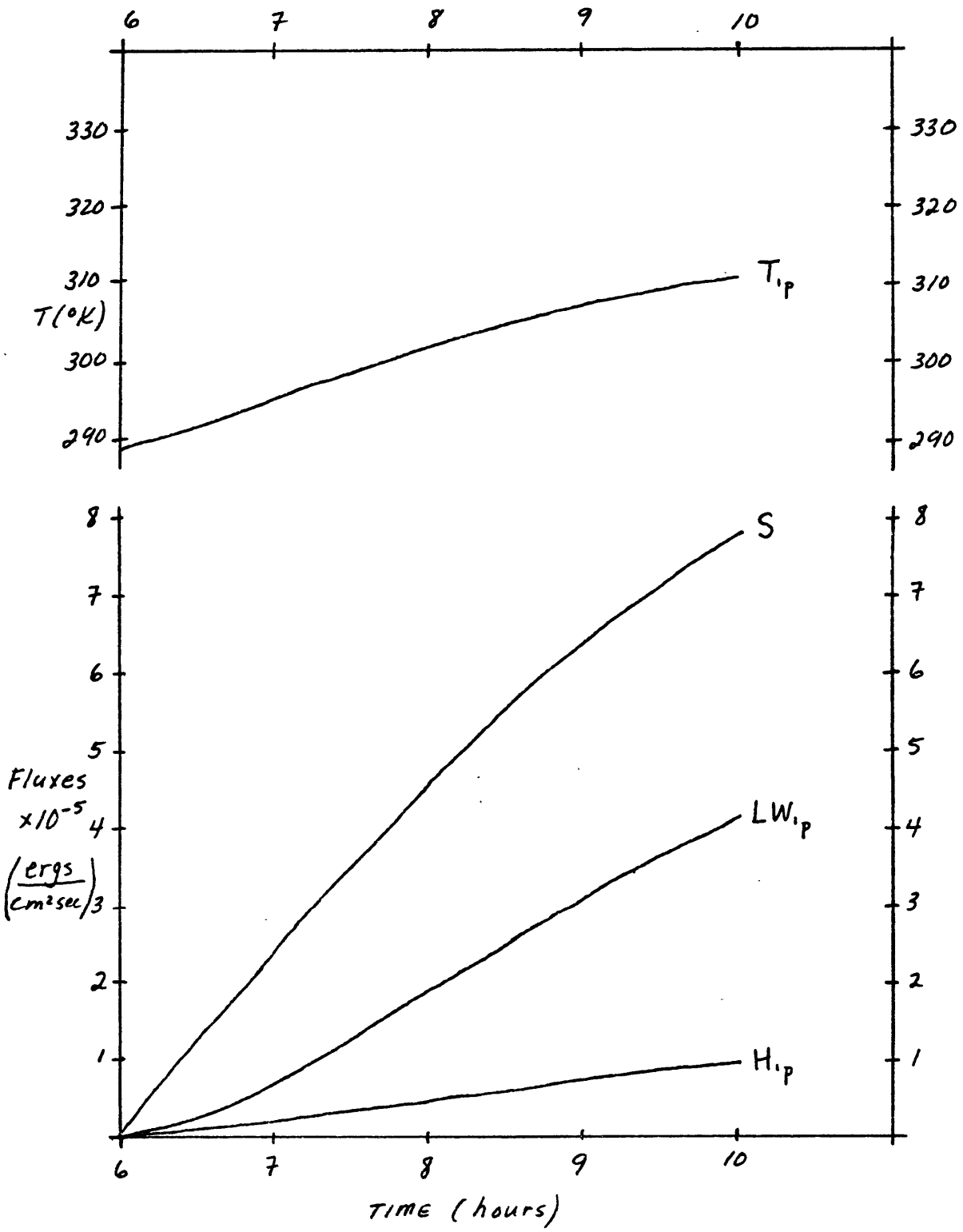

Figure 3.6.5. The ground temperature $T_{1,p}$, and the surface fluxes of sensible heat $H_{1,p}$ and latent heat $LW_{1,p}$ for the perturbed case. S is the solar flux.

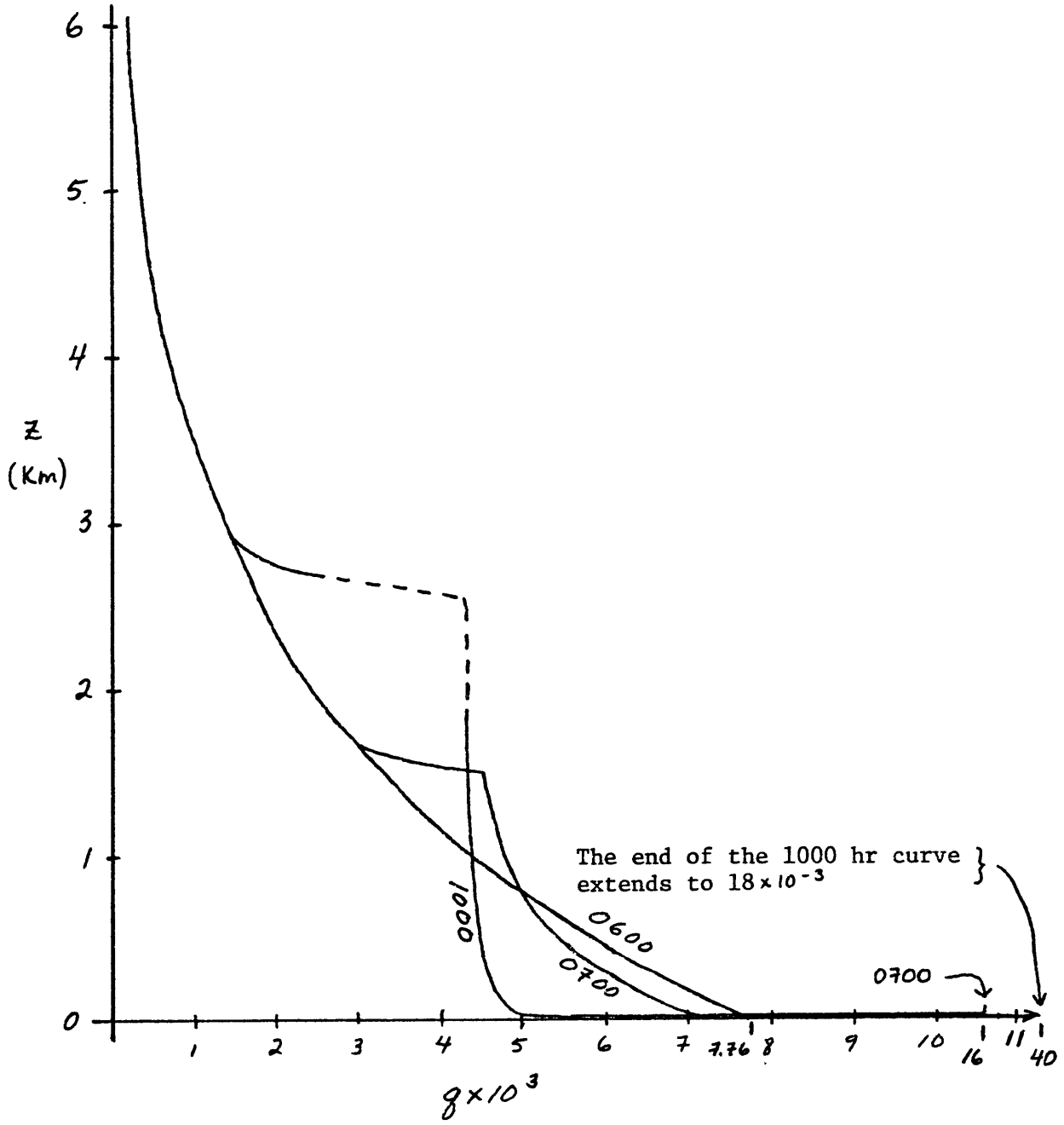

Figure 3.6.6. Specific humidity profiles at different times for the perturbed case. The dashed portion of the 1000 hr curve indicates that q equals or exceeds its saturated value. The tag below each curve is the value of the surface specific humidity. In this case, the humidity jump across the laminar layer is large. The end of the 1000 hr curve extends to $q = 18 \times 10^{-3}$.

at 1000 hr.).

Figure 3.6.7 presents profiles of soil moisture. The amount of moisture in the upper few centimeters decreases considerably over the period of integration. This is due to two factors: first and most importantly, the combined action of gravitational and capillary forces pulls the moisture downwards, and second, some moisture leaves the soil as the latent heat flux.

The 1000 hr temperature profiles (below 10 meters) for the SM and perturbed case are shown in figure 3.6.8. The slight difference between the profiles can be attributed to the difference in ground temperatures between the two situations. Above .25 km, the temperatures are virtually identical.

It is interesting to compare the amount of "condensation" (i.e., supersaturation in our model) that occurs during the integrations. We denote this quantity by "C", and it is given by the integral

$$C = \int_{\substack{\text{saturated} \\ \text{region}}} \rho(q - q_s)\, dz \qquad 3.6.1$$

where q_s is the saturated specific humidity (a function of T and p), and the saturated region is wherever $q \geq q_s$.

When C is computed at 1000 hr we find that the amount of condensation is nearly equal in both cases: .102 $\frac{g}{cm^2}$ for the perturbed case and .105 $\frac{g}{cm^2}$ for the SM case. This result is surprising. Intuitively, one would expect much more condensation to take place when the upper part of the soil contains an abundance of moisture. Condensation appears not to be enhanced when the ground is saturated

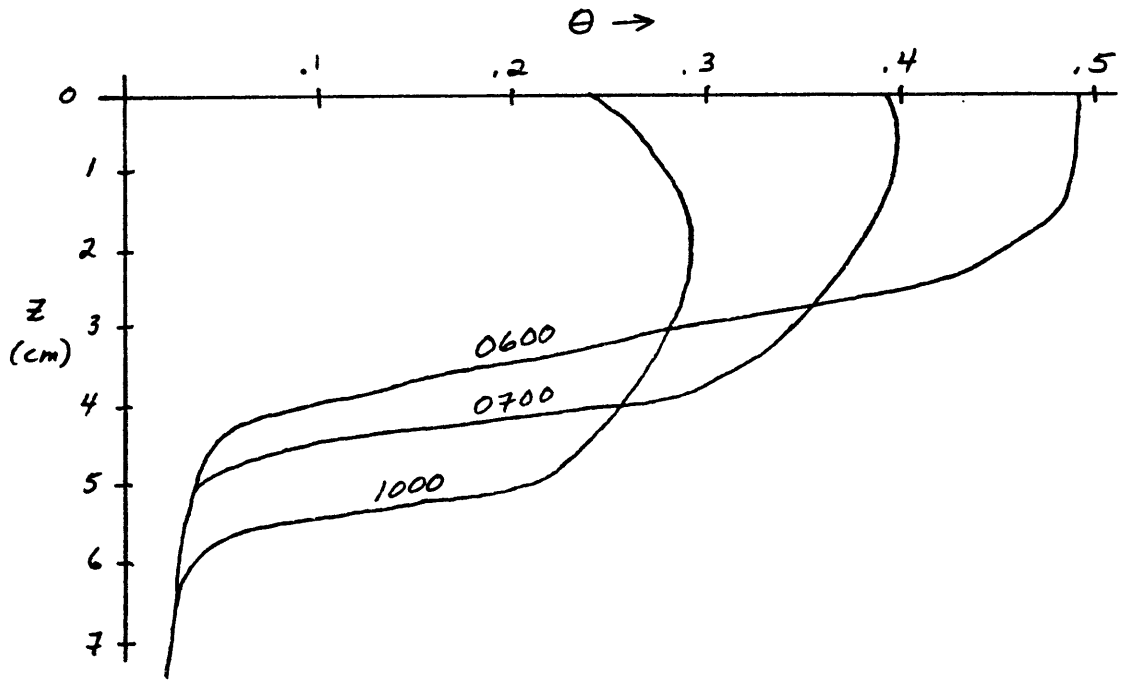

Figure 3.6.7. Soil moisture profiles for the perturbed case.

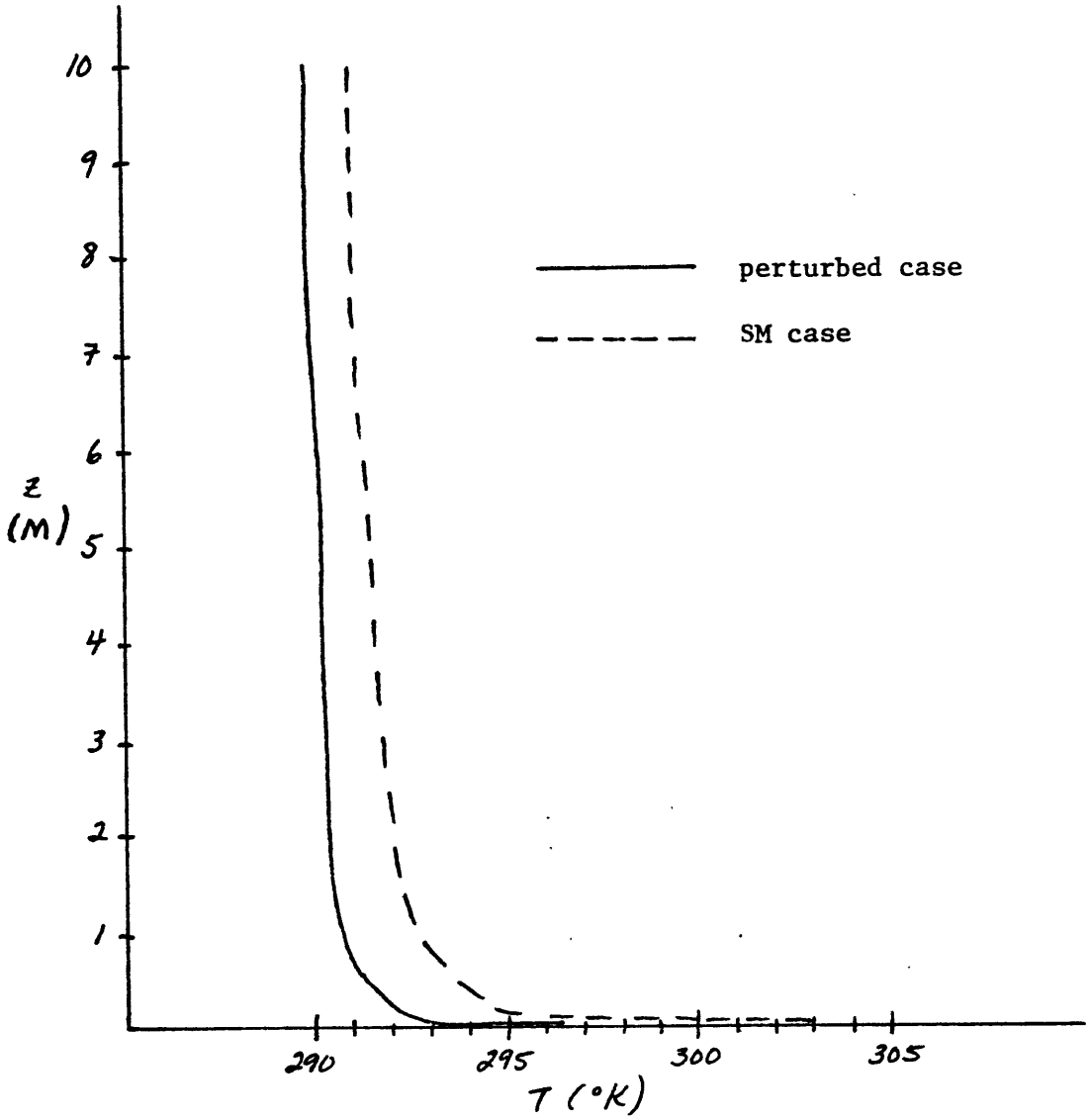

Figure 3.6.8. 1000 hr temperature profiles below 10 meters. The solid line is the perturbed case; the dashed line is the SM case.

because, when compared to a drier soil condition, water is not carried to as high a level in the atmosphere where condensation is encouraged due to the cooler temperatures.

For the above calculations, the initial atmospheric temperature profile up to 7 km had a static stability (σ , defined as $\frac{\partial \theta}{\partial z}$) very close to zero. We shall repeat the calculations but with a different initial temperature profile - one with a static stability of 1.5°K/km. This is designated as PROFILE II in figure 3.5.3. The use of a more stable initial condition retards the onset of condensation, and therefore the results are physically consistent for a longer period of integration. In the following set of calculations, condensation occurs just before 1000 hrs.

Figure 3.6.9 presents the ground temperatures, and the fluxes of latent and sensible heat for the SM and perturbed cases (both with σ = +1.5). Up until 1000 hr the temperatures and fluxes show the same general characteristics as when the static stability is zero. After 1000 hr in the perturbed situation, intense drying takes place at the soil surface, and the latent heat flux decreases.

This drying, which is shown clearly in the 1000 hr soil moisture profile of figure 3.6.10, is confined to the first half centimeter of the soil. In this layer, the gradient of θ becomes very large, yet the moisture flux decreases since the soil is drier, and the moisture diffusivity ($D(\theta)$) assumes a smaller value. As the soil surface is saturated at 0600 hr, and is quite dry at 1100 hr, the transition interval between a wet and dry surface is about 5 hours.

The 1100 hr atmospheric moisture profiles for both cases are

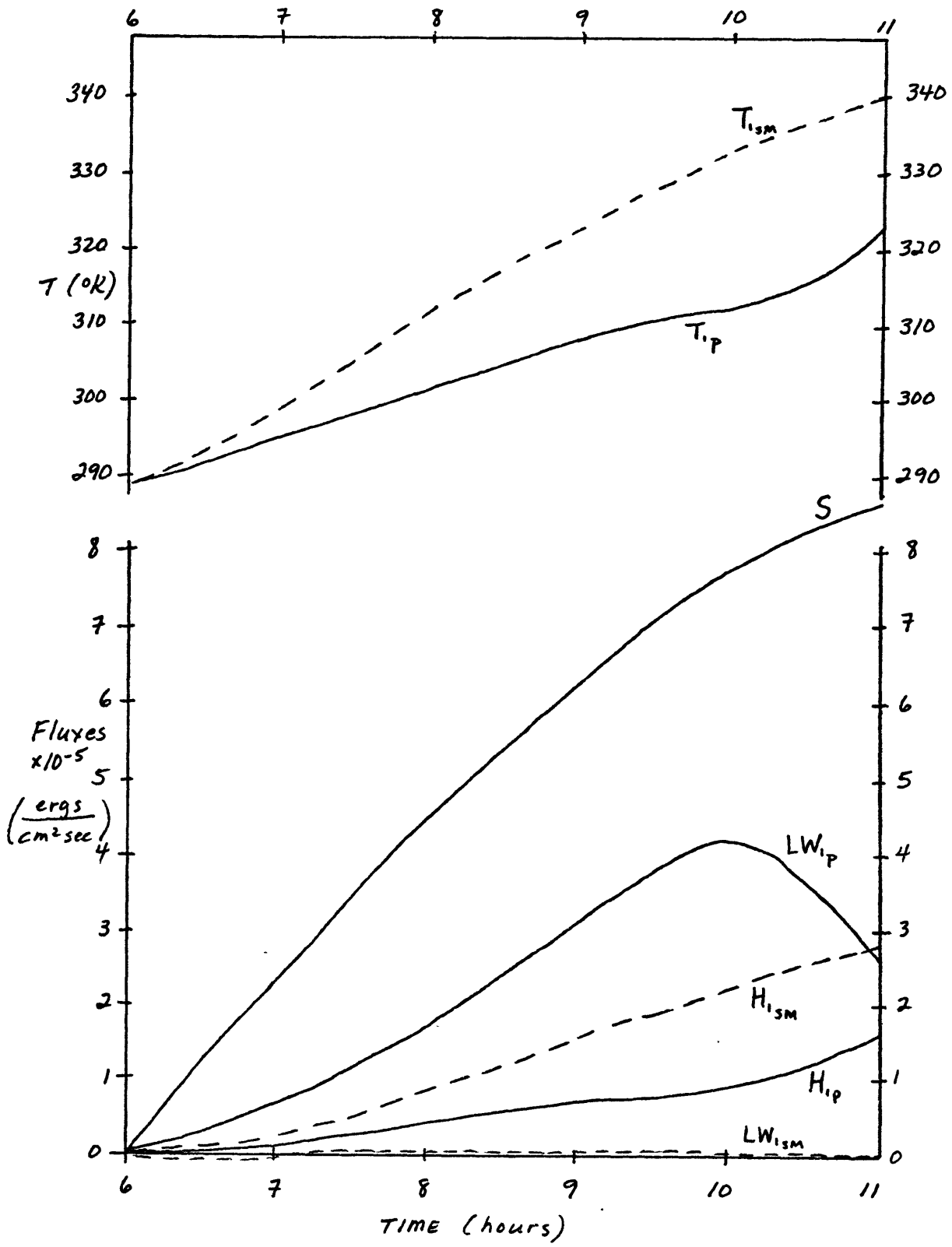

Figure 3.6.9. The ground temperature, and the fluxes of sensible and latent heats for the perturbed and SM cases, (σ = +1.5°K/km). The solid line indicates the perturbed case; the dashed line indicates the SM case. "S" is the solar forcing.

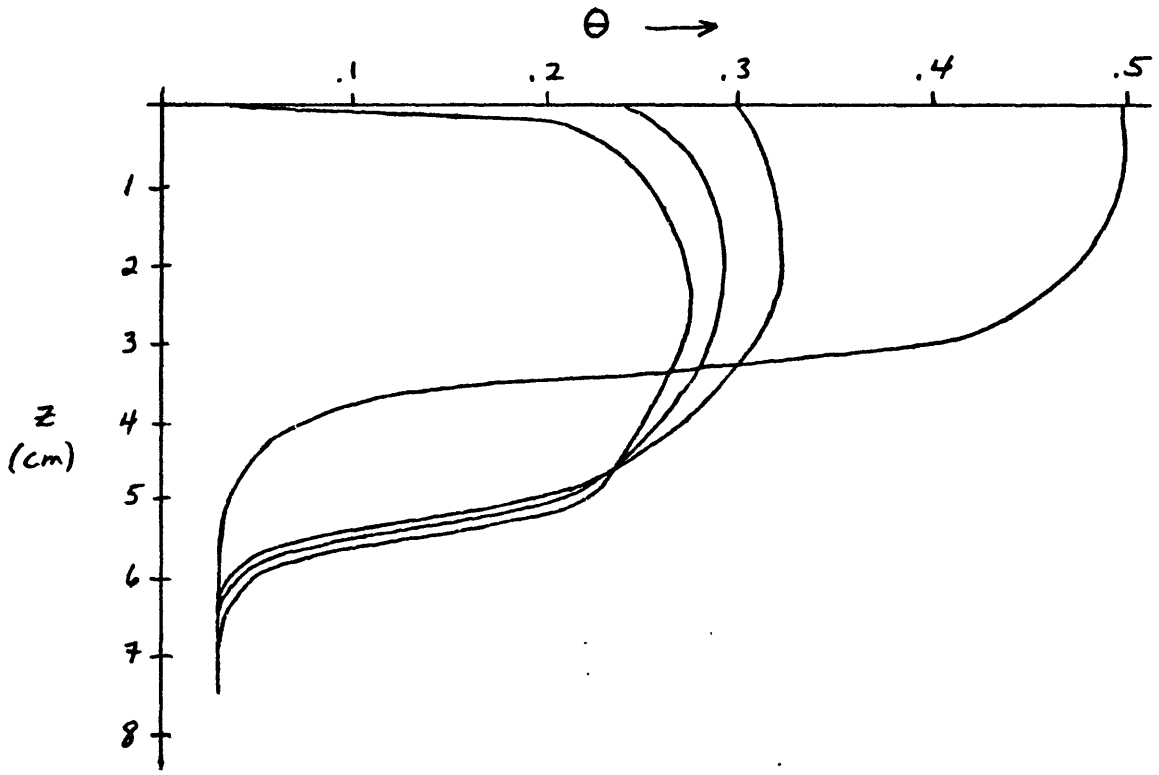

Figure 3.6.10. Profiles of θ for the perturbed case, (σ = +1.5°K/km).

presented in figure 3.6.11. The amount of condensation is again (nearly) equal, with $C \sim 1.5 \times 10^{-2} \frac{g}{cm^2}$ for both cases. This is significantly less condensation than occurs when the initial static stability is zero.

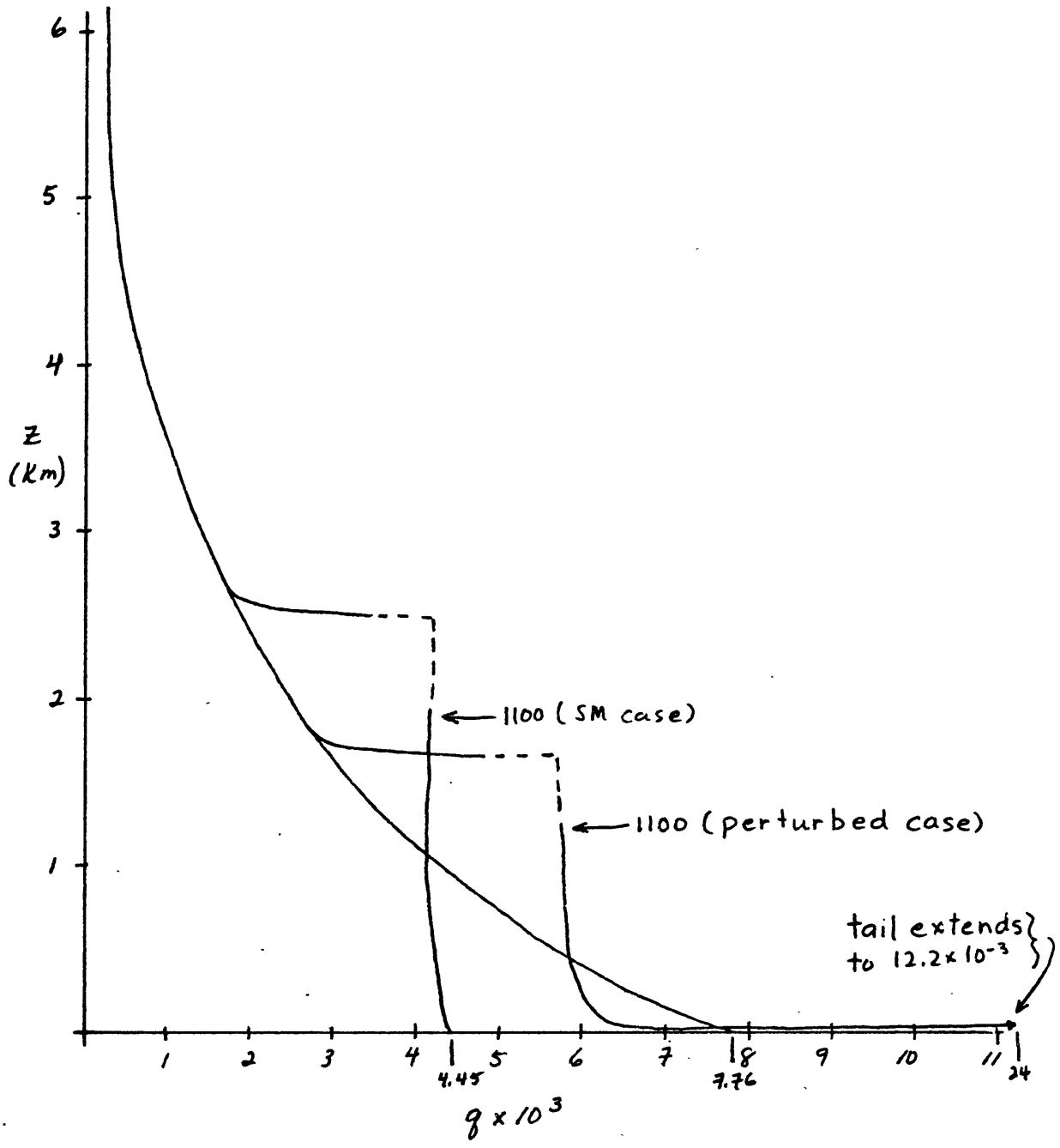

Figure 3.6.11. 1100 hr profiles of specific humidity for the SM and perturbed cases, (σ =+1.5°K/Km). The tag below each profile indicates the value of the surface specific humidity.

IV. Some concluding remarks

This thesis, using a simple coupled soil-atmosphere model, has investigated the sensitivity of the atmosphere to different amounts of soil moisture. The atmospheric component of the model was greatly simplified, so that some important physical processes were ignored (such as condensation, cloudiness, and precipitation) and this limits the usefulness of the calculations. However, some tenative conclusions can be drawn based on the results presented in chapter three. These are:

1) For a very dry soil, the soil moisture has no significant effect on the atmosphere. For all practical purposes, the latent heat flux is neglibible, and a no-flux boundary condition for moisture can be applied at the earth's surface.

2) If a thin layer of soil bordering the atmosphere becomes saturated, say by precipitation (as represented in the calculations by the "precipitation perturbation"), the surface energy balance is greatly altered. The latent heat flux is no longer negligible; instead it becomes several times larger than the flux of sensible heat. The calculations indicate that the transition time for a saturated soil surface to become dry is about five hours.

3) Condensation in the atmosphere appears not be be enhanced when the soil surface is wet - a surprising result. When compared to a dry soil surface, one would intuitively expect more condensation to occur with a wet surface as an abundance of water is available for evaporation. However, this factor appears to be offset by the relative weakness of the turbulent heat flux under wet soil conditions. The

weak flux prevents the transport of water vapor into higher (and cooler) parts of the atmosphere where condensation is most favored.

More study, with an improved model, is needed to confirm the above conclusions. To improve the model and increase its usefulness, it is necessary to relax some of the constraints that have been imposed. First, a simple treatment of condensation, clouds, and precipitation could be put into the model. When this is done, the integrations would not have to be stopped after condensation occurs, and it would be possible for the model to operate for a longer period of time than just a few hours. Second, non-grey radiation could be used instead of the grey approximation. Errors in the radiative heating rates would be reduced, and the temperatures throughout the atmosphere, but particularly in the diurnal boundary layer, could be predicted with greater accuracy.

With these changes, the model should be able to simulate, over a period of a few days, the weather occuring in a region like the Sahel. Numerous experiments could be performed by varying the amount and distribution of soil moisture, and then observing the response of the atmosphere to these changes. These experiments should yield a greater understanding of the physics of soil moisture-atmosphere interaction. It would also be interesting to add vegetation to the model, to determine how much influence it exerts on the atmosphere.

Finally, when these simple studies are complete and the results understood, a "regional" climate model for an area like the Sahel could be constructed which would include atmospheric dynamics as well as soil hydrology and vegetation. This model could be used to examine

Charney's (1975) hypothesis of desertification.

The above suggestions would take a great deal of time to accomplish. However, the model in its present primitive form, with some slight modifications, could still be used to some profit. The accuracy of the "moisture-budget" soil hydrology parameterization used in the GFDL GCM (Manabe (1969)), has never been tested for accuracy. It is not known whether this simple scheme can adequately predict the latent heat flux, which is often an important component of the surface energy balance. It would be very enlightening to compare this parameterization to the more realistic formulation given in this thesis. The error of the moisture budget scheme could be estimated, and it is possible that an improved simple soil hydrology parameterization could be developed.

Appendix I

In this appendix, we heuristically derive expressions for the diffusive fluxes of heat and moisture which are transferred through the laminar layer.

Let the thickness of the laminar layer be d . Above d , moisture and heat are transfered by turbulent convection, while within the laminar layer, molecular transfer of these quantities takes place. For the diffusive fluxes through the layer, we have

$$H_1 \sim \rho c_p K \frac{\Delta T}{d} \qquad \text{A.1.1}$$

$$W_1 \sim \rho D_m \frac{\Delta q}{d} \qquad \text{A.1.2}$$

where H_1, W_1 = heat and moisture fluxes through the layer

$\Delta T, \Delta q$ = differences of temperature and specific humidity across the layer

K, D_m = molecular diffusivities of heat and moisture in air

An estimate is needed for d . At approximately this height, where molecular transfer ends and turbulent transfer begins the Rayleigh number

$$Ra \equiv \frac{g \Delta T d^3}{K \nu \bar{T}} \qquad \text{A.1.3}$$

assumes its critical value, Ra_c . Solving for d we obtain

$$d \sim (Ra_c)^{-1/3} \left(\frac{K\nu\bar{T}}{g\Delta T}\right)^{1/3} \qquad \text{A.1.4}$$

This expression for d is substituted into equations A.1.1 and A.1.2 to get

$$H_1 \sim A\rho c_p K \left(\frac{g}{K\nu\bar{T}}\right)^{1/3} (\Delta T)^{1/3} \qquad \text{A.1.5}$$

$$W_1 \sim A\rho D_m \left(\frac{g\Delta T}{K\nu\bar{T}}\right)^{1/3} \Delta q \qquad \text{A.1.6}$$

where A is a constant, roughly equal to $(Ra_c)^{-1/3}$. (With $Ra_c \sim 1000$, $A \sim .1$). Gierasch and Goody (1968) argue that $A \sim .089 \cdot 2^{4/3}$ $(= .22)$ and this is the value that is used in the thesis.

Appendix II

Derivation of the elements of the matrix $[A_{mi}]$

We recall that Q_{rad} is defined as:

$$Q_{rad} = -\frac{d}{dz} F(\tau(z)) \qquad \text{A.2.1}$$

Putting this in finite difference form, we get

$$Q_{rad_m} = -\frac{F_m - F_{m-1}}{z_m - z_{m-1}} = \frac{F_{m-1} - F_m}{z_m - z_{m-1}} \quad , \quad m \geq 2 \qquad \text{A.2.2}$$

where $F_m = F(\tau(z_m)) =$

$$\sigma T_1^4 \, 2\int_0^1 e^{-(\tau_1 - \tau_m)/\mu} \mu \, d\mu$$

$$+ 2\sigma \int_0^1 \left(\int_{\tau_m}^{\tau_1} T^4(\tau') \, e^{-(\tau' - \tau_m)/\mu} \, d\tau' \right) d\mu \qquad \text{A.2.3}$$

$$- 2\sigma \int_{-1}^0 \left(\int_0^{\tau_m} T^4(\tau') \, e^{-(\tau' - \tau_m)/\mu} \, d\tau' \right) d\mu$$

(In the above expression for F_m, we recall that in our indexing notation, $\tau_1 = \tau_g$ and $T_1 = T_g$).

By making the substitution $\mu = -\mu$ in the last term of equation A.2.3, we get, after simplification,

$$F_m = \sigma T_1^4 \, 2 \int_0^1 e^{-(\tau_1 - \tau_m)/\mu} \mu \, d\mu$$

$$+ 2\sigma \int_0^1 \left(\int_{\tau_m}^{\tau_1} T^4(\tau') \, e^{-(\tau' - \tau_m)/\mu} \, d\tau' \right.$$

$$\left. - \int_0^{\tau_m} T^4(\tau') \, e^{-(\tau_m - \tau')/\mu} \, d\tau' \right) d\mu \qquad \text{A.2.4}$$

and the heating rate is given by

$$Q_{rad_m} = \frac{1}{(z_m - z_{m-1})} \left\{ \sigma T_1^4 \, 2 \int_0^1 \left(e^{-(\tau_1 - \tau_{m-1})/\mu} - e^{-(\tau_1 - \tau_m)/\mu} \right) \mu \, d\mu \right.$$

$$+ 2\sigma \int_0^1 \left(\int_{\tau_{m-1}}^{\tau_1} T^4(\tau') \, e^{-(\tau' - \tau_{m-1})/\mu} \, d\tau' - \int_{\tau_m}^{\tau_1} T^4(\tau') \, e^{-(\tau' - \tau_m)/\mu} \, d\tau' \right.$$

$$\left. \left. - \int_0^{\tau_{m-1}} T^4(\tau') \, e^{-(\tau_{m-1} - \tau')/\mu} \, d\tau' + \int_0^{\tau_m} T^4(\tau') \, e^{-(\tau_m - \tau')/\mu} \, d\tau' \right) d\mu \right.$$

A.2.5

We now split some of the integrals up, in this manner,

$$\int_0^{\tau_{m-1}} (\text{integrand}) = \int_0^{\tau_m} (\quad) + \int_{\tau_m}^{\tau_{m-1}} (\quad)$$

$$\int_{\tau_m}^{\tau_g} (\quad) = \int_{\tau_{m-1}}^{\tau_g} (\quad) + \int_{\tau_m}^{\tau_{m-1}} (\quad)$$

and rearrange to get

$$Q_{rad_m} = \frac{1}{(z_m - z_{m-1})} \Bigg\{ \sigma T_1^4 \, 2 \int_0^1 \left(e^{-(\tau_1 - \tau_{m-1})/\mu} - e^{-(\tau_1 - \tau_m)/\mu} \right) \mu \, d\mu$$

$$+ 2\sigma \int_0^1 \left(\int_{\tau_{m-1}}^{\tau_1} T^4(\tau') \left(e^{-(\tau' - \tau_{m-1})/\mu} - e^{-(\tau_1 - \tau_m)/\mu} \right) d\tau' \right.$$

$$\left. - \int_0^{\tau_m} T^4(\tau') \left(e^{-(\tau_{m-1} - \tau')/\mu} - e^{-(\tau_m - \tau')/\mu} \right) d\tau' \right) d\mu$$

$$- 2\sigma \int_0^1 \left(\int_{\tau_m}^{\tau_{m-1}} T^4(\tau') \left(e^{-(\tau' - \tau_m)/\mu} + e^{-(\tau_{m-1} - \tau')/\mu} \right) d\tau' \right) d\mu$$

A.2.6

By regarding the temperature in a layer as a constant, we can express equation A.2.6 as a sum over all layers:

$$Q_{rad_n} = \frac{1}{(z_n - z_{n-1})}\Bigg\{ 2\sigma \int_0^1 \left(e^{-(\tau_1 - \tau_{n-1})/\mu} - e^{-(\tau_1 - \tau_n)/\mu}\right)\mu\, d\mu\; T_1^4$$

$$+ \sum_{i=2}^{i=n-1} 2\sigma \int_0^1 \left(\int_{\tau_i}^{\tau_{i-1}} e^{-(\tau' - \tau_{n-1})/\mu} - e^{-(\tau' - \tau_n)/\mu}\, d\tau' \right) d\mu\; T_i^4$$

$$+ \sum_{i=n+1}^{i=59} -2\sigma \int_0^1 \left(\int_{\tau_i}^{\tau_{i-1}} e^{-(\tau_{n-1} - \tau')/\mu} - e^{-(\tau_n - \tau')/\mu}\, d\tau' \right) d\mu\; T_i^4$$

$$- 2\sigma \int_0^1 \left(\int_{\tau_n}^{\tau_{n-1}} e^{-(\tau' - \tau_n)/\mu} + e^{-(\tau_{n-1} - \tau')/\mu}\, d\tau' \right) d\mu\; T_n^4$$

A.2.7

The above expression is valid for all $n, n \geq 2$. If in the summation sign, the initial index equals or exceeds the final index, for example $\sum_{2}^{1}$ the term is ignored.

We now seek the elements of the matrix $[A_{ni}]$. Some careful scrutiny reveals that $A_{ni}, n \geq 2$ is given by:

$$A_{m,i} =$$

$$\frac{1}{(z_m - z_{m-1})} \begin{cases} -2\sigma \int_0^1 \left(\int_{\tau_m}^{\tau_{m-1}} e^{-(\tau' - \tau_m)/\mu} - e^{-(\tau_{m-1} - \tau')/\mu} \, d\tau' \right) d\mu, & m = i \\ & i \neq 1 \\ 2\sigma \int_0^1 \left(\int_{\tau_i}^{\tau_{i-1}} e^{-(\tau' - \tau_{m-1})/\mu} - e^{-(\tau' - \tau_m)/\mu} \, d\tau' \right) d\mu, & m > i \\ & i \neq 1 \\ -2\sigma \int_0^1 \left(\int_{\tau_i}^{\tau_{i-1}} e^{-(\tau_{m-1} - \tau')/\mu} - e^{-(\tau_m - \tau')/\mu} \, d\tau' \right) d\mu, & m < i \\ & i \neq 1 \\ 2\sigma \int_0^1 \left(e^{-(\tau_1 - \tau_{m-1})/\mu} - e^{-(\tau_1 - \tau_m)/\mu} \right) \mu \, d\mu, & i = 1 \end{cases}$$

A.2.8

When doing the numerical calculation, it is convenient to define the first row of the matrix $[A_{m,i}]$ so that "$Q_{rad,}$" is actually the downward long wave flux at the surface, F^-. This is done by defining $A_{1,i}$ as:

$$A_{1,i} = \begin{cases} 0, & i = 1 \\ 2\sigma \int_{\tau_i}^{\tau_{i-1}} \left(\int_0^1 e^{-(\tau_1 - \tau')/\mu} \, d\mu \right) d\tau', & i > 1 \end{cases}$$

A.2.9

In practice, the integrals over μ are done first. They can be calculated by using Gaussian quadratures, or if the numerator of arguement of the exponent (for example, $\tau_{m-1} - \tau'$) is small, by a series expansion given in Goody (1964), appendix 8. The following integration over τ is trivial.

Appendix III

For the differential equation

$$\frac{\partial T}{\partial t} = F(T) \qquad \text{A.3.1}$$

the central-implicit (i.e. Crank-Nicolson) method can be represented as:

$$\frac{T^{j+1} - T^{j}}{\Delta t} = f\left(\frac{T^{j+1} + T^{j}}{2}\right) = f\left(T^{j+1/2}\right) \qquad \text{A.3.2}$$

As we see, the function f is evaluated at the average value of T^{j} and T^{j+1}. For more information, see Gerald (1970).

Let the subscript "ℓ" represent the index of the top of the convective region. In the computer program, ℓ is located by starting from the bottom and checking each lapse rate until the first subadiabatic lapse rate is found - its index is "ℓ".

Let $\left.\frac{\partial T}{\partial t}\right)_c$ be the temperature change due to convection. From the heat equation we have

$$\rho c_p \left.\frac{\partial T}{\partial t}\right)_c = -\frac{\partial}{\partial z} H \qquad \text{A.3.3}$$

which when put in centered-implicit form becomes:

$$\rho_m c_p \frac{T_m^{j+1} - T_m^{j}}{\Delta t} = \frac{H_{m-1}^{j+1/2} - H_m^{j+1/2}}{z_m - z_{m-1}}, \quad 2 \le m \le \ell \,. \qquad \text{A.3.4}$$

$H_m^{j+1/2}$ is given by:

$$\begin{cases} 0, & m = \ell \\ \rho_m c_p h z_m^2 \left(\frac{g}{T_m^j}\right)^{1/2} \Big/ \left(\frac{\frac{T_m^{j+1} + T_m^j}{2} - \frac{T_{m-1}^{j+1} + T_{m-1}^j}{2}}{\delta_m} + \Gamma \right)^{3/2}, & 2 \le m < \ell \\ .089\, 2^{4/3} \rho_2 c_p K \left(\frac{g}{T_2^j K \nu}\right)^{1/3} \left(\frac{T_1^{j+1} - T_1^j}{2} - \frac{T_2^{j+1} + T_2^j}{2} \right)^{1/3}, & m = 1 \end{cases} \qquad \text{A.3.5}$$

(To economize on space, from henceforth we let $X_m = \rho_m c_p h z_m^2 \left(\frac{g}{T_m^j}\right)^{1/2}$ and $Y = .089 \cdot 2^{4/3} \rho_2 c_p K \left(\frac{g}{T_2^j K \nu}\right)^{1/3}$).

When equation A.3.4 is applied to each layer in the convective region, a set of $\ell - 1$ non-linear algebraic equations is formed, with unknowns $T_1^{j+1}, \ldots, T_\ell^{j+1}$. As there is one more unknown than the number of equations, an extra equation is needed, which is the surface energy balance equation. It is (in centered-implicit form),

$$-K_g \left(\frac{\frac{T_1^{j+1} + T_1^j}{2} - T_{s_2}^j}{\Delta z_{s_2}} \right) + F^{-j+1/2} + S^{j+1/2}(t) - H_1^{j+1/2} - \sigma \left(\frac{T_1^{j+1} + T_1^j}{2} \right)^4 = 0 \qquad \text{A.3.6}$$

The first term of equation A.3.6 is the soil heat flux at the surface in finite difference form. $T_{s_2}^{j}$ is the soil temperature at the depth Δz_{s_2} $(= \sqrt{2\tilde{K}\Delta t})$.

Making the substitution $\Delta T_{c_m} = T_m^{j+1} - T_m^{j}$ (where ΔT_{c_m} is the convective temperature change) into equations A.3.5 and A.3.6 gives:

$$H_m^{j+1/2} = X_m \left| \left(\frac{T_m^j + T_{m-1}^j}{\delta_m} + \Gamma \right) + \frac{\Delta T_{c_m} - \Delta T_{c_{m-1}}}{2\delta_m} \right|^{3/2} \qquad 2 \le m \le \ell \qquad \text{A.3.7}$$

$$H_1^{j+1/2} = Y \left(T_1^j - T_2^j + \frac{\Delta T_{c_1}}{2} - \frac{\Delta T_{c_2}}{2} \right)^{4/3} \qquad \text{A.3.8}$$

$$- K_g \frac{(T_1^j - T_{s_2}^j)}{\Delta z_{s_2}} - \frac{K_g}{\Delta z_{s_2}} \frac{\Delta T_{c_1}}{2} + F^{j+1/2} + S^{j+1/2}(t)$$

$$+ Y \left(T_1^j - T_2^j + \frac{\Delta T_{c_1}}{2} - \frac{\Delta T_{c_2}}{2} \right)^{4/3} - \sigma \left(T_1^j + \frac{\Delta T_{c_1}}{2} \right)^4 = 0 \qquad \text{A.3.9}$$

If the time step is small, ΔT_{c_m} is presumably small, and the above equations can be linearized with a good degree of accuracy. We obtain:

$$H_m^{j+1/2} \cong H_m^j + \frac{3}{2} X_m \left| \frac{T_m^j - T_{m-1}^j}{\delta_m} + \Gamma \right| \left(\frac{\Delta T_{c_m}}{2\delta_m} - \frac{\Delta T_{c_{m-1}}}{2\delta_m} \right) \qquad \text{A.3.10}$$

$$H_1^{j+1/2} \cong H_1^j + \frac{4}{3} \cdot Y \cdot (T_1^j - T_2^j)^{1/3} \left(\frac{\Delta T_{c_1}}{2} - \frac{\Delta T_{c_2}}{2} \right) \qquad \text{A.3.11}$$

$$\left.\begin{aligned} & H_s^j - \frac{K_g}{\Delta z_{s_2}} \frac{\Delta T_{c_1}}{2} + F^{-j} + S^{j+1/2}(t) \\ & + H^j + \frac{4}{3} \cdot Y \cdot (T_1^j - T_2^j)^{1/3} \left(\frac{\Delta T_{c_1}}{2} - \frac{\Delta T_{c_2}}{2} \right) \\ & - \sigma T_1^{j\,4} - 4\sigma T_1^{j\,3} \frac{\Delta T_{c_1}}{2} = 0 \end{aligned}\right\} \qquad \text{A.3.12}$$

In the surface energy balance equation, we have approximated $F^{-j+1/2}$ by the term F^{-j}. This is a reasonable approximation since the temperature does not change very much during each time step.

We now have a set of ℓ <u>linear</u> equations with the same number of unknowns $\Delta T_{c_1}, \Delta T_{c_2}, \ldots\ldots, \Delta T_{c_\ell}$. This set can be put in the form:

$$\left.\begin{aligned} a_{11} \Delta T_{c_1} + a_{12} \Delta T_{c_2} &= B_1 \\ a_{21} \Delta T_{c_1} + a_{22} \Delta T_{c_2} + a_{23} \Delta T_{c_3} &= B_2 \\ \vdots \qquad\qquad \vdots \qquad\qquad \vdots & \\ a_{\ell,\ell-1} \Delta T_{c_{\ell-1}} + a_{\ell,\ell} \Delta T_{c_\ell} &= B_\ell \end{aligned}\right\} \qquad \text{A.3.13}$$

The matrix $[a_{nm}]$ is a tridiagonal symmetric matrix, with elements:

$$a_{11} = \frac{K_g}{\Delta z_{s_2}} + 4\sigma T_1^{i} + \frac{4}{3} \cdot \gamma \cdot (T_1^{i} - T_2^{i})/2 \qquad \text{A.3.14}$$

$$a_{12} = a_{21} = -\frac{4}{3} \cdot \gamma \cdot (T_1^{i} - T_2^{i})/2 \qquad \text{A.3.15}$$

$$a_{m,m-1} = a_{m-1,m} = -\frac{3}{4} \frac{\chi_{m-1}}{\delta_{m-1}} \left| \frac{T_m^{i} - T_{m-1}^{i}}{\delta_m} + \Gamma \right|^{1/2}, \qquad \text{A.3.16}$$

$$2 < m \leq \ell$$

$$a_{m,m+1} = a_{m+1,m} = -\frac{3}{4} \frac{\chi_m}{\delta_m} \left| \frac{T_{m+1}^{i} - T_m^{i}}{\delta_m} + \Gamma \right|^{1/2}, \qquad \text{A.3.17}$$

$$2 < m < \ell$$

$$a_{mm} = \begin{cases} \rho_m c_p \frac{(z_m - z_{m-1})}{\Delta t} - a_{m,m+1} - a_{m,m-1}, & 2 \leq m < \ell \\ \rho_\ell c_p \frac{(z_\ell - z_{\ell-1})}{\Delta t} - a_{m,m-1}, & m = \ell \end{cases} \qquad \text{A.3.18}$$

The column matrix $[B_m]$ is given by

$$\left.\begin{aligned} B_1 &= F^{i} + S^{i+1/2}(t) + H_s^{i} - \sigma T_1^{i\,4} - H_1^{i}, \quad m = 1 \\ B_m &= H_{m-1}^{i} - H_m^{i}, \quad 1 < m \leq \ell \end{aligned}\right\} \qquad \text{A.3.19}$$

As the matrix $[a_{nm}]$ is tridiagonal, this set of linear equations is easily solved by elimination.

Appendix IV

To solve for the new atmospheric specific humidities q_m^{j+1} and the surface soil moisture content, θ_1^{j+1} an implicit difference scheme is employed. For the differential equation:

$$\frac{\partial q}{\partial t} = f(q) \qquad \text{A.4.1}$$

the implicit method is written as

$$\frac{q^{j+1} - q^j}{\Delta t} = f(q^{j+1}) \qquad \text{A.4.2}$$

The function $f(q)$ is evaluated at the new humidities q^{j+1} instead of q^j, as would be done in an explicit method.

Let " ℓ " denote the index of the top of the convective region. In implicit form the equation of moisture transfer (eq 3.3.2) can be written as:

$$\rho_m \left(\frac{q_m^{j+1} - q_m^j}{\Delta t} \right) = \frac{W_{m-1}^{j+1} - W_m^{j+1}}{z_m - z_{m-1}} \qquad \text{A.4.3}$$

where W_m^{j+1} equals:

$$\begin{cases} \mathcal{Z}\,(q_1^{j+1} - q_2^{j+1}), & m = 1 \\ -\bar{\rho}_m K_{H_m}^j \dfrac{q_{m+1}^{j+1} - q_m^{j+1}}{\delta_m}, & 2 \le m < \ell \\ 0, & m = \ell \end{cases} \qquad \text{A.4.4}$$

In the above expression for W_m^{j+1}, Z represents the quantity "$.089\, 2^{4/3} \rho_2 D_m \left(\frac{g}{T_2^j K_N}\right)^{1/3} (T_1^j - T_2^j)^{1/3}$" and $\bar{\rho}_m$ is the density at the level z_m. Also we have used the eddy diffusivity $(K_{H_m}^j)$ and the temperatures (T_1^j, T_2^j) from the previous time step j. This is an excellent approximation because of the small time step.

By making the substitution $q_m^{j+1} = q_m^j + \Delta q$ into equations A.4.3 and A.4.4 we obtain:

$$\rho_m \frac{\Delta q_m}{\Delta t} = \frac{W_{m-1}^{j+1} - W_m^{j+1}}{z_m - z_{m-1}} \qquad \text{A.4.5}$$

with

$$W_m^{j+1} = \begin{cases} Z(\Delta q_1 - \Delta q_2) + W_1^j, & m = 1 \\ -\bar{\rho}_m K_{H_m}^j \left(\frac{\Delta q_{m+1} - \Delta q_m}{\delta_m}\right) + W_m^j, & 2 \le m < \ell \\ 0, & m = \ell \end{cases} \qquad \text{A.4.6'}$$

When equation A.4.5 is applied to each layer in the convective region, a set of $\ell - 1$ linear algebraic equations is formed:

$$\Delta q_1 (-Z) + \Delta q_2 \left(\rho_2 \frac{(z_2 - z_1)}{\Delta t} + Z + \frac{\bar{\rho}_2 K_{H_2}^j}{\delta_2}\right) + \Delta q_3 \left(\frac{-\rho_2 K_{H_2}^j}{\delta_2}\right) = W_1^j - W_2^j$$

$$\cdots\cdots$$

$$\Delta q_{m-1} \left(\frac{\bar{\rho}_{m-1} K_{H_{m-1}}^j}{\delta_{m-1}}\right) + \Delta q_m \left(\rho_m \frac{(z_m - z_{m-1})}{\Delta t} - \frac{\bar{\rho}_{m-1} K_{H_{m-1}}^j}{\delta_{m-1}} - \frac{\bar{\rho}_m K_{H_m}^j}{\delta_m}\right)$$
$$+ \Delta q_{m+1} \left(\frac{\bar{\rho}_m K_{H_m}^j}{\delta_m}\right) = W_{m-1}^j - W_m^j \qquad \text{A.4.6}$$

$$\cdots\cdots$$

$$\Delta q_{\ell-1} \left(\frac{\bar{\rho}_{\ell-1} K_{H_{\ell-1}}^j}{\delta_{\ell-1}}\right) + \Delta q_\ell \left(\rho_\ell \frac{(z_\ell - z_{\ell-1})}{\Delta t} - \frac{\bar{\rho}_{\ell-1} K_{H_{\ell-1}}^j}{\delta_{\ell-1}}\right) = W_{\ell-1}^j$$

In the above set of equations there are ℓ unknowns, $\Delta q_1, \Delta q_2, \ldots, \Delta q_\ell$. This is one more unknown than the number of equations.

To obtain a closed set of equations we must employ the conditions stated in section 3.3 First, q_1^{j+1} is a function (which we denote as Q) of the surface moisture content as stated by equation 3.3.11. We have

$$q_1^{j+1} = Q(\theta_1^{j+1}) = \frac{\epsilon}{p_s} e^{\frac{g\,\psi(\theta_1^{j+1})}{R_w T_1^j} \cdot 6.11} e^{\frac{L}{R_w}\left(\frac{1}{273} - \frac{1}{T_1^j}\right)} \qquad \text{A.4.7}$$

With the above relation, we obtain

$$\Delta q_1 = Q(\theta_1^{j+1}) - q_1^j \qquad \text{A.4.8}$$

Equation A.4.8 along with the equations A.4.6 consists of a set of ℓ equations and $\ell+1$ unknowns $\theta_1^{j+1}, \Delta q_1, \Delta q_2, \ldots, \Delta q_\ell$. The additional equation that makes a closed set is the condition that the moisture fluxes must be continuous at the surface. (eq. 3.3.6). In finite difference form, we have:

$$Z(\Delta q_1 - \Delta q_2) + W_1^j = -\rho_\ell \left[D(\bar{\theta}) \frac{(\theta_1^{j+1} - \theta_2^j)}{\Delta z_{\ell_1}} + K_w(\bar{\theta}) + D_T(\bar{\theta}) \frac{(T_{s_1}^j - T_{s_2}^j)}{\Delta z_{s_1}} \right] \qquad \text{A.4.9}$$

where θ_2^j is the value of the moisture content at the depth Δz_{ℓ_1} and $\bar{\theta}$ is the average value of θ_1^{j+1} and θ_2^j .

The closed set of equations (A.4.6, A.4.8, and A.4.9) contains two non-linear equations A.4.8 and A.4.9. The set can be solved using an iterative scheme. With the m^{th} approximation of the variable X denoted by $(X)_m$ the scheme is as follows:

1) If $m=1$ or $m=2$, we choose a value of $(\theta_1^{j+1})_m$ which is close to the actual solution. In practice

$$(\theta_1^{j+1})_m = \begin{cases} \theta_1^j + .001, & m=1 \\ (\theta_1^j)_1 + .001, & m=2 \end{cases} \qquad \text{A.4.10}$$

If $m>2$, this step is ignored.

2) Given $(\theta_1^{j+1})_m$, $(\Delta q_1)_m$ is calculated from equation A.4.8. With $(\Delta q_1)_m$ known, the equations A.4.6 form a closed set. As the associated matrix of the coefficients is tridiagonal, the set is easily solved by elimination. We obtain $(\Delta q_m)_m$, $m \geq 2$.

3) We define the function $G((\theta_1^{j+1})_m)$ such that

$$G = W_s|_{z=0} - W_1$$

$$= Z(\Delta q_1 - \Delta q_2) + W_1^j + \rho_l \left[D(\bar{\theta}) \frac{(\theta_1^{j+1} - \theta_2^j)}{\Delta z_{s_1}} + K_w(\bar{\theta}) + D_T(\bar{\theta}) \left(\frac{T_{s_1}^j - T_{s_2}^j}{\Delta z_{s_1}} \right) \right] \qquad \text{A.4.11}$$

With $(\Delta q_1)_m$, $(\Delta q_2)_m$, and $(\theta_1^{j+1})_m$ known, the

quantity $\frac{G}{W_1}\left(=\frac{W_s|_{z=0}-W_1}{W_1}\right)$ is calculated.

If it is less than .0001, we stop.

5) If $m=1$, return to step 1 and obtain a value for $(\theta_1^{j+1})_2$.

If $m \geq 2$, the next value of $(\theta_1^{j+1})_m$ is calculated using the so-called "secant method":

$$(\theta_1^{j+1})_{m+1} = -\frac{(\theta_1^{j+1})_{m-1} - (\theta_1^{j+1})_m}{G((\theta_1^{j+1})_{m-1}) - G((\theta_1^{j+1})_m)} \cdot G((\theta_1^{j+1})_m) + (\theta_1^{j+1})_m \quad \text{A.4.12}$$

(This method is just a way of finding the root to the function $G((\theta_1^{j+1})_m)$.

6) Repeat the process until convergence is obtained.

This method requires about 3 iterations to converge.

References

Businger, J.A. and Robert G. Fleagle, 1963: An Introduction to Atmospheric Physics. Academic Press.

Charney, J.G., 1975: Dynamics of deserts and drought in the Sahel. Quart. J. R. Met. Soc., 101, 193-202.

Gerald, C.F., 1970: Applied Numerical Analysis. Addison-Wesley.

Gierasch, P. and R. Goody, 1968: A study of the thermal and dynamical structure of the Martian lower atmosphere. Plant. Space Sci., 16, 615-646.

Goody, R.M., 1964: Atmospheric Radiation, Part I. Oxford University Press.

Hess, S.L., 1959: Introduction to Theoretical Meteorology. Henry Holt and Company.

Izumi, Y., 1971: Kansas 1968 Field Program Data Report. Environ. Res. Pap. No. 379, AFCRL-72-0041 (available from NTIS as AD-739 165).

Kirkham, D. and W.L. Powers, 1972: Advanced Soil Physics. John Wiley and Sons, Inc.

Kraichman, R. H., 1962: Turbulent thermal convection at arbitrary Prandtl Number. Physics Fluids, 5, 1374-1389.

Lettau, H.H. and B. Davidson, 1957: Exploring the Atmosphere's First Mile, Vol 1 and 2. Pergamon Press.

Manabe, S. and F. Möller, 1961: On the radiative equilibrium and heat balance of the atmosphere. Mon. Wea. Rev., 89, 503-532.

Manabe, S. and J.L. Holloway, Jr., 1975: The seasonal variation of the hydrologic cycle as simulated by a global model of the atmosphere. J. Geophys. Res., 80, 1617-1649.

Manabe, S., 1969: Climate and the Ocean Circulation, 1, The atmospheric circulation and the hydrology of the earth's surface. Mon. Wea. Rev., 97, 739-774.

Michelin Tyre Co., Ltd., 1973: Map of Africa, North and West. Map # 153.

Möller, F. and S. Manabe, 1961: Über das Strahlungsgleichgewicht der Atmosphäre, Z. fur Met., 15, 3-8.

Newell, R.E., J.W. Kidson, D. Vincent and G. Boer, 1972: The General Circulation of the Tropical Atmosphere, Vol. I. MIT Press.

Oort, A.H. and E.M. Rasmusson, 1971: Atmospheric Circulation Statistics. NOAA Professional Paper 5, U.S. Department of Commerce.

Philip, J.R. and D.A. de Vries, 1957: Moisture movement in porous materials under temperature gradients. Trans. Amer. Geophys. Union, 38, 222-232.

Philip, J.R., 1957: Evaporation and moisture and heat fields in the soil. J. Meteorology, 14, 354-366.

Priestly, C.H.B., 1959: Turbulent Transfer in the Lower Atmosphere. Chicago University Press.

Sasamori, T., 1970: A numerical study of atmospheric and soil boundary layers. J. Atmos. Sci., 27, 1122-1137.

Sundararajan, A. and S.A. Macklin, 1976: Comments: "On the Heat Flux and Friction Velocity in Free Convection Near the Ground". J. Atmos. Sci., 33, 715-718.

Walker, J. and P.R. Rowntree, 1977: The effect of soil moisture on circulation and rainfall in a tropical model. Quart. J. Roy. Met. Soc., 103, 29-46.